The Role of Hydrothermal Degradation in the Wear Behaviour of Zirconia

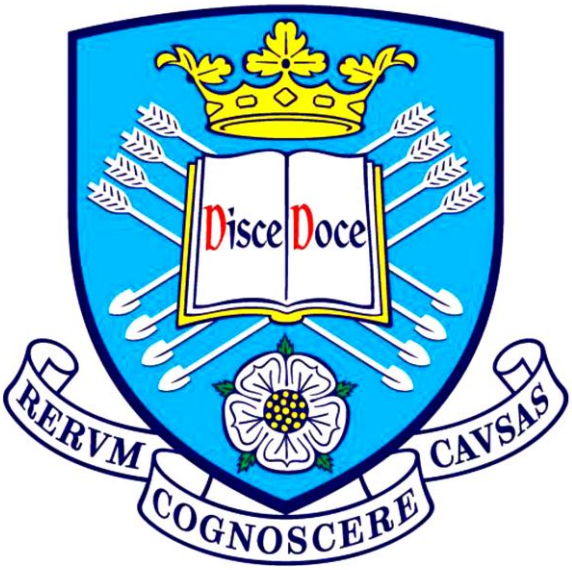

Submitted for the Degree of Doctor of Philosophy

Leili Shirkhan

Supervisor: Professor W. Mark Rainforth

The Department of Materials Science and Engineering
The University of Sheffield
September 2014

با عشق و سپاس بی پایان تقدیم به پدر،مادر وتارای نازنینم

Acknowledgements

First and foremost I would like to sincerely thank my PhD supervisor Professor Mark Rainforth for his unlimited support throughout my doctorate. Without his continues guidance and patience I would not have got here.

I would like express my appreciation to the Engineering and Physical Sciences Research Council (EPSRC) for financial support of the present study, members of staff in the Department of Materials Science and Engineering at the University of Sheffield, members of staff in Sorby Centre especially, Dr Peter Korgul, Dr Peng Zeng and for their electron microscopy assistance, Dawn Bussey for her help on the AFM, Phil Staton and Andrew Mould in sample preparation laboratories and all the clerical and technical staff who have been very helpful and friendly all the time.

Big love to all of my friends in H6 office in the Hadfield building. In particular, my biggest appreciation goes out to Akemi, Amit, Samira, Erfan and Zahra for their advice, discussions and helping me to over the past few years.

Last but not least my most sincere gratitude must go to my beloved family. Only whose infinite love and support would have been possible to pursue a PhD. To my parents and my wonderful daughter Tara who were with me in every second of this work. I love you all very dearly!

To all of you that I may have forgotten, I am equally grateful too.

Thank you!

Abstract

Yttria stabilised tetragonal zirconia polycrystal (Y-TZP) ceramics have attracted particular attention in medical applications due to their outstanding mechanical properties. In particular they have increased toughness compared to other ceramics such as alumina. Transformation toughened zirconia has the highest fracture toughness of the oxide ceramics, but its engineering applications are currently limited because hydrothermal degradation can catastrophically degrade its strength. Hydrothermal degradation is the autocatalytic transformation of the metastable tetragonal (*t*-ZrO_2) to the equilibrium monoclinic (*m*-ZrO_2) which occurs at a free surface when held in a moist atmosphere at elevated temperature (typically 100-200^{o}C). The underlying cause of this degradation process is still a matter of considerable debate and attempts to improve the resistance of Y-TZPs to hydrothermal degradation have generally resulted in unacceptable loss of toughness. The most prominent example of zirconia hydrothermal degradation is the failure of femoral heads in hip prosthetics. Hydrothermal degradation is not the only cause of hip joint failure, but tribological behaviour is also important, and the interaction between wear and ageing is crucial to developing zirconia applications. The origin of the detrimental effects of ageing on the wear of zirconia remains controversial. In the current work the wear behaviour of zirconia against alumina was investigated. In particular, a series of Y-TZPs have been developed with ternary and quaternary dopant additions designed specifically to reduce the rate of hydrothermal degradation to see whether these additions affected the wear behaviour. Ceramics with 0.1%wt Al_2O_3 and 0.1%(La_2O_3+Al_2O_3) doped 3Y-TZP ceramics were manufactured under conditions that yielded materials with the same grain size and fracture toughness. TEM of sintered materials demonstrated that the ternary oxide additions segregated to grain boundaries. Prior to degradation the surfaces were prepared by careful polishing to produce an extremely flat surface, followed by thermal etching to minimise residual surface strains and to ensure the starting surface was fully tetragonal zirconia. After degradation surfaces were examined using atomic force microscopy and X-ray diffraction and measurements were taken of the transformation depth on cross-sectional samples. Materials with ternary oxide additions exhibited superior degradation resistance to the base zirconia material. To study the ageing behaviour on wear behaviour in zirconia the specimens were aged at 134 °C in superheated steam (one hour in these

conditions is believed to equate to approximately one year *in vivo*). A UMT tribometer in pin–on–disk configuration was used for the tests. The effect of two different lubricants (water and bovine serum) was also investigated. The specific wear rates were measured to be at or below 10^{-6} mm^3/Nm for all samples, indicating that mild wear predominated throughout. Surprisingly, the wear rate of some of the aged specimens was lower than that for the non-aged samples. The worn surfaces exhibited evidence of surface fracture and grain pull-out. Cross-sectioning the surface by FIB and examination in the TEM showed that transformation from tetragonal to monoclinic zirconia occurred, with grain pull out resulting from loss of material from within the monoclinic zirconia layer. TEM also revealed an amorphous tribolayer formed on top of the worn surface, which appeared to be a combination of the substrate material and the lubricant.

CONTENTS

Abbreviations

TZP Tetragonal Zirconia Polycrystals

Y Y_2O_3

Z 3Y-TZP sample

AZ 0.1 wt. % Al_2O_3 doped 3Y-TZP sample

LAZ 0.1 wt. % Al_2O_3 / 0.1 wt. % La_2O_3 doped 3Y-TZP sample

DZ Degraded 3Y-TZP sample

DAZ Degraded 0.1 wt. % Al_2O_3 doped 3Y-TZP sample

DLAZ Degraded 0.1 wt. % Al_2O_3 / 0.1 wt. % La_2O_3 doped 3Y-TZP sample

W Water lubricant

B Bovine lubricant

COF Coefficient of friction

AFM Atomic force microscopy

SEM Scanning electron microscopy

TEM Transmission electron microscopy

FIB Focused ion beam microscopy

1. Introduction

Total hip replacement (THR) is a major operation to replace a damaged hip with an artificial part to improve the mobility of patients suffering from a wide range of hip joint diseases. A broad range of the hip joint health problems such as osteoarthritis, bone disease, wear, and trauma have been treated since total hip joint replacement were first successfully introduced by Mackee Farrar and Charnley in 1956 [1]. Earlier attempts with materials such as pyrex and teflon failed due to the poor design and inadequate material properties [2]. The current life time of the hip joint implant is between 10 and 15 years which is insufficient for the increasing numbers of younger and more active patients seeking treatment [3]. Hence, the demand for new materials and longer lasting designs is increasing. Current designs of the hip joint and the acetabular cup (large pelvic bone) may be either hard-on-hard or hard-on-soft combinations i.e. metal-on-metal, metal-on-ultra high molecular weight polyethylene (UHMWPE), metal-on-ceramic, UHMWPE-on-ceramic and ceramic-on-ceramic.

A polyethylene cup in conjunction with cobalt chrome metal head is a popular configuration, but unfortunately the wear rate of the polymer cup is quite high. The liberated wear debris reacts with body fluids leading to aseptic loosening, adverse tissue reactions and bone resorption [4]. Despite this drawback survival rates as high as 75% over 20 years implant life time have been reported for this implant type [5].

The biocompatible nature of ceramics has been commercially recognised since the 1970s, and alumina has always led the field. The world's leading ceramic hip joint (Biolox Delta),

manufactured by Ceramtec Germany, uses the fourth generation of alumina developed - zirconia toughened alumina (ZTA).

Zirconia has three times higher fracture toughness than alumina. Since 1985, more than 600,000 stabilized zirconia femoral heads for THR have been implanted worldwide in the form of Y-TZP. However, the effects of ageing, mechanical stresses and low thermal conductivity on wear of zirconia implants is complicated by interaction of these processes with some unexpected consequences. Clinical studies demonstrated that those patients with stabilized zirconia implant can experience problems related to wear and phase instability. The most high profile zirconia failure occurred in 2001 when more than 350 Y-TZP implanted hip prostheses failed requiring revision surgery. The French manufacturers, SGCA Desmarquest, voluntarily suspended the use of prostheses from the batches involved in the failure [6].The catastrophic failures were linked to an "accelerated transformation" in zirconia.

Pure zirconia at room temperature has three polymorphic phases, cubic, tetragonal and monoclinic. The tetragonal phase becomes stabilised at room temperatures by dopant additions such as yttrium, calcium and magnesium. Doping introduces oxygen ion vacancies within the structure and which are essential for tetragonal phase retention [7]. However, tetragonal zirconia is metastable at room temperature and it can transform to the monoclinic phase. This tetragonal to monoclinic phase transformation (t→m) is the main reason for zirconia's outstanding fracture toughness. Kobyashi was the first to discover tetragonal to monoclinic phase transformation at low temperature in a moist environment, known generally as ageing or low temperature hydrothermal degradation [7]. Doping

zirconia with some metal oxides decelerates the kinetics of this transformation. The effects of this on the wear and ageing of zirconia are the main subjects of this project.

One of the main concerns with using zirconia as a tribological material is the concern over hydrothermal degradation. However, Nogiwa and Rainforth [23] demonstrated ways in which the degradation rate can be substantially reduced without any detrimental effect on mechanical properties.

In the current study, a key objective was to understand whether the additions of ternary and quaternary dopants, that reduce the rate of degradation, have any effect on the wear rate.

Test conditions were chosen to maximise the likely hood that degradation would occur. In addition, the effect of degrading the surface of the zirconia before the wear test on the subsequent wear behaviour was also investigated. This has not been undertaken before, but it believed to be a potential problem arising with sterilisation of zirconia components prior to insertion in the body.

2. Literature

2.1. Total Hip Joint Replacement

Total hip replacement (THR) is a major operation to replace a damaged hip with an artificial part to improve the mobility of patients suffering from a wide range of hip joint diseases. In this operation real joint performance is mimicked using an acetabulum cup fixed inside the pelvis, and the ball component is inserted inside the femur bone, Figure 2.1.

Figure2.1: Hip joint implants [8].

THR is an efficient and a practical solution, reducing severe pain in these patients, leading to increased global demand as a treatment method for hip joint disfunctionality, such as arthritis or trauma. The earliest THR was an ivory ball and socket joint invented by Gluck, in Berlin, in 1891. Pyrex and acrylic have also been utilised. Initially both material and design contributed to a very short life for replacement parts, and revision surgery was necessary [2]. Clinical performance has been improved through both design modification and materials development, particularly since the 1950s, when more long lasting pairs were introduced to the biomaterial market. The McKee-Farrar metal-on-metal [3] and Charnley metal-on-polymer prosthesis [2] were both successful designs. Ceramic-on-ceramic (C-O-C) components were introduced for the first time in France by Boutin in the early 1970s using alumina-on-alumina [9]. The early C-O-C hip design by Ceraver Osteal Hip was used in

Europe only, but the Mittlemeier and Heisel design in Germany gained worldwide success [10]. Initial ceramic-on-ceramic results were very encouraging with satisfactory results in the first 200 cases, and no reported failures or fractures in the early years.

Pairs in current use may be categorised into hard-on-hard and hard-on-soft combinations with either Ceramic-on-(ceramic, polymer and metal) or metal-on-(ceramic, polymer and metal) are currently used, Figure 2.2.

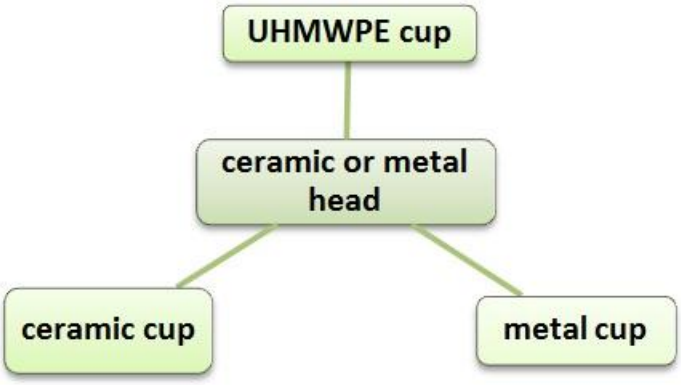

Figure 2.2: Potential and existing combination for THR combinations

The wear rate is one of the main concerns in this application because it affects the life of the replacement joint. Table 2.1 [4] gives a brief summary of the in vitro wear rate reported in the literature. The most commonly used hard-on-soft pair is metal-on-polymer (ultrahigh molecular weight polyethylene) yet the polyethylene generates wear particles at a very high rate. The same problem arises with alumina-on-polyethylene and zirconia-on-polyethylene.

Longer life time and lower failure rates have been achieved in recent years using hard-on-hard combinations. For example a cobalt–chromium (CoCr) alloy introduced in 1938 as a general wear resistant material used in a metal-on-metal (MOM) design showed up to 100 times less wear debris generation. The market for this configuration grew until 2007 when a voluntary warning notice issued by Depuy (French hip joint manufacture) alerted high wear

debris of MOM pairs. Metallosis is the given name to metal ion release on MOM wear and MOM implants were found to cause inflammatory diseases and suffer long term catastrophic failure. Since 2012 the FDA have advised that patients with MOM implants have regular blood and urine tests for prompt identification of any adverse tissue reaction and excessive levels of cobalt or chromium ions within their blood stream [11].

Attention is therefore now focussed on ceramic-on-metal pairing inhibiting the fracture risk in ceramics [12].

Table 2.1: Wear rate of bearing components of hip joint prostheses [4]

Ball-on-socket material	Clinical wear rate (µm/year)
Metal-on-polymer	100-300
Ceramic-on-polymer	50-150
Metal-on-metal	2-20
Ceramic-on-ceramic	2-20

2.2. Ceramic-On-Ceramic THRs

The emergence of ceramics-on-ceramic pairs (COC) in the arthroplasty industry arose from its success as a femoral head when paired with UHMWPE cups. Table 2.2 provides a brief history in ceramic innovations [13]. The excellent mechanical properties of alumina, such as high hardness and biocompatibility have resulted in it replacing metals, and its popularity continues to increase.

Table 2.2: A brief history of ceramic innovation [13]

Year	Ceramic	Diameter(cm)	Details	Manufacture company
1970	Alumina	32	Non-modular ceramic ball and 1 piece cemented ceramic cup	Ceraver Inc: Boutin MD
1973	Alumina	28,32,35	Modular ceramic balls	Feldmuhle Inc: Griss; Mittlemeier MD
1977	Alumina	28,32	Modular ceramic balls	Ceraver Inc: Cedel MD
1985	Zirconia (Y-TZP)	22,26,28,32	Modular zirconia balls	JMMC Japan, Metoxic Switzerland, Morgan Matrock –UK,NGK –Japan, Saint Gobain-France
1989	Alumina	28,32	Modular ceramic cup, threated with hydroxyapatite coating	JRI Inc; Furlong MD
1989	Alumina-zirconia	26,28,32	Various alumina and Y-TZP zirconia approved by FDA, for use with polyethylene bearing	
1997	Alumina	36	Large ball. approved by FDA, for use by Write Medical with PE cups	Biolex forte Ceram Tec AG
1999	Zirconia(Y-TZP)	28-32	Beginning of problem in manufacturing and major fracture	Prozyr, Saint Gobin Descmarquest Inc , France
2000	Alumina-zirconia	28-32	Biolox Forte and delta ceramic balls and liners	Ceram Tec AG
2000	Alumina-zirconia	28-32	Biolox Delta ball approved by FDA ,with PE cups	Ceram Tec
2003	Alumina	28-32	Ceramic liners FDA approved	Biolex forte
2006	Alumina-zirconia	36	Large ball of Biolox Forte approved by FDA, for use with Polyethylene cups	Ceram Tec AG

Alumina and zirconia can both be used in hip joint replacements, but alumina's performance has gained more market success than zirconia. The development of alumina occurred through four different generations of materials. The third generation alumina by benefit of a hot isostatic pressing technique achieved a density near theoretical density. Low density was the main disadvantage of the older generations in alumina implants. The addition of zirconia (fourth generation) increases both the strength and fracture toughness (primarily through the introduction of the transformation toughening mechanism in the zirconia). By 2005 over 5,000,000 alumina femoral heads and around 500,000 alumina acetabular cups had been implanted worldwide [13]. However, the low fracture toughness of ceramics

remains a big concern with some sections of the orthopaedic community deeming fracture rates >0.004 % as being unacceptably high [6]. Revision surgery is a very complicated and therefore expensive procedure which puts patients at risk so there is strong market demand for a material with greater chemical and mechanical stability, which produces minimal wear particles and adverse body reactions.

Regardless of the materials combination used then aseptic loosening of the joint is one of the most common reasons for THR revision surgery. Loosening is believed to result from wear debris migrating into the surrounding tissue provoking a physiological reaction that causes rejection of the prosthesis. Wear of the joint can be uniform, but is usually localised in a region of severe wear on the head or cup, commonly known as stripe wear. This area usually has a different contrast from the original surface which can be observed with the naked eye, Figure 2.4 [16]. Stripe wear is believed to form as a result of microseparation during the walking cycle. Figure 2.3 [14], [15] shows a schematic diagram of how microseparation occurs during the swing phase of the walking cycle, Figure 2.3A. During vertical movements of the head in the heel strike phase, large amounts of load transfer to the head, which causes partial contact of the head and rim, Figure 2.3B, and severe wear damage is initiated due to edge loading. Material detachment during progressive wear changes the original geometry and in severe cases, the actual size of the implant. Revision surgery becomes necessary in such cases. While there are limitations to access real retrieved hip joints, in vivo experiments are well designed to create such a pattern for further study.

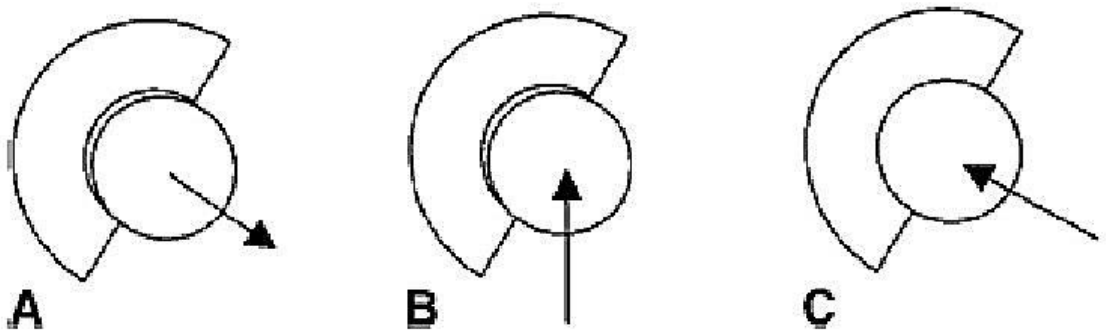

Figure 2.3: Schematic drawing to show walking cycle applied stress to C-O-C implant and part failures performance [14, 15].

Figure 2.4: Stripe wear region on ceramic head and cup [16].

2.3. Zirconia in THR

Christel [17] was the first to recognise zirconia as a bio material and its higher fracture toughness and higher flexural strength offer potential advantages for implants compare to alumina. Zirconia has the advantages of non-cytotoxicity, less inflammation reaction, outstanding fracture toughness. Zirconia has a polymorphic crystal structure, and its ability to transform from tetragonal to monoclinic phase enhances the fracture toughness (see next section for detail). Ceramic steel was the name given to zirconia after discovery of the ''transformation toughening process'' by Garvie [18]. Tetragonal zirconia polycrystalline (TZP) is a toughened zirconia with the addition of 3 mol % of yttrium oxide to partially

stabilise the tetragonal phase. In the 1990s Y-TZP material opened a new way for design of implants which were not successful with alumina. Manufacturing of smaller hip joints for example 22mm head size and Y-TZP knee implants [6] were in this field. In recent years, some zirconia-based ceramics such as Mg-PSZ and TZP have been employed in biomaterial applications due to their low chemical reactivity and high strength [7]. Table 2.3 compares the properties of zirconia based ceramics with those of alumina.

There are conflicting reports of the success of zirconia implants for hip joint replacements. Some reports show very low rates of failure of 0.002%, whereas others reveal disastrous performance [6]. The high failure rates are believed to be associated with “ageing” or “hydrothermal degradation” [7]. Saint Gobain Ceramiques Avances Desmarquest (France) was one of the manufacturers of hip joint prostheses that were suspended by the FDA in 2002. This was due to reports of a higher than expected rate of hip breakages inside the patient’s body, sometimes within a few months of surgery. The high failure rate was originally thought to be a result of hydrothermal degradation; it was later shown to be a result of poor ceramic properties. In this series of hip joints, the sintering stage had been changed from a batch process to a continuous process, resulting in unacceptably high porosity and poor strength. These catastrophic events seriously eroded the medical community’s confidence in zirconia as a biomaterial, triggering renewed research efforts to address this weakness and develop this otherwise promising material [6].

Table 2.3: Properties of zirconia based ceramics in compare with alumina [7]

Property	units	Alumina	Mg-PSZ	TZP
Chemical composition		99.9% Al_2O_3+MgO	ZrO_2	ZrO_2
Density	gcm^{-3}	≥3.97	5.74-6	>6
Porosity	%	<0.1	-	<0.1
Bending strength	MPa	>500	450-700	900-1200
Compression strength	MPa	4100	2000	2000
Young modulus	GPa	380	200	210
Fracture toughness	$MPam^{-1}$	4	7-15	7-10
Thermal expansion coefficient	K^{-1}	$8x10^{-6}$	$7\text{-}10x10^{-6}$	$11x10^{-6}$
Thermal conductivity	WmK^{-1}	30	2	2
Hardness	H.V 0.1	2200	1200	1200

The following sections will first consider the tribological behaviour of zirconia followed by discussion of wear, microstructure, phase transformation, transformation toughening process and hydrothermal degradation behaviours.

2.4. The Structure of Zirconia

Zirconia is a natural oxide mineral found in two forms, baddeleyite and zircon ($ZrO_2.SiO_2$). There are numerous ways to produce pure zirconia from these ores but commonly used

ones are vapour phase reaction and sol-gel processing. Zirconia's toughness, wear and corrosion resistance have numerous industrial applications e.g. extrusion dies, machinery wear parts and piston caps. Ion conductivity and thermal fracture resistance of partially stabilized zirconia are utilised in oxygen sensors and fuel cells, and its low thermal conductivity in thermal barrier coatings for aerospace parts. Well-polished zirconia is used for feeler gauges. The outstanding mechanical properties of toughened zirconia compared to the other ceramic oxides have been extensively demonstrated.

Zirconia has three well defined polymorphs at ambient pressure, which are stable in different temperature ranges, Figure 2.5. The monoclinic structure (space group $P2_1/c$) with seven fold coordination is the thermodynamically stable phase from room temperature up to 1170°C. At this temperature the structure transforms to tetragonal (space group $P4_2/nmc$), which is stable up to 2370 °C. The cubic polymorph (space group CF2) nucleates in this temperature and remains stable up to 2680 °C (the melting point of zirconia). Both the later phases are in eight fold coordination [7].

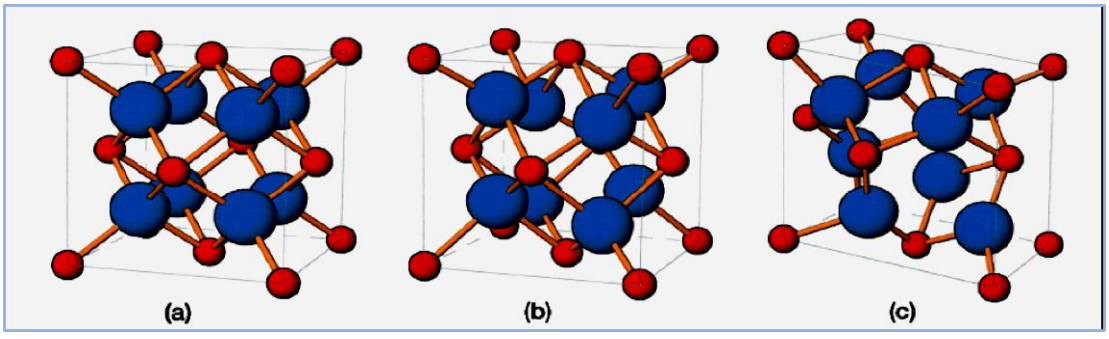

Figure 2.5: Schematic representation of the three main zirconia polymorphs: cubic (a), (b) tetragonal and (c) monoclinic [7]. Red and blue spheres show Zr^{4+} and O^{2-} respectively.

2.4.1. Stabilisation of Zirconia

During the transformation from the tetragonal to the monoclinic phase the zirconia lattice undergoes a 2-5 % volume expansion and 16% shear strain. This transformation, which occurs for example during the post sintering cooling cycle, is martensitic in nature. As part of this martensitic phase transformation, twins are formed in the monoclinic phase, often with associated microcracking, in order to relieve the lattice strain resulting from the transformation. The importance of the creation of oxygen ion vacancies in the lattice to stabilize both the tetragonal and cubic zirconia phases is well documented [19]. Additions of appropriate concentrations of metal oxide dopants such as CaO, MgO, Ce_2O_3 and Y_2O_3, generates these oxygen ion vacancies. Tuning the concentrations of the dopants yields different varieties of the toughened zirconia [7]. The two main classes are partially stabilised zirconia (PSZ), where the metastable tetragonal zirconia is contained within a cubic zirconia matrix, and tetragonal zirconia polycrystals (TZP), where a fully metastable tetragonal structure is obtained. TZPs may also contain small fractions of cubic and/or monoclinic phases. In Table 2.4 the ionic radii of some dopants added to the zirconia are given. Generally ions with a radius within 40% of Zr^{4+} are able to stabilize or partially stabilise the zirconia.

Table 2.4. Ionic radius of different dopant cations [19].

Cation	Ionic radius (nm)
Mg^{2+}	0.089
Ca^{2+}	0.112
Y^{3+}	0.102
Ce^{4+}	0.097
Nb^{5+}	0.074
Ta^{5+}	0.074

Reducing the oxygen partial pressure during sintering and doping the material with oversized (Y^{3+} and Gd^{3+}) and undersized (Fe^{3+} and Ga^{3+}) trivalent cation in the ZrO_2 lattice generates oxygen vacancies. The homogeneity of the dopants (i.e. whether they are present throughout the lattice or are segregated to the grain boundaries), as well as the sintering condition, has a considerable influence on the microstructure (grain size, phase constitution etc).

2.4.2. Transformation Toughening Process

Various toughening mechanisms, such as transformation toughening, microcrack toughening and crack deflection toughening may be applied to zirconia ceramics. The t-m phase transformation which occurs at < 900^{o}C is a consequence of an athermal, diffusionless and displacive solid-state phase change known as martensitic transformation. This involves the simultaneous movement of a large number of atoms by distances smaller than one atomic spacing. In un-doped zirconia, this transformation results in considerable loss of mechanical strength, due to the inherently low strength of the monoclinic phase and the extensive microcracking. However, in a TZP or PSZ, where the combination of grain size and

dopant concentration are optimised, the transformation to monoclinic zirconia can be constrained to around a propagating crack, Figure 2.6. The volume expansion associated with the tetragonal to monoclinic transformation results in a compressive stress inside the transformed region. It is specifically the action of closing the crack in the area behind the crack tip, called the crack wake (Figure 2.6) that is responsible for slowing crack propagation and thereby toughening the ceramic. The expansion associated with the transformed zone in the wake zone that results in closure of the crack, is referred to as 'crack shielding'. As the crack grows, the size of the wake zone expands and therefore the amount of transformed monoclinic phase becomes larger [7]. This can result in R curve behaviour, i.e. where the value of K increases with an increase in crack length, until eventually, K reaches K_{1C} and failure occurs. In fact K is the stress-intensity factor which determines the fracture toughness of most materials.

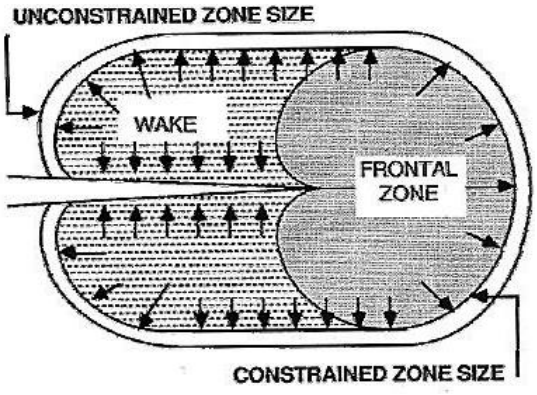

Figure 2.6: Crack Propagation: The propagating crack exerts a compressive force around the crack tip, which can toughen the ceramic [7].

2.4.3. Hydrothermal Degradation

The Achilles heel of transformation toughened zirconia based ceramics is the spontaneous phase transformation of metastable tetragonal zirconia to monoclinic phase at temperatures between 100-500 °C, particularly in the presence of water vapour, known as hydrothermal degradation or aging. Kobayashi, who discovered this phenomenon for the first time in 1981, reported significant loss of strength due to the microcracking which was detected after aging [7]. Water molecules and even water vapour in air is a strong trigger for this ageing process. The metastable tetragonal grains undergo martensitic transformation during water penetration inside the lattice. The transformation initiates at the surface and propagates into the interior. The transformation to monoclinic phase is associated with microcracking, which is believed to provide a mechanism for the ingress of water to the transformation front, encouraging the transformation to propagate further into the bulk.

Masaki in 1986[20] showed that degradation of different TZPs was strongly dependent on the amount of yttria at 200 °C, Figure 2.7[7]. The specimens were aged in air.

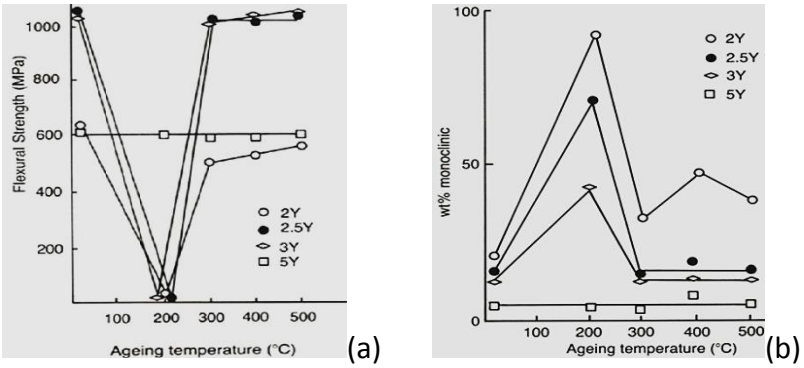

Figure 2.7: Zirconia failure by increasing the monoclinic content in doped materials [7]. Bend strength (a) and monoclinic percentage (b) respectively versus ageing temperature for Y-TZPs. Y represents the Y_2O_3 content.

Despite numerous theories the main cause of ageing has yet to be confirmed. An early model proposed by Lange (1986) suggested that degradation occurs because a reaction between Y_2O_3 and water results in the loss of Y^{3+} from the tetragonal zirconia matrix leading to the formation of α-Y $(OH)_3$. Since Y^{3+} stabilises the tetragonal structure, the loss of Y^{3+} from the lattice results in spontaneous transformation to monoclinic zirconia [21]. However, this theory is controversial and has not been subsequently pursued since, as Lange pointed out, for Y $(OH)_3$ to form then Y^{3+} must diffuse through the zirconia lattice, and this process is believed to be very slow taking perhaps 10^{21} years for 1 nm diffusion.

Schubert and Frey suggested that when the water molecules penetrate into the lattice they dissociate into OH^- and H^+, and the hydrogen settles in the interstitial site. The vacancies, brought about by the addition of the Y^{3+}, are crucial to the retention of the tetragonal structure. The presence of H^+ in the interstitial site results in a lattice contraction, which generates tensile stress, destabilizing the tetragonal grains [22].

The hydrothermal degradation mechanism of TZP is considered to be a nucleation and growth process which starts at the surface and propagates inwards, according to kinetics which can be described by the standard Mehl-Avrami-Johnson law. The transformation is not a random process in terms of the monoclinic nucleation and growth, rather following transformation to a monoclinic grain, transformation is then nucleated in the adjacent grain, a process which continues until the monoclinic phase covers a specific area, a process known as autocatalytic transformation. Large grains, and also the grains with inhomogeneous dispersion of the stabiliser, are more prone to transform [23].

Sato's model (1985) was based on the reaction of the water molecules with Zr-O-Zr at the crack tip. He proposed that breaking of the Zr-O bonds and formation of Zr -OH induces a stress at the crack that releases the crack tip stress encouraging the transformation to occur more rapidly [24]. His model was based on the assumption that degradation was only a surface phenomenon, however it has since been convincingly evidenced that transformation starts at the surface but does then invade the bulk.

In 1987, Yoshimora proposed the formation of the hydroxyl ions and diffusion of them into the zirconia lattice when Zr-OH bonds are created. He postured that absorption of the water molecules on the Y-TZP surface produces Zr-OH bonds at the stress sites. Surface diffusion of the OH^- ions creates nucleation sites for phase transformation on the surface so that surface and near surface micro- and macrocracking occurs [25].

An alternative model considers crack growth to be a stress corrosion mechanism. Diffusion of the corrosive species (OH^-) occurs from the environment to the crack tip; the OH^- anions react with Zr-O-Zr releasing crack tip stresses generated from the tetragonal to monoclinic phase transformation and accelerating the transformation process [26]. Since the hydrothermal degradation process does appear to involve anion vacancy removal in the lattice, particularly in a moist atmosphere, inducing local lattice strain accelerates the transformation. Conversely, a higher anion vacancy concentration within the grain boundary decelerates it.

2.4.4. Ternary Oxide Addition

Hydrothermal degradation in TZP ceramics limits its wide scale use due to the loss of strength. In severe cases complete fracture of the material occurs. Micro-cracking along the

grain boundaries accelerates the degradation kinetics; so anion vacancy creation in the grain boundaries could reduce the tetragonal to monoclinic phase transformation rate and increase the toughness of the material.

It has been known for some time that the addition of small amounts of alumina to TZPs improves their resistance to hydrothermal degradation. Alumina is usually added to ZrO_2 at the initial powder processing stage to enhance density, but it also improves hydrothermal degradation resistance. It has been demonstrated that the trivalent structure of the Al^{3+} enhances the number of oxygen ion vacancies in the grain boundary. Ross et al. [27] discovered that when adding Al_2O_3 (0.05, 0.1, and 0.25 wt %) to TZP the Al^{3+} segregates and modifies the grain boundary structure enhancing oxygen ion vacancy concentration, Figure 2.8. More recently their research also showed that homogeneity of the precursor has a great influence on the microstructure.

Lawson (1996), performing degradation tests on different TZPs powder at 180 °C for 48 h, found that the presence of a glassy phase improved resistance to ageing. The glassy phase decreases the thermal expansion mismatch stress due to the thermal anisotropy in the TZP [28]. The drawback of grain boundary glass in Y-TZP microstructure is the reduced toughness due to the loss of yttria within the glassy phase.

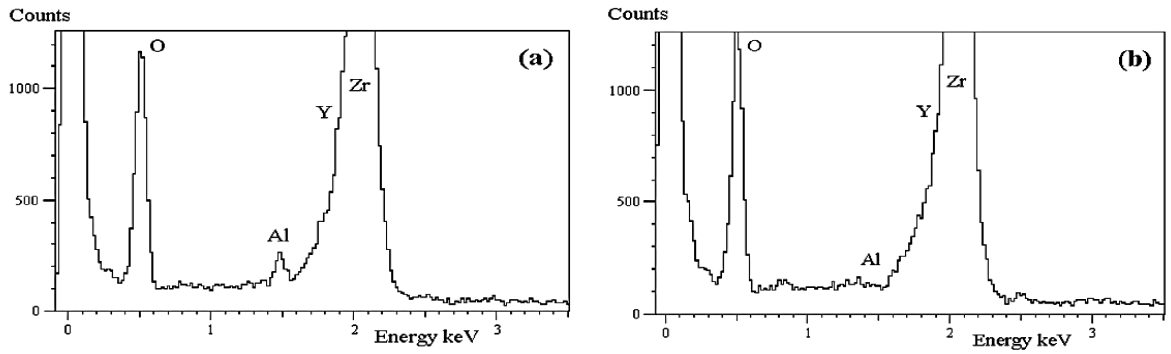

Figure 2.8: EDS trace derived from a) two grain interface showing Al trace and b) from the adjacent rain interior [27].

2.5. Wear

Tribological wear is defined as the progressive loss of material when two surfaces rub against each other, either in dry or lubricated conditions. Material detachment can occur through a wide range of mechanisms as summarised in Table 2.5[29]. In fact friction and consequent wear between sliding components is a major factor in high energy cost and equipment life reduction but can be significantly reduced with lubrication. Knowledge of fluid dynamics and surface engineering is essential optimising a lubrication regime in tribological studies. During wear multiple wear mechanisms, with varying wear rates can simultaneously occur. Only the wear mechanisms, most relevant to the wear of ceramic on ceramic hip joints are discussed here.

Table 2.5: A brief summary of wear mechanism [29]

Wear mechanism	The way it occurs
Adhesion	Material deposition from one surface to another, leaving craters and pits known as galling as well.
Abrasion	The softer surface material removal through ploughing or gouging in contact by harder surface. Detached particles can embed to the surface (2 body abrasion) or roll freely between two surfaces (3 body abrasion).
Fatigue	Cyclic sliding stresses which initiates deformation such as cracks underneath the surface which results in material fragmentation.
Erosion	It is a kind of abrasive wear which through that the material removal occurs by particles that striking the surface in fluid flow.
Delamination	The wear debris pack up makes a sheet like structure which would remove from surface during sliding contact.
Fretting	Material removal by oscillatory movement.
Polishing	Abrasive wear type wear which in very fine particles during continues movement, strike the surface
Tribochemical wear	Mechanical stresses of wear trigger chemical reaction of the surface and environment.
Corrosive	This type of wear occurs when environmental chemicals attack strikes the surface.

2.5.1. Wear of C-on-C in THR

Ceramics, due to their inherently brittle nature, mostly wear through microcracks and chipping. Wear of the ceramics has been broadly separated into the mild and the severe wear regime. In the mild wear regime the ceramic surface remains smooth, sometimes smoother than the original surface. Ceramics will be useful for tribological applications if their specific wear rate is less than 10^{-6} mm^3/Nm i.e. the upper limit for the mild wear [30, 31]. During progressive wear then beyond a critical load/speed/time the wear mechanism changes and the condition transforms from mild wear to severe. During this transition, the specific wear rate usually increases by several orders of magnitude, exceeding $10^{-4}mm^3/Nm$ in ceramics where it is accompanied by the onset of brittle fracture. Table 2.6[32], [33] provides information about wear behaviour in the mild and severe wear zone.

Table 2.6: General differences between mild and sever wear in ceramics [32] [33]

	Mild wear	**Severe wear**
Wear rate	Low, $<10^{-6}$ mm^3/Nm	High, $>10^{-4}mm^3/Nm$
Worn surface morphology	Extremely smooth, often smoother than original surface	Rough, pitted from original surface
Friction	Steady	Fluctuating
Wear mechanism	Plastic flow /tribochemical	Fracture
Wear Particles	Fine particles and often chemically different from the bulk material(chemical interaction of surface and wear environment	Large angular particles with structure similar to the wear surfaces

2.5.2. Wear Rate

The specific wear rate provides a convenient way to compare the wear data from different sources. For homogeneous materials the specific wear rate (k) is defined by well-known Archard theory, equation 2.1. In this equation the wear volume, V, is assumed to be proportional to the applied load (N) and sliding distance (S) [34].

$$k=V/NS \qquad (2.1)$$

The specific wear rate is usually reported in mm^3/Nm.

Wear debris generation is the direct consequence of wear and can be formed early in the implant life. Debris as large as 5µm has been detected within the body an implant recipient. Although ceramics such as alumina and zirconia are biocompatible materials, but wear debris can still be seen as a foreign body, stimulating the immune system and triggering pro-inflammatory cytokines followed by osteoclast activation and bone resorption [35]. This could be lead to aseptic loosening which is the most common reason for revision surgery. Wear particles can also act as third body abrasive particles, further increasing implant wear.

2.5.3. Friction and Wear in Simulation Tests

Friction factor (*f*) or coefficients of friction (µ) are used in tribology studies for estimating the resistance of motion. The coefficient of friction is a non-dimensional ratio which is derived from the first law of friction, equation 2.2:

$$\mu=F/N \qquad (2.2)$$

In this equation F is the friction force and N is the applied load. The friction factor (*f*) in a hip joint simulator is defined in by equation 2.3 [36] where (T) is friction toque, R_1 is the radius of ceramic head and R_2 is the radius of the ball-socket configuration.

$$f=T/R_1N \qquad (2.3)$$

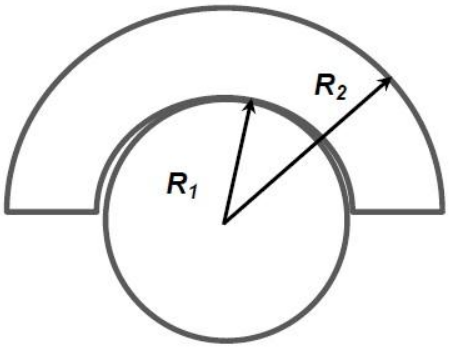

Figure 2.9: Hip joint schematic diagram R_1, is femoral head diameter and R_2 is diameter of head and cup.

The anatomy of a hip is a ball-and-socket configuration where the acetabulum is the socket and the femur head is the ball portion. A slippery tissue, cartilage, covers the ball and socket surface to produce a smooth and low friction movement. The synovial membrane produces synovial fluid which is a natural lubricant designed to continuously lubricate natural human joints. The behaviour of synovial fluid in the presence of artificial parts is markedly different and the wettability and lubricant contact angle of artificial parts with the wear surface significantly affects wear behaviour [37].

During wear, the efficiency of the bearing couples depends on the lubrication regime. The design for the bearing pairs should suit a range of full-fluid film and mixed lubrication regimes during its lifetime. Where there exists enough lubricant between wearing parts to avoid asperity contact the system is in full fluid film lubrication regime. As wear progresses the stress state alters due to changes in the wear environment e.g. the rheology of the

lubricant, consequently the lubricant regime transforms from hydrodynamic to boundary or mixed.

Friction measurements in the reciprocating wear tests determine the lubrication regime by reference to its Sommerfeld Number. Variations in the Sommerfeld Number are usually reported by plotting a Stribeck curve, Figure 2.10. The X- axis of the Stribeck curve is the Sommerfeld number (Z) which is defined as: Velocity (v) X Viscosity of the lubricant (η)/applied load (N) combines the factors which directly influence friction. The chemical reaction of the lubricant with wearing surfaces can dramatically influence the lubricant regime.

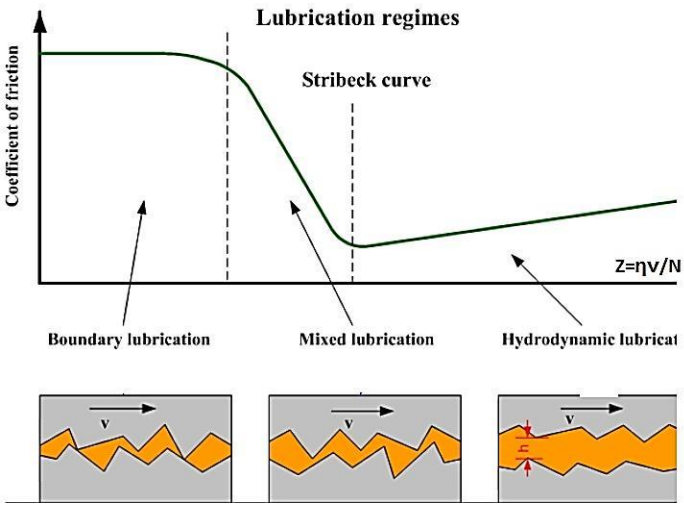

Figure 2.10: Stribeck curve to determine lubricant regime [39]

2.5.4. Zirconia's Wear

The contribution of the tetragonal to monoclinic phase transformation in zirconia to wear resistance remains controversial, with some reports suggesting that it can reduce wear rate, while others suggest it can increase the wear rate [40]. In-vitro experiments of zirconia-on-

alumina wear showed a catastrophically high wear rate for zirconia [41]. The rapid formation of microcracks caused surface fractures leading to severe wear. In the wear of a zirconia ball against UHMWPE cup, severe damage of the acetabulum demonstrates the poor performance of a polymer against high toughness zirconia, compounded by localised wear damage due to the low thermal conductivity of zirconia. In this test high sliding speed could be a main factor for this severe wear. Modification of the UHMWPE surface structure can significantly improve its performance [42], as can doping the zirconia to improve its thermal conductivity [43].

The low thermal conductivity of zirconia is 2.9 W/ m·K, results in substantial frictional heating during sliding, which along with hydrothermal degradation makes zirconia's tribological behaviour more complex and unpredictable than other ceramics.

Recent research on an explanted zirconia femoral head [44] in conjunction with polyethylene cup reports topographical and compositional changes on the zirconia surface, Figure 2.11. In this research the intrinsic coupling of ageing and wear was considered. The mixed effects of temperature and mechanical stresses on these retrieved zirconia heads show monoclinic clusters of up to 20% on the surface of implant as young as 3 years. Figure 2.11a shows a surface of an unused implant with scratches that are likely to have been produced during surface preparation. Deeper scratches on the surface in image 2.11c are a sign of the abrasive wear damage. As is clear in Figure 2.11f, on the 8 year old zirconia head, a self-polishing mechanism occurred which decreased the intensity of the abrasive grooves. VSI imaging indicates reductions in the scratch lines occurred as monoclinic clusters increases. This is in line with those from a simulated ageing experiment reported by Chevalier [6]. From the result it could be understood that the transformed zone penetrates

into the bulk and causes grain pull out. The loose grains then cause further wear damage through abrasive wear mechanisms.

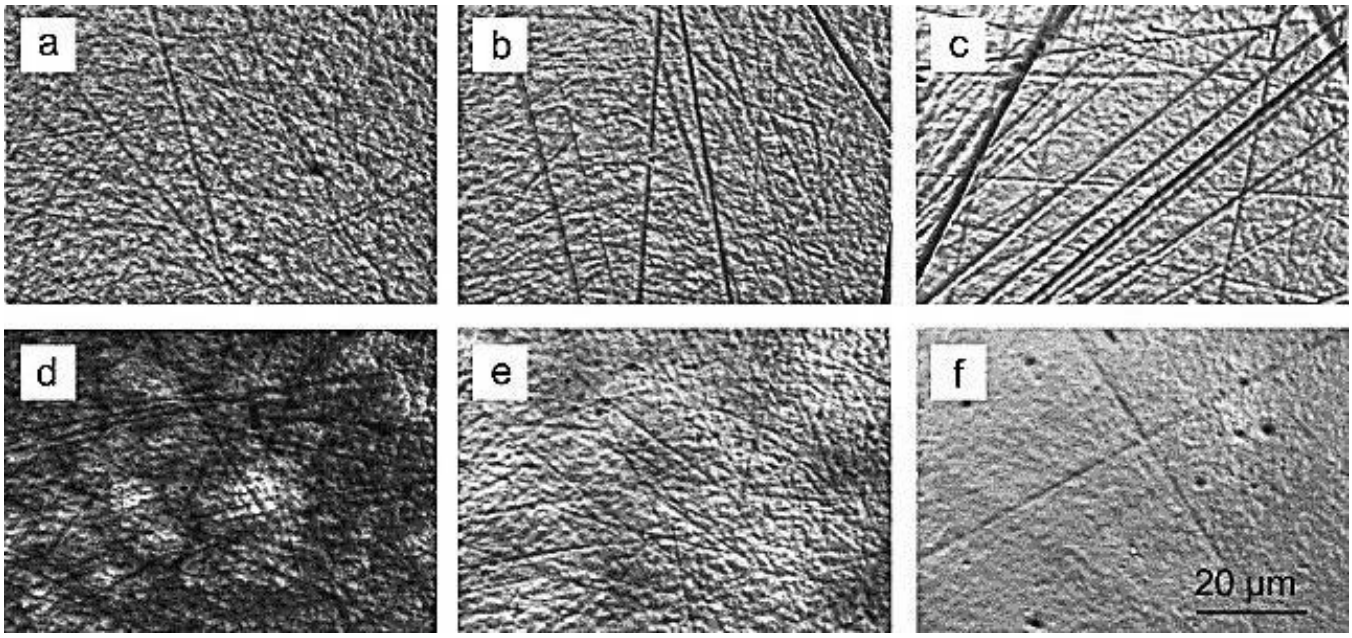

Figure 2.11: Optical imaging of zirconia head worn against polyethylene cup after different implantation periods: (a) unused, (b) 1 year and 6 months, (c) 5 years and 1 month, (d) 9 years and 1 month, (e) 11 years (f) 12 years and 8 months. [44]

The role of the toughening in zirconia's tetragonal phase retention was detailed in Chapter 2. Fischer et al. [45] evidenced that the wear resistance of the Y-TZP depends on its yttria content and considered transformation to be advantageous. They suggested that the dominant mechanism of wear of Y-TZP was plastic deformation. They considered the tetragonal to monoclinic phase transformation to be a critical factor in material removal during wear, and they linked the wear resistance to the fourth power of the toughness, after investigating a wide range of fracture toughness values (11.6, 8.7 and 2.5 $MPa.m^{1/2}$) with a mixed structure of tetragonal and cubic zirconia. Rainforth and Birkby challenged this view, considering transformation to be a wear driven mechanism and that the importance of fracture toughness for zirconia was being over-stated [45].

Lee's wear maps for Y-TZP under dry and lubricated conditions, Figure 2.12, indicate that a sudden increase in wear rate can be attributed to the combined effects of load and the velocity variations [46]. Lee postulated that the rheological properties of a lubricant dramatically influence the onset of wear transition where the coefficient of friction varies between 0.03 and 0.7. He also tested the combined effect of speed and load on the wear rate of self-mated Y-TZP where it was in the range of 10^{-1}-10^{-6} mm^3/m.

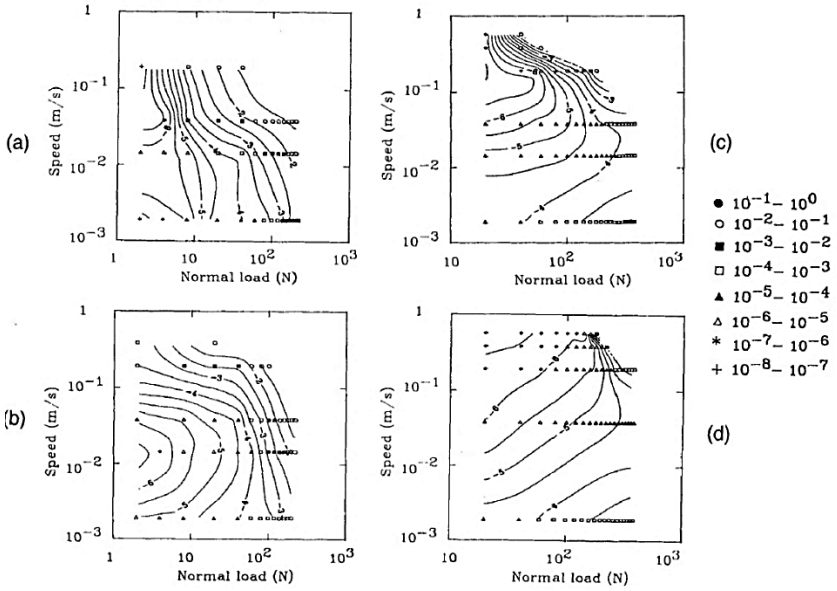

Figure 2.12: Wear contour maps for Y-TZP under various lubrication conditions: (a) in dry air, (b) in water, (c) in paraffin oil and (d) in formulated oil [47].

Lee also introduced a velocity model to describe the speed influence on wear transition, Figure 2.13.

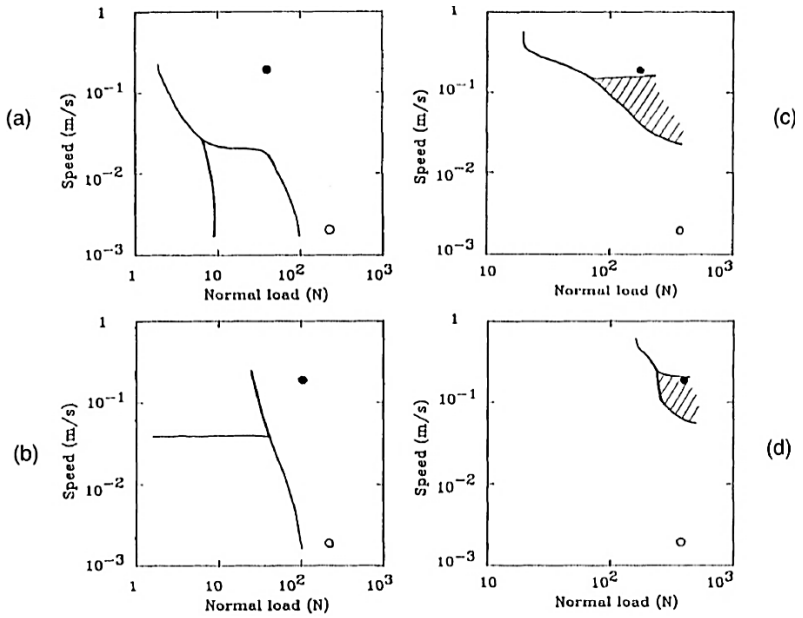

Figure 2.13: Wear transition diagrams for Y-TZP under different lubrication conditions: (a) in dry air, (2) in water, (3) in paraffin oil, and (4) in formulated oil. The solid and hollow circles represent the conditions where SEM observations were taken [47].

A summary of tribological behaviour of Y-TZP in Table 2.7 provides some information about wear of this material. Some researchers believe that the fine microcracks produced during the phase transformation are the main reason for zirconia's high wear rate. Bikby's comparison of 2Y-TZP (K_{1c} about 11 MPa.$m^{1/2}$) and 3Y-TZP (K_{1c} about 7 MPa.$m^{1/2}$) support the view that phase transformation is the main reasons for zirconia's high wear rate because he observed a higher wear rate in the former compound than the latter. He considers transformation to be the dominant wear mechanism and that his results evidence that transformation has a catastrophic influence on the wear transition in zirconia [45].

Water lubrication is regularly used in wear test experiments to decrease wear rate by reducing frictional heating, and to reducing contact stress by creating a full fluid film lubrication regime. However, hydrothermal degradation of zirconia in the presence of water complicates the use of water lubrication and there are conflicting reports of its benefits/detriments.

Barceinas-Sanches and Rainforth studied the wear rate of 3Y-TZP wear against Mg-TZP in both dry and wet wear environments. They measured $6.8x10^{-4}$ and $2.2x10^{-4}$ mm^3/Nm wear rate in water and dry conditions respectively. They did not detect any wear resistance improvement in the water worn specimens or any reduction in frictional heating despite using water. This behaviour was attributed to the hydrophilic nature of a zirconia surface [49].

Rainforth [52] in his research of Y-TZP wear against a ZTA ball concluded that zirconia's low thermal conductivity was the main cause of severe wear damage. He estimated that surface flash temperatures of 800 °C occurred due to the asperity contact. Phase transformation of zirconia occurs at a much lower temperature than this.

In contrast, Rainforth and Stevens observed quite a different mechanism for the sliding of Mg-PSZ in water against steel. The presence of grain relief on the surface suggested tribochemical wear. They found that preferential wear was influenced by the crystal orientation. From TEM analysis of Mg-PSZ material [52], they identified that a severe wear zone was created due to coalescence of the microcracks along a band with tetragonal precipitates with a certain orientation. These microcracks were already formed due to the phase transformation. Stevens and Rainforth detected microstructural changes due to the mechanical stresses from wear well below the surface. They concluded that the frictional temperature on the surface was too high to trigger the phase transformation process [50].

Unlubricated wear of self - mated TZP studies by Stachowiak et al. [53] recorded surface temperature rises and its destructive effect on both strength and toughness. They also reported a coefficient of friction of around 0.5-0.6 which is high for zirconia. The abrasive

grooving caused further wear of their TZP surface. The intensity and depth of these grooves varied with temperature.

Khanna and Basu found that the wear rate of zirconia decreased with environmental humidity. They reported detection of the plastic deformation as the wear mechanism with surface delamination under both lubricated and non-lubricated conditions. They detected zirconium and yttrium hydroxide inside the wear debris, which it was believed formed a tribofilm layer improving wear resistance [51].

The characteristic wear morphology of a zirconia surface is that of a delaminated surface where accumulated wear debris is located in above the original surface. This detachment of surface material and its smearing over the surface increases the thermal gradient which causes increased wear. Some studies show that the addition of a solid lubricant to the surface of the ceramic produces a self-lubricated condition for zirconia by improving its thermal conductivity [47].

Table 2.7: Tribological properties of Y-TZP in different environments [48].

Material	Configuration	environment	Speed (mm/s)	Load(N)	COF	Wear rate (mm^3/Nm)	Ref
3Y-TZP	Pin-on-disk	Water	1	9.8	0.6	0.15	Fischer
3Y-TZP	Pin-on-disk	Hexadecane	1	9.8	0.11	0.03	Fischer
3Y-TZP	Ball-on-disk	Paraffin oil	1-570	40-200	0.03-0.57	$0.1\text{-}10^{-4}$	Lee
3Y-TZP	Pin-on-disk	Water	240	10	0.62-0.67	230	Rainforth
3Y-TZP	Pin-on-plate	Air	60-90	65	0.68	2.3	He

2.5.5. Tribofilm Creation

The formation of a tribolayer which has been widely observed on zirconia surfaces is due to a tribochemical wear mechanism involving interaction between the surface and its environment. The same tribolayer formation also occurs in alumina ceramics. Barceinas-Sanchez and Rainforth consider tribochemical wear to be the main wear mechanism in ceramics in the mild wear zone. Further investigation of the protein reaction at the surface of implants is needed, but the in-vitro experiments in bovine serum demonstrate significant chemical changes in both the bovine serum and the zirconia surface after wear.

In general the environmental effects on the wear behaviour of zirconia can be occurred in several steps:

- Formation of an absorbed layer on the surface under tribochemical and tribomechanical activities.
- Modification of the surface properties and surface stress state by the absorbed layer.

Ma [30], in her TEM study of ZTA-on-alumina pairs, detected an amorphous layer containing nanocrystalline wear debris. EEELs observation of the tribolayer detected traces of Na as well as the presence of both surface and lubricant components, indicating reaction with the bovine serum. By contrast, Rainforth et al. reported an amorphous structure to the tribolayer of his alumina wear, leading him to conclude that surface hydration was the primary process [54].

Fischer in his study on alumina tribolayer detected rolling wear debris throughout the layer, from which he concluded that the tribolayer aided wear resistance by acting as if it was a lubricant [55].

Kalin *et al*. [56] and Novak *et al.* [57] in their observation on alumina tribological behaviour showed that in acidic and alkaline aqueous environment no alumina tribolayer appeared. They attributed the high wear rate in alumina to the dissolution of alumina.

2.5.6. Effect of the Counterface

A range of socket materials can be used in conjunction with a zirconia ball in a hip implant. In vitro studies of unlubricated Al_2O_3, SiC, Si_3N_4 and ZrO_2 found the highest wear rate occurred with Al_2O_3 and ZrO_2 counterfaces [58]. Ionic materials sliding over each other are believed to form an adherent film form that has not been observed in the wear of covalently bonded ceramics. In most of the combinations of these materials then transfer of materials in both directions was observed, but in the zirconia/alumina counterface then zirconia transferred to alumina but not vice versa.

2.5.7. Abrasive Wear Mechanisms

Abrasive wear damage occurs by two different mechanisms, as shown by the schematic images in Figure 2.14 and 2.15 [59]. In two body abrasion, the abrasive is part of the counterface, and material removal occurs by the machining action of the abrasive. In contrast, third body abrasion mechanism occurs when the wear particles move freely between the two surfaces and they do not bond to any surfaces. Abrasive particle geometry, size and hardness has a critical role in abrasive wear damage in ceramics.

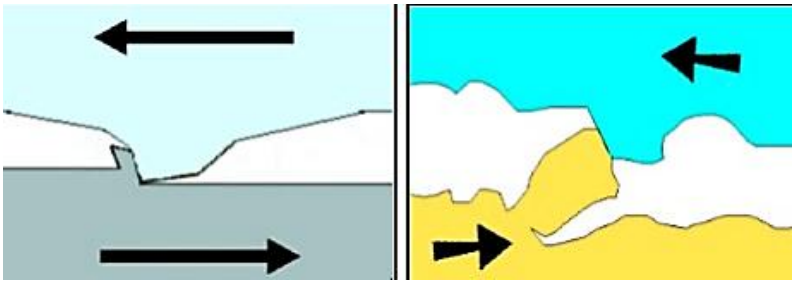

Figure 2.14: Schematic image of second body abrasion

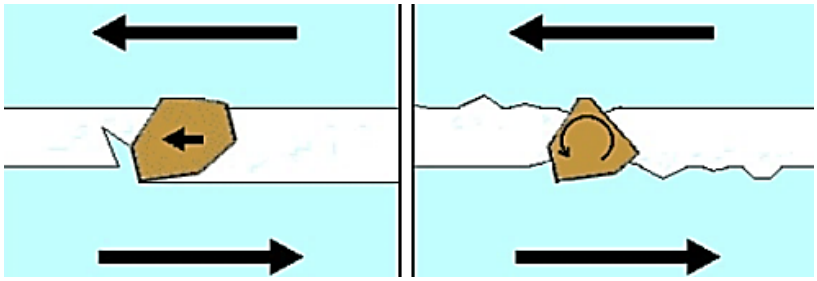

Figure 2.15: Schematic image of third body abrasion

3. Experimental Procedure

3.1. Powder Processing and Specimen Sintering

The current research was focused on the hydrothermal degradation behaviour and reciprocating sliding wear mechanisms in Y-TZP ceramics with and without dopant additions. Partially stabilized zirconia powder with uniform dispersion of 3 mol % Yttria (TZ-3YB, Tosoh Corporation) and <0.034% impurities was selected as a base material. A summary of the composition is given in Table 3.1. The low level of impurities was important to enable investigation of the effects of ternary additions. The selected supplier was able to guarantee this low level, making their zirconia powder the purest commercially available, and their processing method creates a very fine powder with improved strength, high fracture toughness, and resistance to wear and ageing compared to other suppliers.

Table 3.1: Tosoh powder specification provided by vendor [66]

powder	wt%Y_2O_3	wt%HfO_2	wt%Al_2O_3	wt%SiO_2	wt%Fe_20_3	wt%Na_2O
Tosoh TZ3YB	4.95	~2	~0.005	0.006	<0.002	0.028

High purity Al_2O_3 (AKP50, Sumitomo Chemical Co., Japan) and La_2O_3 (Sigma Aldrich) were added to the base powder as ternary and quaternary oxides to aid the hydrothermal degradation resistance.

Equal-sized disk-like specimens with surface roughness, r_a, less than 3 nm were prepared for degradation and wear testing as follows:

- 50 g batches of TZ-3YB, TZ-3YB + 0.1 wt % Al_2O_3 and TZ-3YB +0.1 wt. % (Al_2O_3 +La_2O_3) were weighed separately. These composites hereafter will be called Z, AZ and LAZ

respectively. Each batch was added to 120 ml methanol and 1 kg 3Y-TZP zirconia balls (2 mm ball dimension).They were attrition milled in a Teflon lined jar at 350 rpm for 3.5 hours to produce homogenous slurries. After that the milling media was separated from the slurries.

- To avoid any contamination the slurry containers were covered while drying at 80 °C for 24 h inside an oven.
- The dried product was crushed by agate mortar and pestle and was sieved out through a 355 µm stainless steel mesh to obtain a fine homogenous powder.
- 2 cm diameter pellets were formed by uniaxial (20 MPa) and cold isostatic (200 MPa) pressing from the resulting powder.
- The compacted powders were sintered for 3 hours at 1450 °C at a heating rate of 2 °C/min and a cooling rate of 3°C/min inside a clean furnace in an air environment.

It was essential to achieve an extremely uniform flat and defect-free surface for both the high temperature degradation and reciprocating sliding wear tests. Any residual strains on the surface would act as nucleation sites for the monoclinic phase. To achieve this surface then hot resin was used to attach the sintered sample to a metal stub. The sample was ground manually with SiC papers starting with the coarsest (120 grit), and then progressing through 240, 400, 800 and finally 1200 to create a planar scratch free surface. The polishing stage was carried out in an automatic machine (Buhler USA, water lubricant, 150 rpm) using first a diamond grinding disc (APEX DGD 45 µm, Buhler USA) and then a diamond particle embedded grit disk (Cameo Disk Platinum 3-Yellow and 4-Red, Leco, France). At each grinding/polishing stage the surface quality was checked using an optical microscope. The polished samples were deep cleaned in an ultrasonic bath for 5 minutes in isopropanol. The

clean samples were thermally etched at 1400 °C for 5 min at a heating and cooling rate of 5°/min in order to reveal the grain boundaries and remove any residual stresses.

3.2. Sample Characterization

3.2.1. Density Measurement

The Archimedes water immersion method was used to measure the density of thermal etched specimens, by applying equation (3.1) [60].

$$\rho = \frac{m_{air} - m_{water}}{m_{air*} m_{water}} \qquad (3.1)$$

In this equation m_{air} is the mass of the pellets measured in air and m_{water} is the mass of the pellets measured in the water. The average measured density for the specimens was 6.1 g/cm³, similar to those values reported in the literature.

3.2.2. Grain Size Measurement

The average grain size of the thermal etched samples was estimated by the conventional linear intercept method of SEM image at x10000 magnifications, by applying equation 3.2[61].

$$\frac{S(\overline{L})}{L} = \frac{S(\overline{N})}{N_L} \qquad (3.2)$$

In this equation N_L is the number of grains, $(\overline{L})$ is mean linear intercept grain size and N is total number of grains. Around 3000 grains were counted for each material to obtain an accurate value for the grain size.

3.2.3. Hardness and Fracture Toughness Measurement

The fracture toughness and hardness of the materials were measured using the Vickers hardness indentation technique. For this purpose a 10 kg load was applied on the thermal

etched surface. 15 dents were performed on each surface sufficiently well separated to avoid interconnection of the created cracks. The length of the Palmqvist cracks (l) and indentation half diagonal (a) were measured by optical microscopy (Leica Polyvar) immediately after indentation in order to minimise any errors associated with slow crack propagation. In order to enable comparison with previous work in this area then Equation 3.3 was selected from the range of available fracture toughness (K_{IC}) models [62].

$$K_{IC} = 0.0319P/(al^{\frac{1}{2}}) \qquad (3.3)$$

3.3. Hydrothermal Degradation Test

Hydrothermal degradation was simulated by placing specimens in 2 ml of distilled water within a conventional sealed Teflon lined general purpose vessel (Parr Instruments Co., USA), Figure 3.1. The vessel was heated at a rate of 3 °C/min to 134 °C and held at that temperature for periods of 6 , 12 and 24 hours then cooled down to room temperature. The extent of degradation was examined using different microscopy techniques.

Fig 3.1: Sealed Teflon lined general-purpose vessel

3.4. Characterization of the Degraded Material

3.4.1. XRD Phase Determination

Original Tosoh powder and disk samples after thermal etching were characterised by X-ray diffraction prior to degradation.

The condition of the as-received Y-TZP powder was analysed by X-ray diffraction (Siemens D500 diffractometer, CuKα radiation with 0.02° step size, 0.2°/min) at 2theta angles 27-33 °. Two monoclinic phases and one tetragonal peak at $(-111)_m$, $(111)_m$ and $(101)_t$ respectively were identified.

The intensity ratio of the monoclinic phase was calculated using the method proposed by Garvie and Nicholson [63]:

$$X_m=\frac{I(-1\,1\,1)_{m+}I(1\,1\,1)_m}{I(-1\,1\,1)_{m+}I(1\,1\,1)_{m+}I(1\,0\,1)_t} \qquad (3.4)$$

In this equation, $I_{m(hkl)}$ is the integrated intensity of the monoclinic peaks and $I_{t(hkl)}$ corresponds to the tetragonal phase. The volume fraction was calculated using Toraya et al.'s model (Equation 3.5) [64]:

$$V_m=\frac{0.311Xm}{1+1.311Xm} \qquad (3.5)$$

Where V_m is the volume fraction of the monoclinic phase and X_m is the intensity ratio of that phase.

3.4.2. Optical Microscopy

Lattice volume expansion caused by monoclinic to tetragonal phase transformation can be detected by optical microscopy. For this purpose, a Veeco Instruments Contour GT 3D

interferometer was used to visualize the regions containing monoclinic spots after propanol cleaning of the samples.

3.4.3. Atomic Force Microscopy

Atomic force microscopy (AFM) is an effective technique for detecting the onset of transformation. AFM was performed on a Veeco NanoscopeIIIa (Digital Instrument, USA) using a silicon nitride probe in contact mode. Samples tested ranged from those with the original surface through to the most degraded. The acquired images were scanned at a rate of 0.5 Hz with a resolution of 256 samples per line.

3.4.4. Scanning Electron Microscopy

Since the ageing process in zirconia initiates at the surface and penetrates into the bulk the depth of the transformation zone and its microstructure were analysed using scanning electron microscopy, SEM, (Inspect F, FEI Company) on cross sectional samples which had been mounted in resin before grinding, polishing and gold coating.

3.4.5. Raman Spectroscopy

A Raman Spectrometer (LabRam HR, Joriba Jobin Yvon, France) with a 532 nm line of a He-Ne laser was used to obtain the Raman spectrum of aged specimens. Spectra were recorded from 100-900 cm^{-1} on accumulation of 5 seconds per point. Point analysis and surface mapping were both used, and the latter was found to be a more useful technique to study transformation. The monoclinic phase is characteristically double peaked as shown in Fig. 3.2 [66].

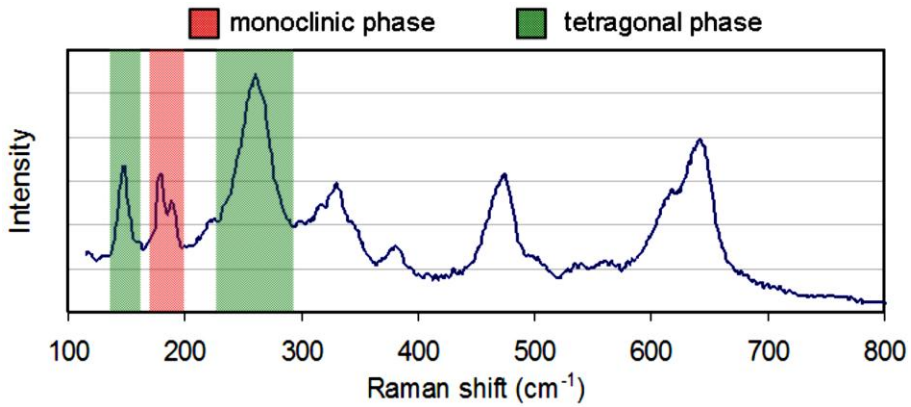

Figure 3.2: Typical Raman spectra of a 3Y-TZP specimen containing a mixture of monoclinic and tetragonal phases [65].

3.5. Reciprocating Wear Test

Since wear is a system property rather than a material one then wear behaviour is difficult to monitore and measure, particularly for in-vitro tests where access to the simulated condition of the body is restricted. In the current study then reciprocating sliding wear tests were performed on a ball-on-flat (alumina-on-zirconia) lubricated configuration using a UMT tribometer (Centre for Tribology, Inc, USA), (Fig 3.3). In a ball–on-flat configuration the lower specimen slides back and forth against an upper specimen tightly held in a holder with a gap of up to 15 cm in the machine used. In the current study the upper surface was an ultra-pure alumina ball (Oakwade Ltd, UK) with 4 mm diameter and roughness about 5-8 nm. The lower liquid chamber contained a metal stub on which the disk sample was secured and had sufficient capacity to also accommodate the lubricant. For these work two kinds of lubricant, ultra-pure water and 25 vol% new-born calf serum solutions were chosen. Lower specimen speed was controlled in the range 0.001 rpm to 5000 rpm by a spindle load control was applied through an ultra-accurate strain-gauge sensor with 0.00003% resolution.

All tests were conducted at 10 Hz (0.02 m/s) and a 10mm stroke length for 24h. Surface loads of 0.5 N, 1 N, 2 N, and 4 N, generating pressures of up to 24MPa were used to simulate the rim-contact stress range of ceramic-on-ceramic hip joint articulation which results in mild to severe wear of the zirconia. Initial Hertzian contact pressure for this reciprocating sliding contact is in the range 2.4-7.1MPa, but rapidly reduced as the surfaces became more conformal [55]. The vertical motion controller was paired with a normal load sensor to confirm the consistency of the applied load. A stroke length of 10mm was selected in order to enable comparison with previously reported results. UMT software recorded real time data on F_X, Fz, W_R, Z, T, F_f and coefficient of friction (COF. In total 17278 individual COF

values were computed from the 24hr duration tests and the total distance travelled by the lower specimen was 17.28 Km. The accuracy of 0.05 µm was performed by for wear measurements.

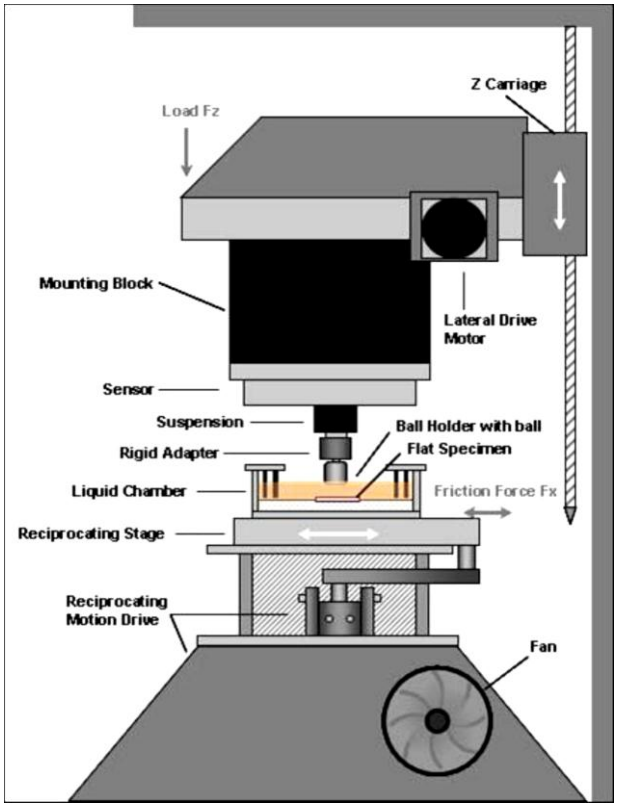

Fig 3.3: The UMT tribometer[66]

3.5.1. Lubricants

Ultra-pure water, HPLC Gradient grade, supplied by Fisher Scientific, UK, with viscosity of 0.001 Pa·s was the first lubricant used in this study. Referring to the ISO 6474 [67] water has been used for studying tribological behaviour in most of the researches with destructive and constructive effects on zirconia's wear performance. The second used lubricant was 25 vol% bovine serum solutions. Bovine serum is a natural protein concentration commonly used as a substitute for synovial fluid in tribological studies, 25 vol% bovine serums were obtained

by diluting the sterile new-born calf serum supplied by First Link (UK) Ltd with phosphate buffered saline (PBS). The PBS was made by dissolving one (1814.5 - 2005.5 mg/tab) Phosphate Buffered Saline tablet (Sigma-Aldrich, UK) in 200ml of ultra-pure water (Fisher Scientific, UK). 0.1 wt% sodium Azide (Fisher Scientific, UK) was added as anti-bacterial agent. This lubricant solution of 25vol% bovine serum had a viscosity of 0.0012 Pa·s.

3.5.2. Lubricant Regime Definition

The lubricant regime of each sample was identified using a Stribeck Curve in which Sommerfeld Number is plotted against COF. The Sommerfeld number, equation (3.6) [68], is applied to study the wear performance of two rubbing surfaces in dynamic state, in the presence of a lubricant and relates speed (V), viscosity (η) and load (N).

$$Z = \frac{\eta V}{N} \qquad (3.6)$$

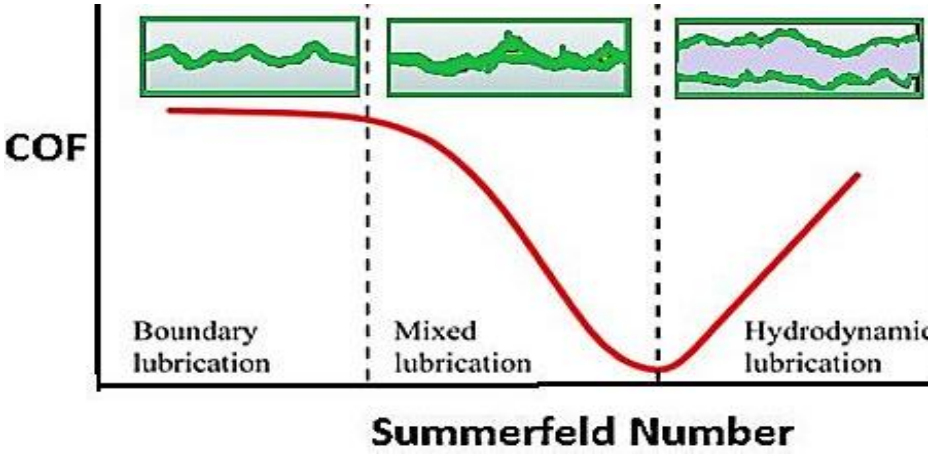

Fig 3.4: Stribeck curve and lubricant regime

3.5.3. Wear Rate

The specific wear rate (k) for each lubricant used to analyse the lubricant effect on the wear rate of each sample in the 24h reciprocation sliding test was calculated using Archard theory

(Equation (3.7)). This equation is commonly used to estimate the specific wear rate of homogeneous materials. In this equation S is the total sliding distance after 24 hours reciprocation, V is the volume loss of the material after wear and N represents the applied load:

$k=V/NS$ (mm³/Nm) (3.7)

To calculate the volume loss of the material after wear, the average area lost, A, was measured by a profilometer, Dektak 150(Veeco instrument, US) across the 10 mm wear scar length and on 15 different locations of the surface. The average of these values was used for calculating the wear rate.

3.6. Wear Scar Analysis

Different kinds of microscopes such as counter GT optical microscope, Atomic force microscope, Raman spectroscopy, scanning electron microscope, and focused ion beam microscope and transmission electron microscope were used to characterise the worn surface.

3.6.1. Profilometer

The cross-sectional profile of the wear tracks was measured by using a surface profilometer, Dektak 150 (Veeco Instruments, US). The Profilometer is a straightforward contact quantitative measuring technique. Due to the hard nature of the surface the stylus load was set as 3 *mg* and scan length was varied in different wear regions in accordance with wear scar width. The scan durations were set to 50 s Hills & Valleys profile type. Levelling up the acquired graph gave the lost area of the worn scar.

To achieve the extremely clean surface needed for area measurement to apply this technique samples were cleaned prior to measurement in ultra-sonic bath for 15 minutes and then they dried by spray air.

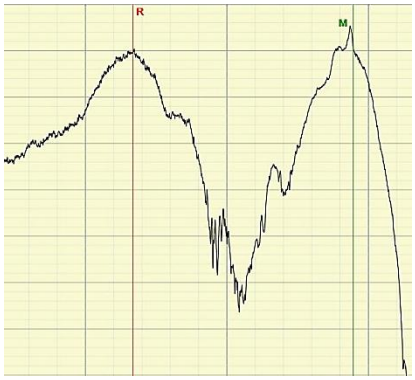

Figure 3.5: Volume lost was measured by tribometer of AZ surface worn under 4N load in water after 24 hours sliding with 0.02 m/s speed.

3.6.2. 3D Optical Microscopy-VSI Imaging

To visualize the wear scar features throughout the wear track and the accumulated wear at the tail of the wear scar the vertical scanning interferometer (VSI) in Mirau assembly with white light illumination (Contour GT, Veeco Instruments Inc., USA) was employed.

3.6.3. Atomic Force Microscopy

A Dimension™ 3100 scanning probe microscope (Veeco Instruments, US) was operated in general contact and lateral mode to study topography of the worn surface.

3.6.4 Scanning Electron Microscopy

Roughness variability and plastic deformation on the worn surface was determined using a field emission gun scanning electron microscope (Inspect F, FEI Company). Samples were cleaned in ultra-sonic bath and they were dried by compressed air before gold coating. The microscope was operated at an acceleration voltage of 10 keV. The bovine serum worn

specimens needed thicker layer of gold coating plus a carbon depositing on top of the gold coat to minimise the electron beam causing protein contamination on the surface during focusing.

3.6.5. Focused Ion Beam Microscopy

Focused ion beam microscopy (Quanta 200 3D FIB/SEM, FEI, Netherlands) was employed to prepare TEM samples of the worn surface where mechanical thinning was not practical on the worn surface. AZ specimen worn under 4N load in both lubricants was the subject for near surface microstructure investigation. In this technique a focused beam of accelerated gallium ions milled the material from a selected region at a rate controlled beam current to achieve a transparent TEM specimen.

In this test the specimen's surface first was gold coated. This coat with around 50 nm thickness was created a dark contrast layer on surface to label the original surface during TEM observation. On top of the gold coat a thicker carbon coat was deposited to protect the real surface from gallium ion beam damage. After specimen was inserted inside the SEM chamber it was tilted to 52 ° to become perpendicular to the radiated ion beam. In this stage a carbon layer with 15x2x1 μm^3 dimensions was deposited on the area of interest on the surface to protect that from ion implantation and surface erosion during milling. In the tilted position, on both opposite sides of the deposited strap two trenches were milled sequentially starting from 5.0 nA and finishing at 1.0 nA. The created thin foil with less than 500 nm thickness was cut out at 7 °.Then the sample was lifted out with a microprobe(Omni probe, US) and it was attached *in situ* to a copper grid. Final ion polishing was carried out with 50 pA beam current until reaching a thickness less than 100nm of the foil.

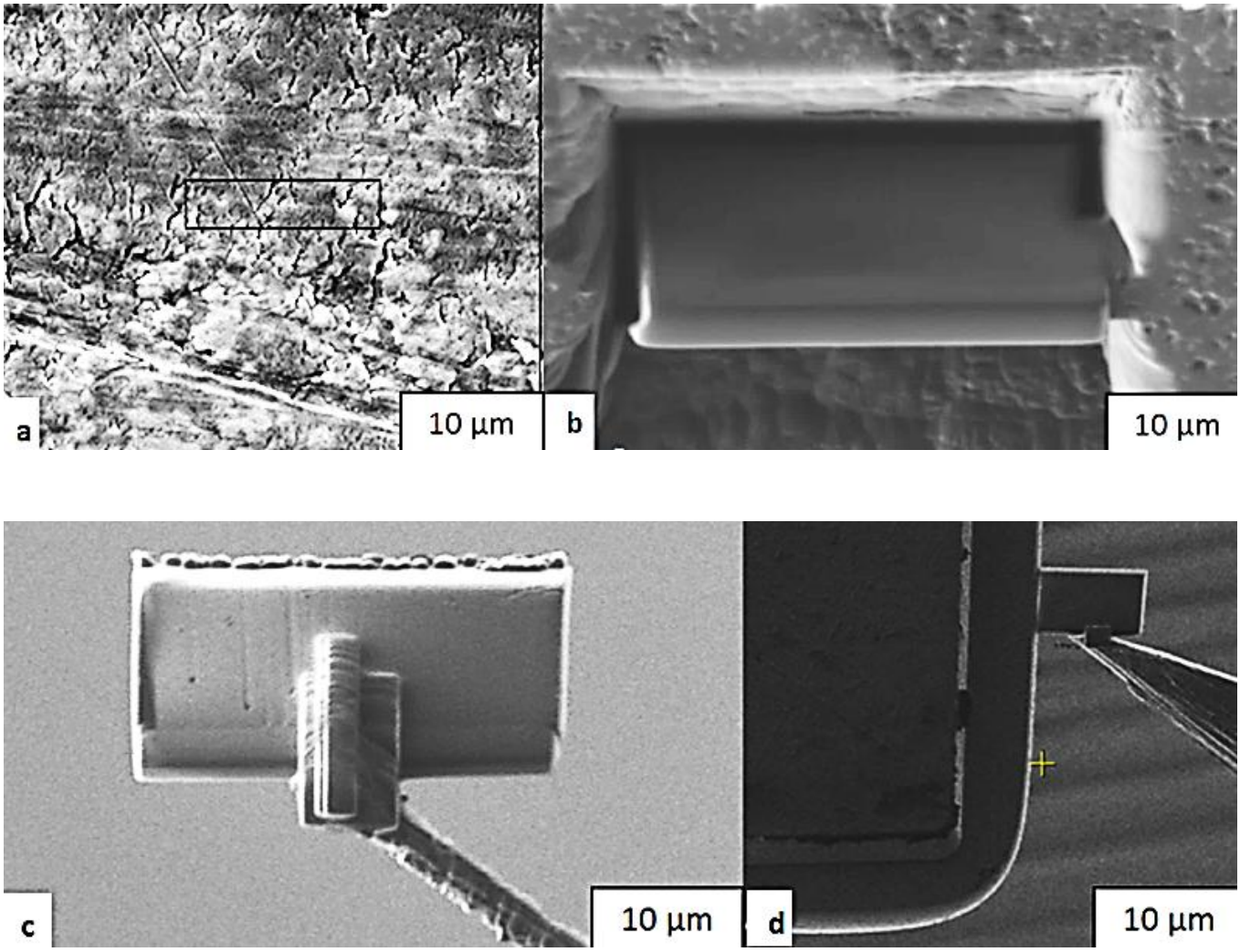

Fig 3.6: Electron (a) and ion beam images of the preparation stage of a FIB-machined: a) point (b) milling and cut out of the foil, (c) sample lift out with microprobe, (d) sample attachment on TEM holder.

4. Results

4.1. XRD of Tosoh Powder

X- ray diffraction of the base 3 mol% Y-TZP Tosoh powder showed a mixture of tetragonal and monoclinic phases at 27°-33° 2θ. The main tetragonal peak $(101)_t$ appeared at about 30.1° 2 θ , and two monoclinic peaks $(-1\ 1\ 1)_m$ and $(1\ 1\ 1)_m$ were detected at 28° and 31.2° 2 θ respectively. It was found that the powder contained 13% monoclinic phase with the balance being tetragonal zirconia.

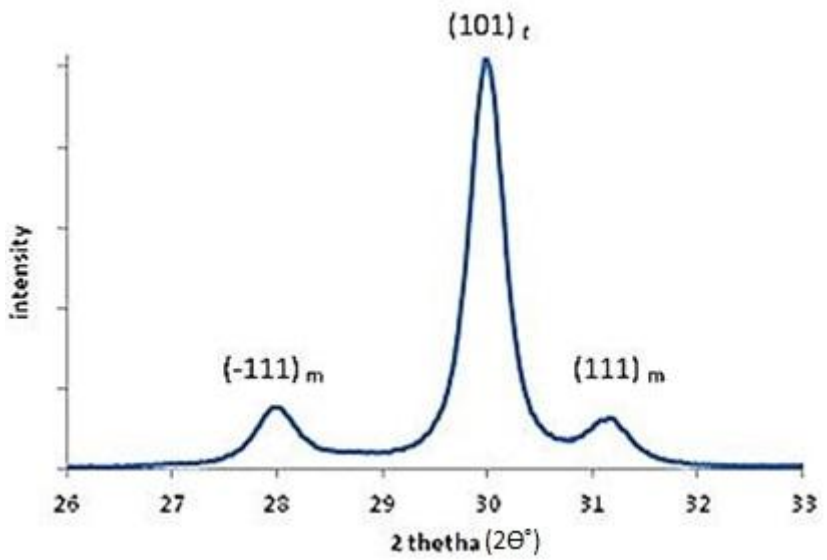

Fig 4.1: X-ray diffraction of as-received Tosoh powder

4.2. Sintered Material Characterization

4.2.1. Mechanical Property and Grain Size Measurement

Table 4.1 gives the grain size, density, Vickers hardness and fracture toughness of the thermal etched pellets. The sintered material's density was measured at about 6.1 g/cm³, which is 99.7% of the theoretical density reported in the literature.

Table 4.1: Mechanical properties of sintered material

Material	Grain size (nm)	Density (gr/cm³) [std dev]	Vickers hardness(GPa) [std dev]	Fracture toughness (MPa.m½) [std dev]
Z	289±8	6.09 [0.01]	12.3 [0.10]	5.62 [0.03]
AZ	302±4	6.10 [0.02]	12.4 [0.17]	5.70 [0.09]
LAZ	268±2	6.09 [0.01]	12.7 [0.27]	5.63 [0.13]

Intercept calculation of the grain size in the SEM images showed values of 260-310 nm grain size distribution with an average of 286 nm. The thermal etched schedule was set for 5 minutes at 1350 °C with a heating and cooling rate of 5°/min. Typical equiaxed grain structure was found in all three composites, Figure 4.2. Grain size distribution does not appear to have been significantly affected by dopant additions, although the LAZ had the smallest grain size of all.

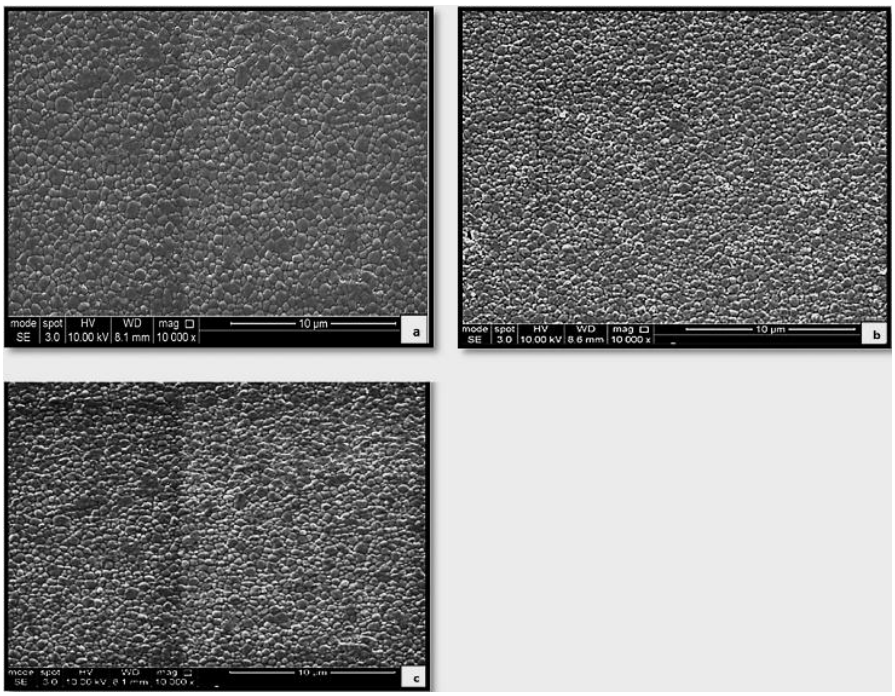

Fig 4.2: Secondary electron SEM images of (a) Z, (b) AZ and (c) LAZ.

Atomic force microscopy was undertaken on the thermal etched samples prior to the degradation tests to check that the starting surface roughness (Ra) was <3nm. A typical AFM image in Figure 4.3 shows homogenous distribution of grains without any abnormal grain growth within the scanned area of the specimens.

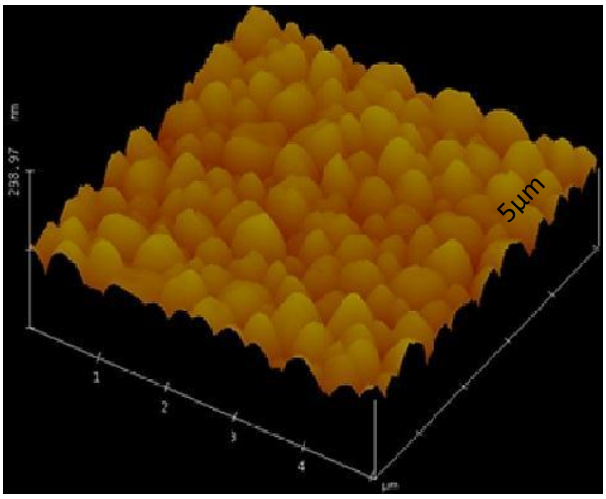

Fig 4.3: AFM image of TZP sample.

4.2.2. XRD Phase Determination

The X-ray diffraction of thermal etched specimens at 27°-33° 2θ did not show any evidence of monoclinic phase on the surface, Figure 4.4. The single tetragonal peak appeared at 30.28° in all the specimens.

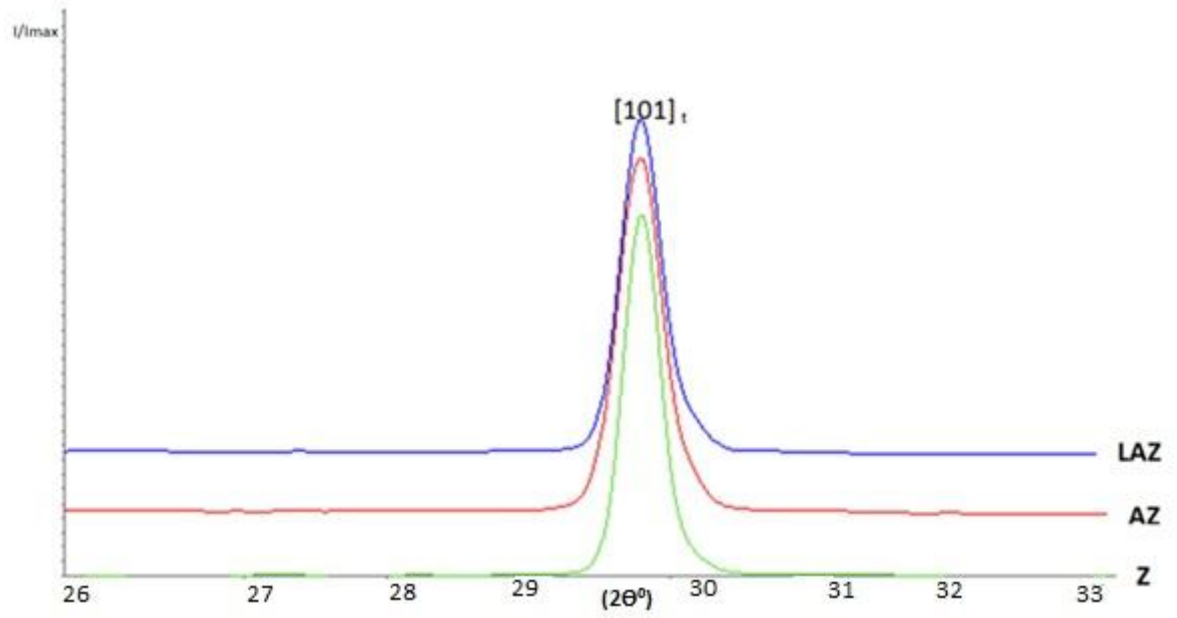

Fig 4.4: XRD of sintered specimens

4.3. Degraded Sample Characterization

4.3.1. Optical Microscopy (OM)

The surfaces of aged specimens were examined with a polyvar optical microscope with Nomarski contrast at 200 x magnification and also using the vertical inferometry imaging method (VSI). The volume increase during tetragonal to monoclinic phase transformation produces monoclinic clusters which are clearly visible in the optical microscope. Figures 4.5, 4.6 and 4.7 give VSI images from the surface showing the monoclinic protuberances for different samples with various growth rates. The radius of monoclinic protuberances was larger in Z sample than AZ and LAZ samples with average radii of 13.3 µm, 13 µm and 1.7 µm respectively. The Z specimens show the highest population intensity of monoclinic clusters with 41 clusters compared to less than one in the equivalent AZ surface area. LAZ monoclinic nucleation did not form in conical protuberances, Figure 4.7. In this image the monoclinic protuberance represents the smallest radius with lowest grain height compared

with other samples. The presence of scratches on the surface resulted in a greater localised transformation to monoclinic zirconia, even though the sample had been thermally etched for stress relief so any residual monoclinic would have been expected to transform back to monoclinic zirconia. While any surface defect such as scratches is a stress point for monoclinic nucleation, Figure 4.6 demonstrates that the monoclinic was nucleated all the way along the scratch line on the aged surface. Figure 4.8 shows how monoclinic clusters covered almost the entire surface of the Z sample after an exposure time of 48h at 134 °C.

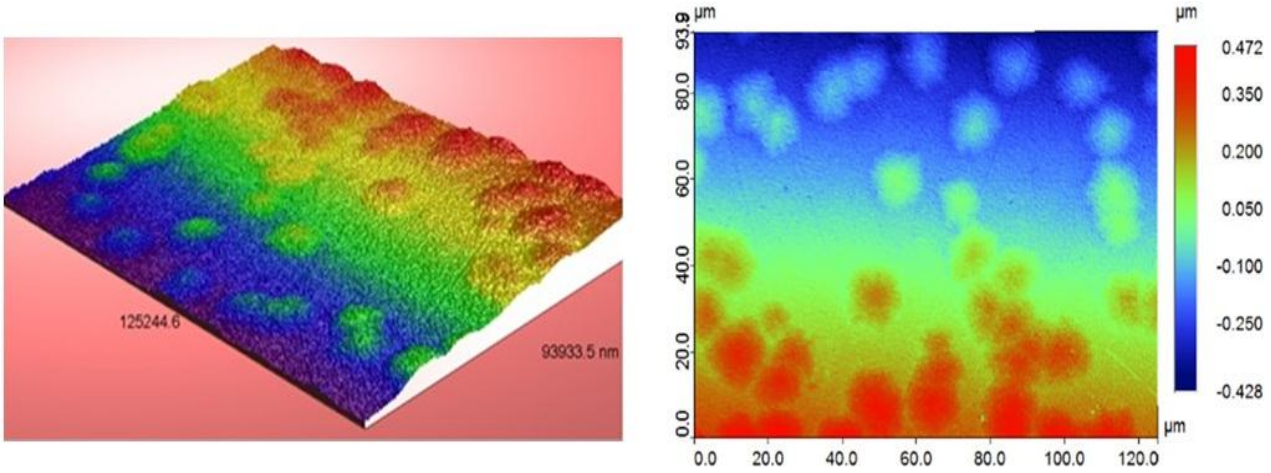

Fig 4.5: VSI image of Z specimen aged for 24hours at 134 °C

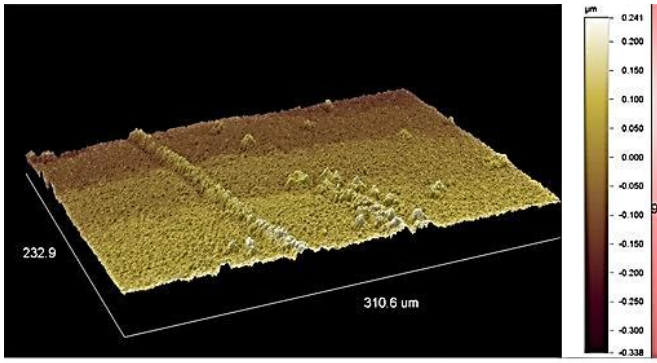

Fig 4.6: VSI image of AZ sample aged for 24 hours

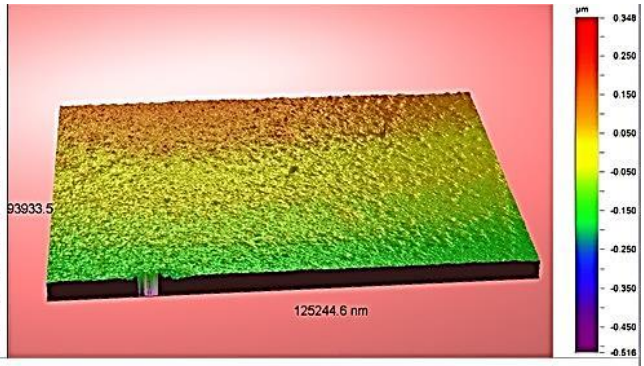

Fig 4.7: VSI image of LAZ specimen aged for 24 hours at 134°

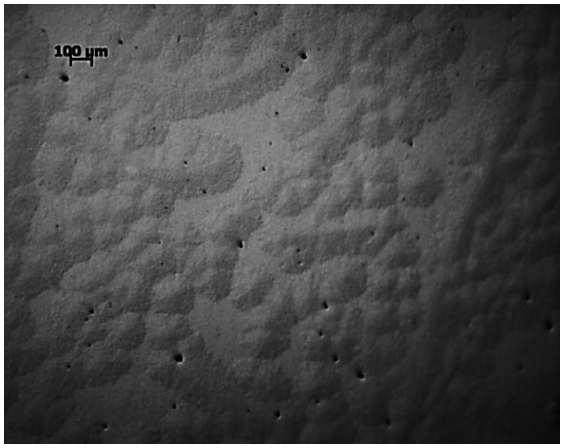

Fig 4.8: Optical image of Z sample aged for 48 hours at 134°

4.3.2. X- Ray Diffraction

After thermal degradation of specimens phase constitution was observed by X-ray diffraction. Figures 4.9 and 4.10 show that there was no sign of monoclinic phase formation at 6 and 12 hours ageing process. Figure 4.11 indicates the presence of the monoclinic phase more clearly at $(-111)_m$ reflection than at $(111)_m$ reflection and tetragonal phase retention in all specimens after 24h exposure at 134 °C.

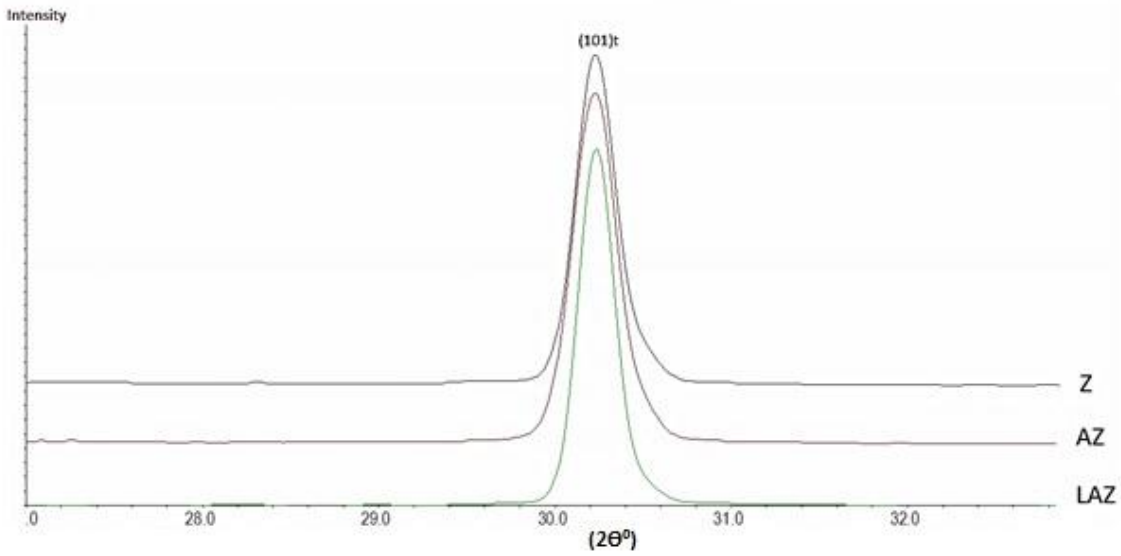

Fig 4.9: Degraded specimens at 134 °C for 6h.

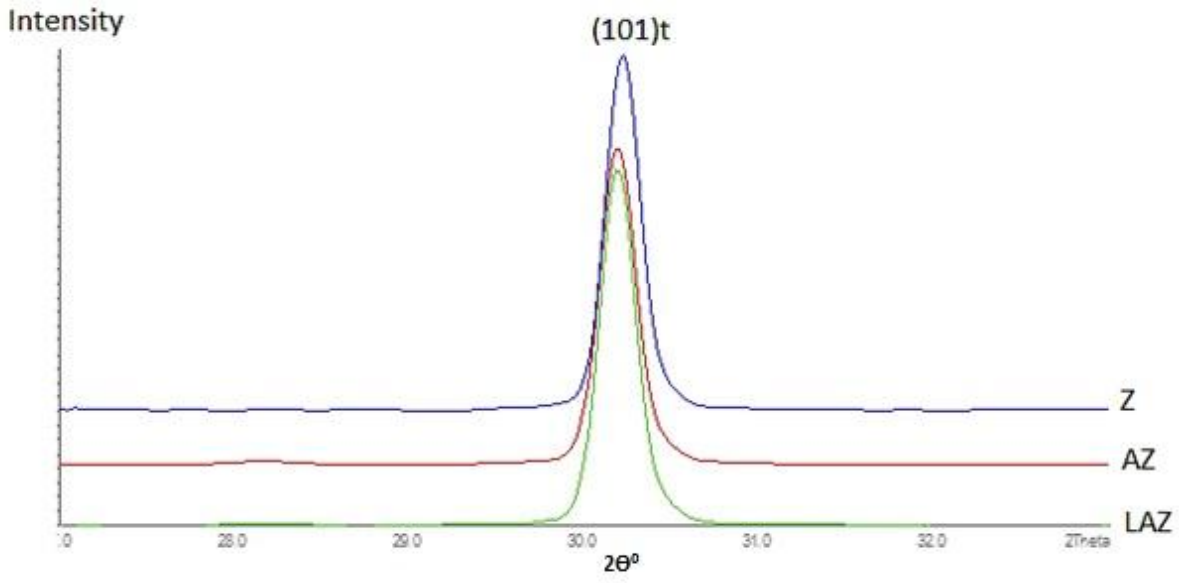

Fig 4.10: Degraded specimens at 134 °C for 12h.

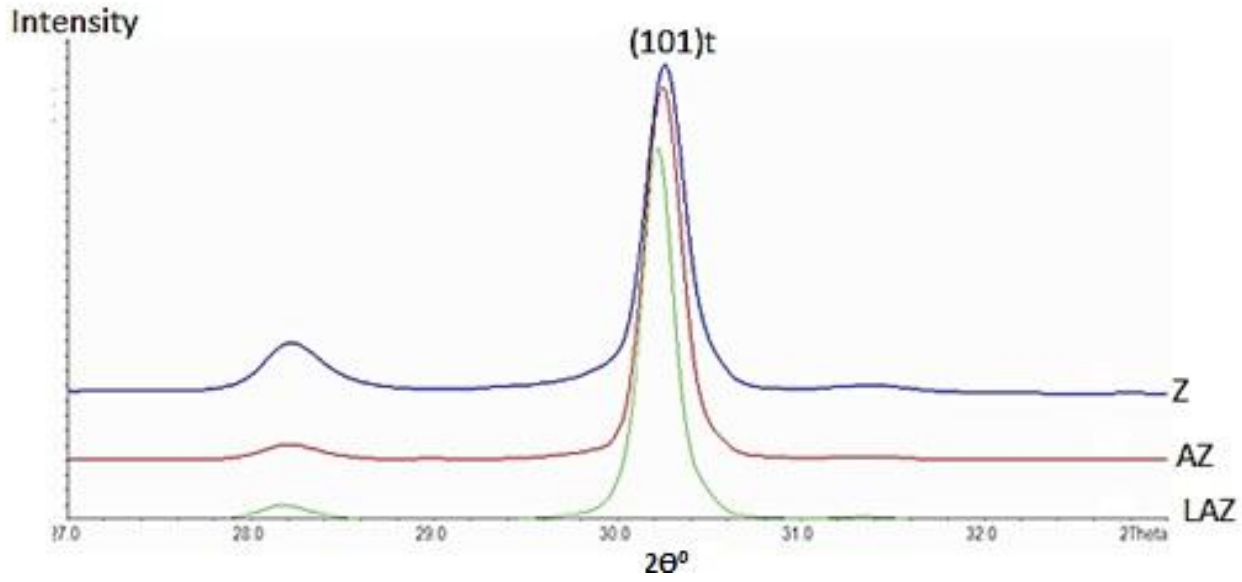

Fig 4.11: Degraded specimens at 134 °C for 24h.

4.3.3. Atomic Force Microscopy (AFM)

In addition to optical microscopy, atomic force microscopy (AFM) was used to study surface evolution through the degradation process. AFM enables higher depth resolution images at nanometer scale. For this purpose a Nanoscope IIIa (Digital Instruments, USA) microscope was used in contact mode with silicon nitride probes. Typical images were acquired at a scan rate of 1 Hz with a resolution of 512 samples per line in the scanned area. In the AFM images, the regions with brighter contrast are associated with monoclinic grains due to the volume expansion on transformation, meaning they stand proud of the surface.

AFM imaging of the aged Z sample, Figure 4.12, indicates individual transformed grains and regions of more extensive transformation to form monoclinic clusters. The AZ and LAZ aged samples (Figures 4.13 and 4.14 respectively) demonstrate different nucleation and growth rate of monoclinic grains at 134 °C for 24 hours compared to the Z specimen. Conical monoclinic coalescence was not observed in the LAZ sample, only in the Z and AZ samples. Figure 4.15a was imaged from a darker contrast region within the section imaged in Figure 4.14. Figure 4.15b was imaged from within a light contrast region and confirms that all the grains in this region were transformed.

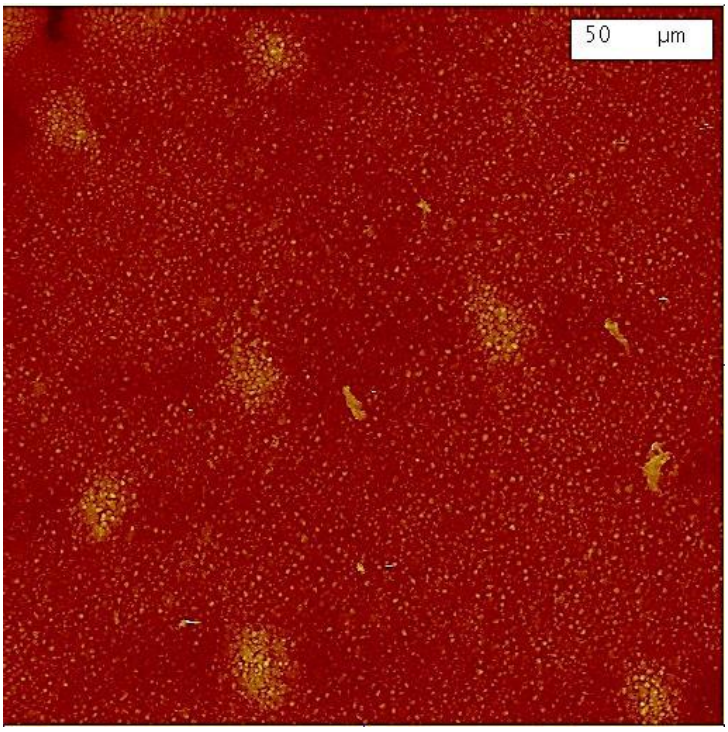

Fig 4.12: Z sample degraded at 134°C for 24 hours

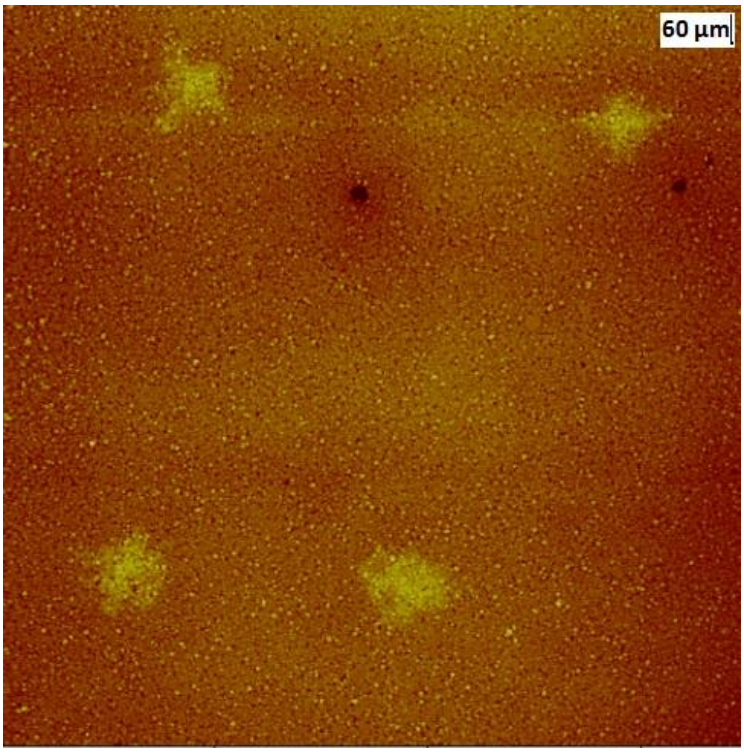

Fig 4.13: AZ sample degraded at 134° for 24 hours

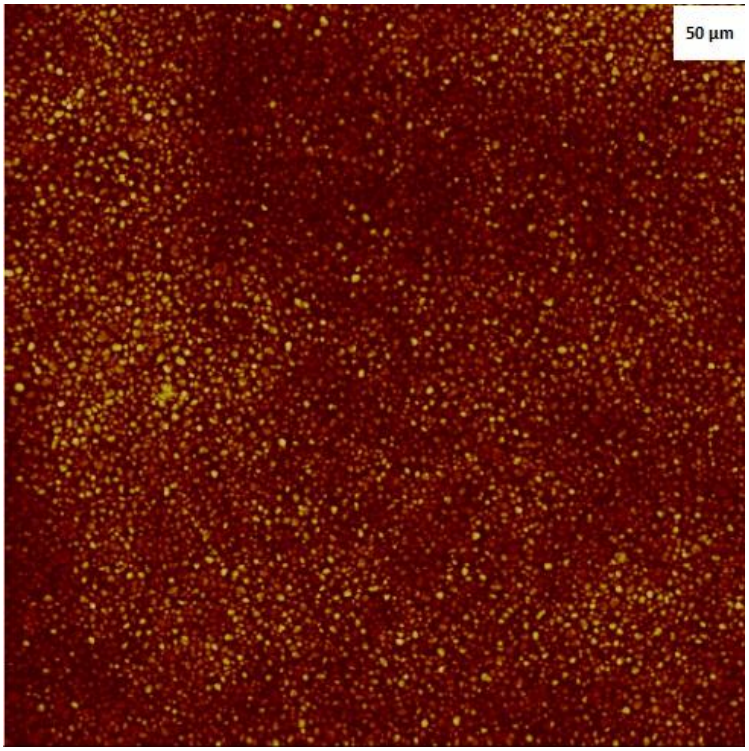

Figure 4:14: LAZ sample degraded at 134 °C for 24 hours

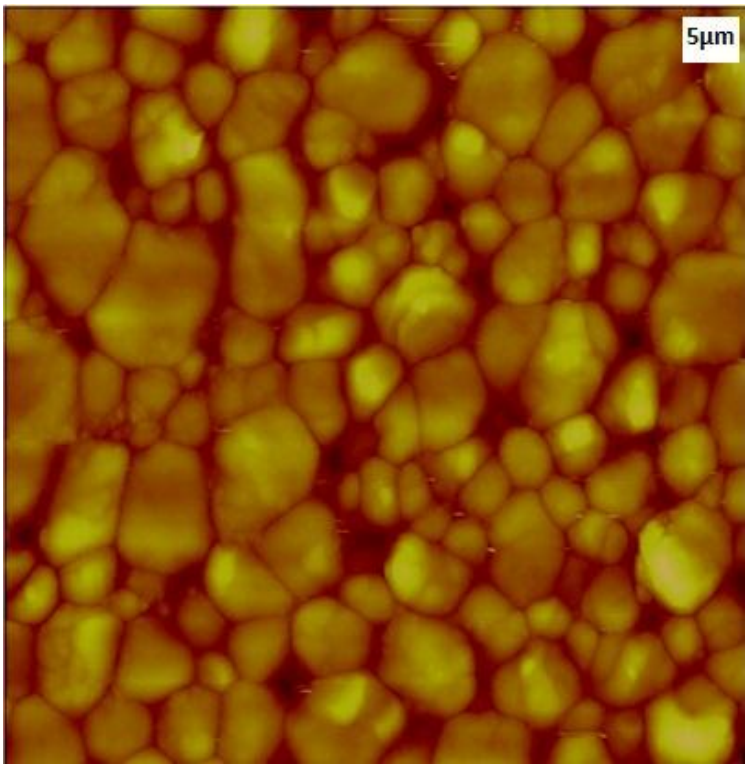

Fig 4.15a: Tetragonal region of Figure 4.14

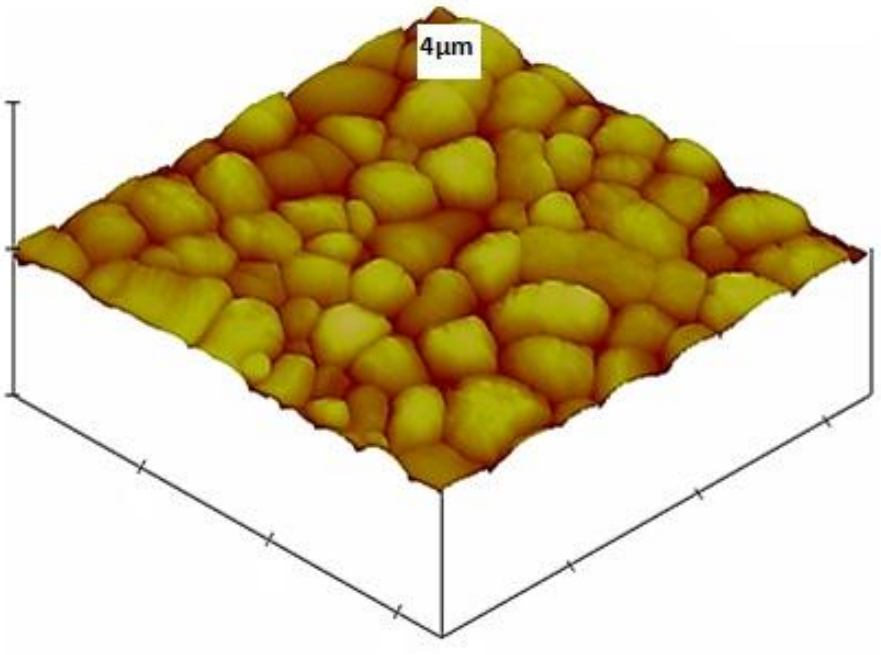

Fig 4.15b: Monoclinic region of Figure 4.14

Section analysis using AFM imaging techniques was used to measure the vertical height difference between transformed monoclinic and untransformed tetragonal grains, Figure 4.16. The height difference between the red and a green marker is about 71.75 nm.

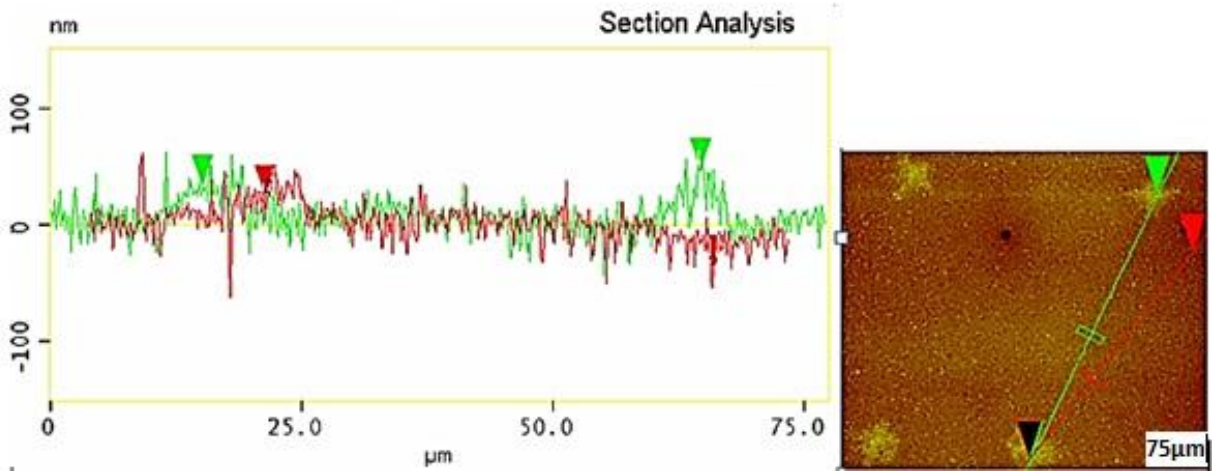

Fig 4.16: Section analysis of AZ specimen aged at 134 °C for 24 h

4.3.4. SEM Imaging of Degraded Specimens (SEM)

Hydrothermal degradation of the specimen at 180 ^{o}C for 48 hours in superheated steam resulted in extensive transformation of the tetragonal to monoclinic phase. In several cases this led to surface microcracks and catastrophic surface fracture Figure 4.17. Figure 4.18 shows that on an AZ surface exposed at 134 °C for 24 hours grain boundaries in some locations are difficult to find.

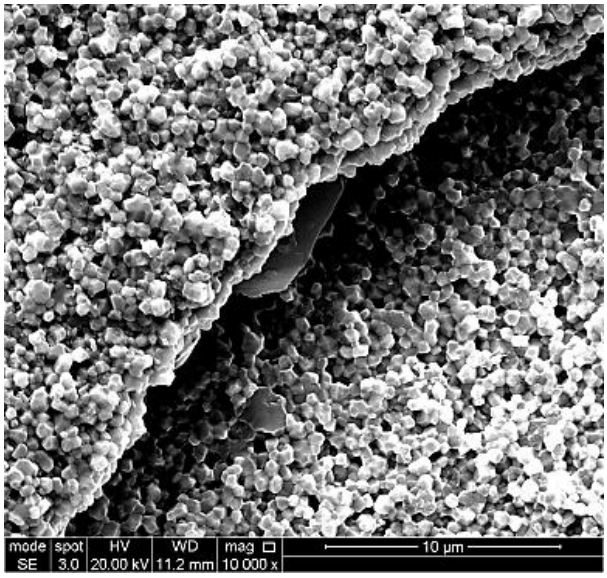

Fig 4.17: Secondary electron SEM image of degraded Z sample exposed for 48h at 180 ^{o}C.

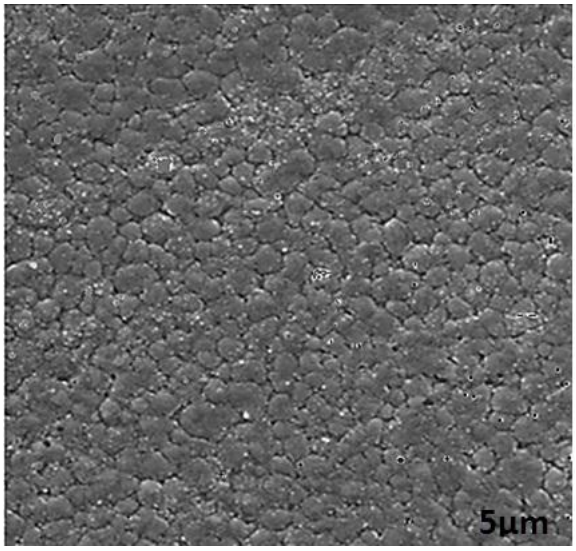

Fig 4.18: Secondary electron SEM image of AZ specimen aged at 134 °C for 24h.

Degradation is a phenomenon which starts from the surface and penetrates into the bulk. SEM imaging on cross section specimens was used to evaluate the total penetration depth of samples exposed for 24 hours at 134 °C. Figures 4.19 (a), 4.19 (b) and 4.19(c) from Z, AZ and LAZ samples respectively present different depths degradation(4.41 µm, 2.68 µm and 1.49 µm) indicating that the LAZ and AZ specimens were more resistant to degradation than the Z sample.

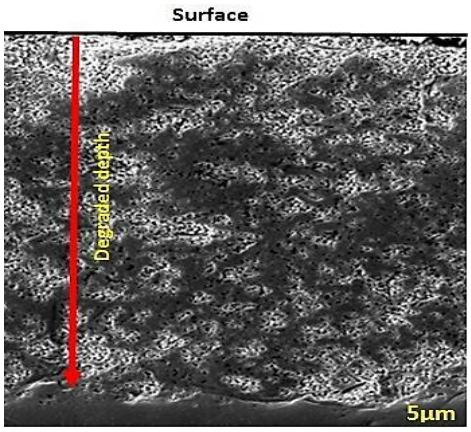

Fig 4.19(a): Secondary electron SEM image of a surface cross section of Z sample aged at 134 °C for 24 hours.

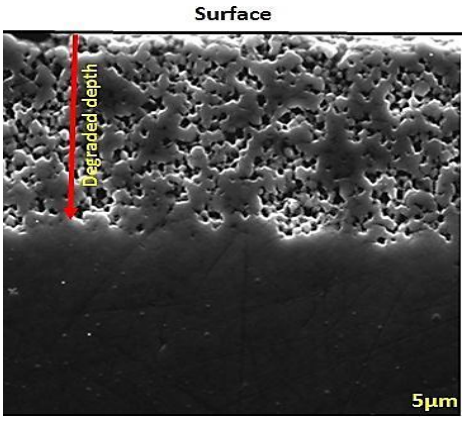

Fig 4.19(b): Secondary electron SEM image of a surface cross section of AZ sample aged at 134 °C for 24 hours.

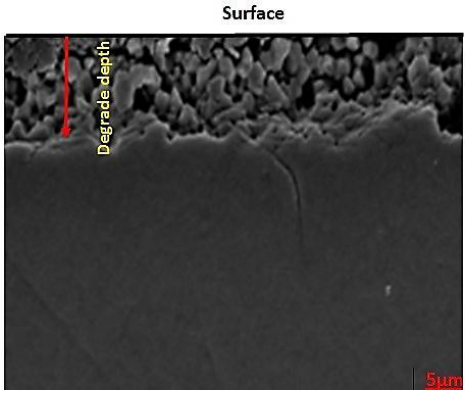

Fig 4.19(c): Secondary electron SEM image of a surface cross section of LAZ sample aged at 134 °C for 24 hours.

4.3.5. Raman Spectroscopy

Although specimens exposed at 134 °C for 24 h revealed monoclinic peaks in X-ray diffraction, no characteristic monoclinic twin peak was detected on the aged surface of the same material through Raman spectroscopy, Figure 5.20a. This twin peak associated with monoclinic phase only appeared on samples aged at 180 °C for 48 hours Figure 5.20b. This shows that Raman spectroscopy was insensitive to small amounts of transformation.

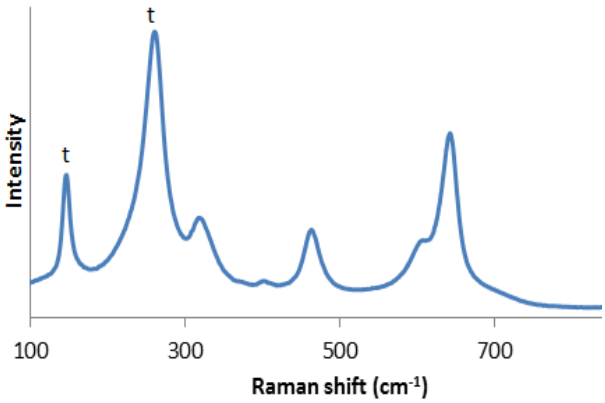

Fig 4.20a: Z sample aged at 134 °C for 24 hours.

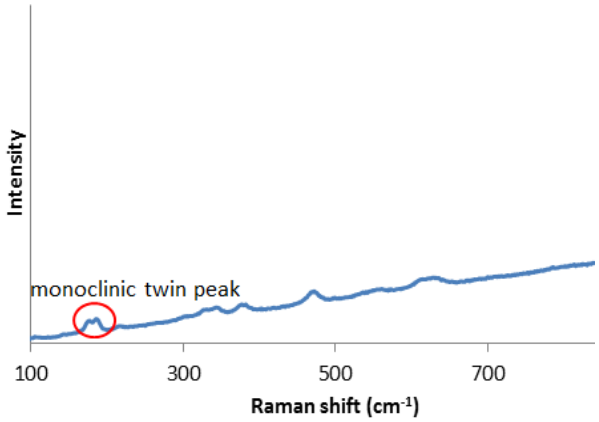

Fig 4.20b: Z sample aged at 180 °C for 48 hours.

4.4. Reciprocating Wear

Reciprocating sliding wear tests were used to partially simulate the conditions in hip joint prosthesis. It is not possible to fully simulate the conditions as this would require a hip simulator that incorporates microseparation. However, reciprocating tests in bovine serum are known to generate worn surfaces that give many of the worn surface characteristics found on retrieved hip joints. In this test two kinds of lubricant were used, ultra-pure water and 25% bovine serum which provide both different lubrication regimes, but also different degrees of tribochemical interaction.

4.5. Water Lubricated Condition

Water lubrication would be expected to maximise hydrothermal degradation. Its influence on the sliding wear mechanism of zirconia surfaces against alumina ball was studied by applying different loads at constant speed to simulate the mild to severe wear zone. Figure 4.21 (reciprocating sliding wear of the AZ specimen under 4N load for 24 hours at 600 rpm in water) shows a typical coefficient of friction (COF) as a function of time graph. Early fluctuation of the COF value at was attributed to initial contact of two intact surfaces and was followed by a period of around 6 hours where the COF gradually increased before attaining a steady state value of around 0.035.

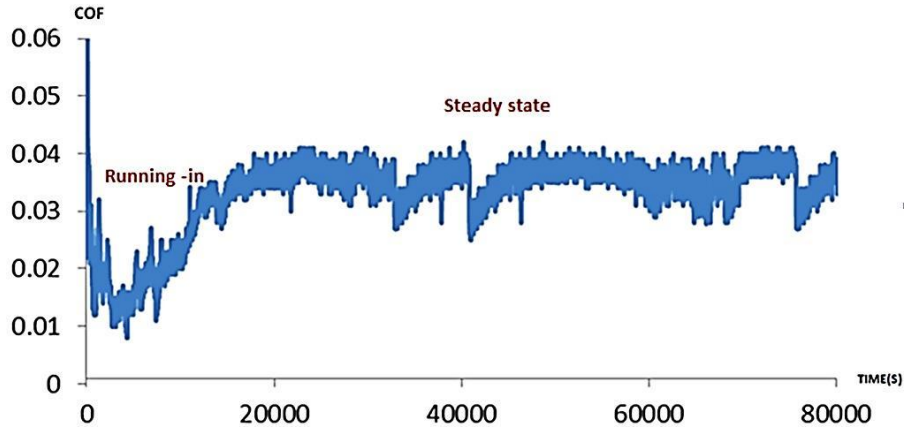

Fig 4.21: A typical COF –Time plot of a reciprocating wear test on AZ specimen *in* ultra-pure water under 4 N contact load, 0.02 m/s speed for 24 hrs.

The lubrication regime for each lubricant was defined by constructing the Stribeck curve, which is a plot of the average COF values as a function of the Sommerfeld number. Sommerfeld number ''Z '' is defined in equation 4.1, where V is the sliding speed, η is the lubricant viscosity and N is the applied load. Lubricant viscosity was assumed constant and sliding speed was set at 600 rpm (equating to 0.02 m/s).

$z = v\eta$ /N (4.1)

Figure 4.22 gives the Stribeck curve for six samples of Z, AZ, LAZ, DZ, DAZ and DLAZ (where D refers to degraded). Two lubricated regimes were identifiable in the majority of the graphs. When the COF increases proportionate to the Sommerfeld number the lubricant regime is considered to be full fluid-film and when it reduces a mixed lubrication regime is indicated. The minimum and maximum average values of COF and the lubrication regimes for the water lubricated wear test are summarized in table 4.2. During this test the value of COF for zirconia surface against alumina ball was quite small and it changes in the range of [0.006±0.001, 0.070±0.062].

Table 4.2: Minimum, maximum of COF with respect to the applied load and lubrication regime for Z, DZ, AZ, DAZ, LAZ and DLAZ specimens in water ("D" represents the degraded specimens) .

Material	Minimum COF(load)	Maximum COF(load)	Lubrication regime
Z	0.013±0.012 (1N)	0.048±0.028(2N)	Mixed-full
DZ	0.021±0.012(1N)	0.070±0.062(4N)	Full-mixed
AZ	0.012±0.004(1N)	0.023±0.010(2N)	Full-mix-full
DAZ	0.006±0.001 (0.5N)	0.021±0.003 (1N)	Mixed-Full
LAZ	0.010±0.001(1N)	0.028±0.016(4N)	Full-Mixed
DLAZ	0.022±0.014(2N)	0.025±0.012 (05,1,4N)	Mixed

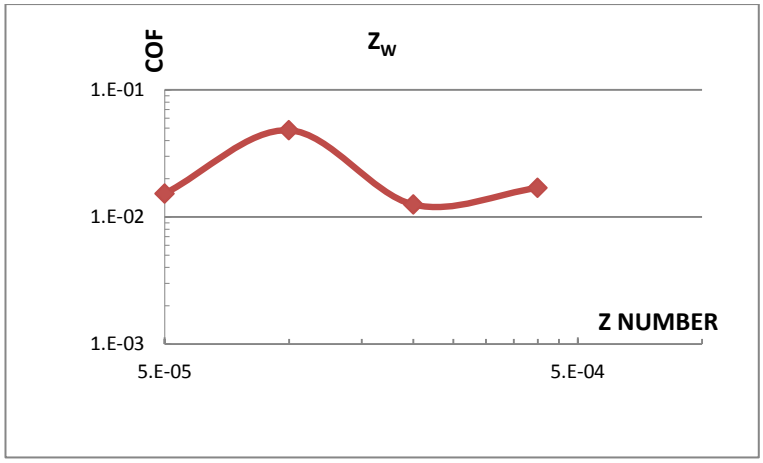
Z_w
COF
1.E-01
1.E-02
1.E-03
5.E-05
5.E-04
Z NUMBER
(a)

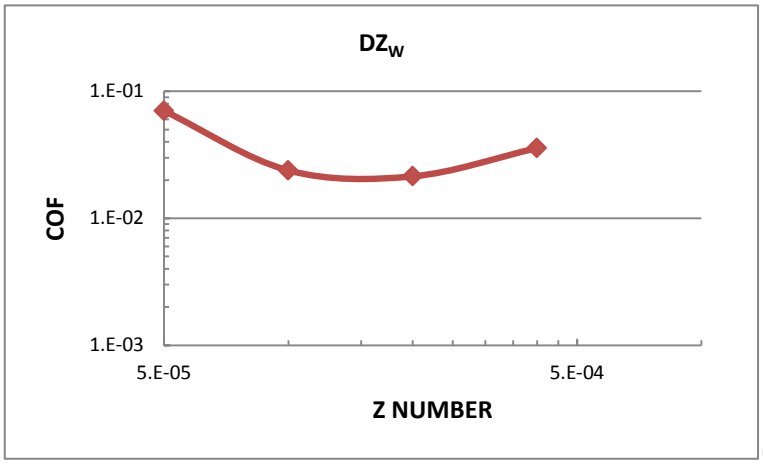
DZ_w
1.E-01
1.E-02
1.E-03
COF
5.E-05
5.E-04
Z NUMBER
(b)

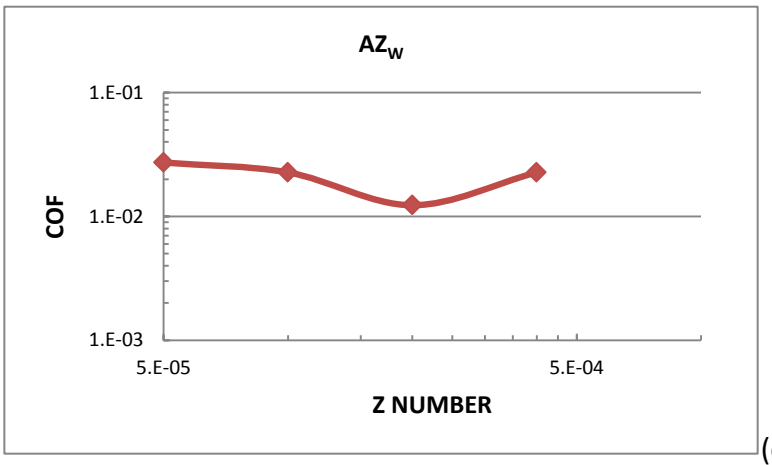
AZ_w
1.E-01
1.E-02
1.E-03
COF
5.E-05
5.E-04
Z NUMBER
(c)

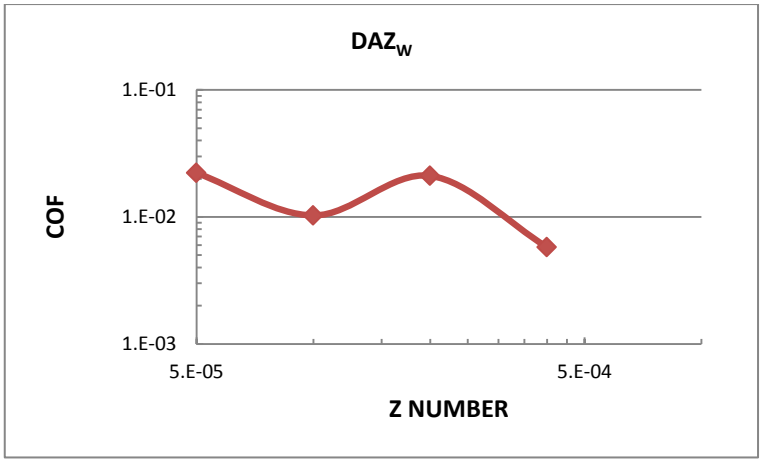

(d)

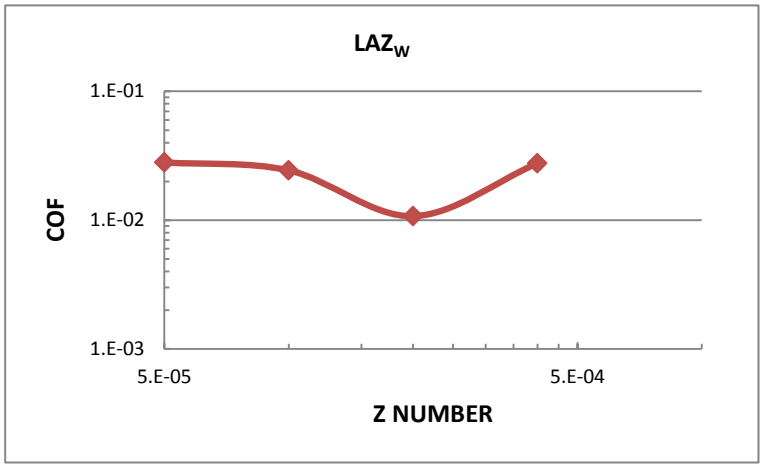

(e)

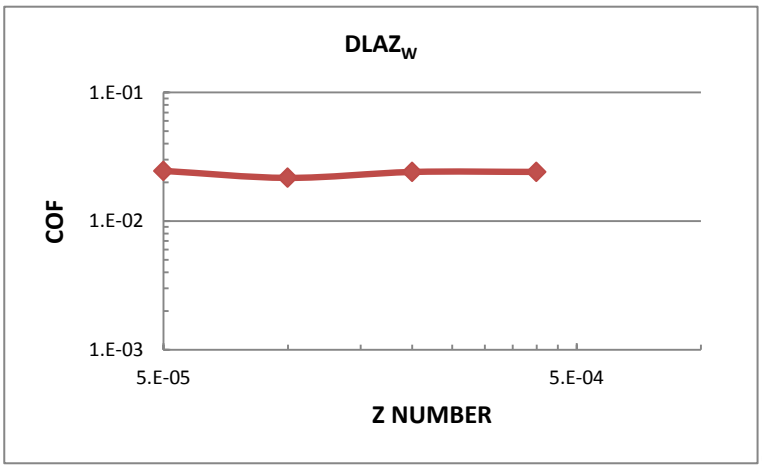

(f)

Fig 4.22: The Stribeck curve for (a) Z, (b)AZ, (c)LAZ,(d) DZ, (e)DAZ and (f) DLAZ samples *lubricated* with ultra-pure water(W) under 4, 2, 1 and 0.5N load. D represents degraded specimens.

4.5.1. Wear Rate

The specific wear rate of each material was determined by equation 4.2, i.e. the volume lost (V) divided by the applied load (F) and travelled distance (S), with units of mm^3/Nm.

$$K=\frac{V}{FS} \qquad (4.2)$$

The specific wear rates of Z, AZ, LAZ, DZ, DAZ and DLAZ specimens sliding against alumina ball in ultra pure water at speed of 0.02 m/s as a function of load and material are plotted in Figure 4.23 and 4.24 respectively. The DZ sample showed a slight decrease in wear rate at 1N load compared with 0.5 N load, but in all other tests the wear rate increased with load, Figure 4.24. The highest wear rate was at 4 N for the Z specimen at 2.04E-6 mm^3/Nm, while the smallest wear rate was obtained at 0.5 N for the LAZ specimen. The magnitude of specific wear rate placed all wear tests within the mild wear regime [ref49]. The wear rates at 0.5N and 1N loads were significantly lower than those at 2N and 4N for all of the specimens. Surprisingly the degraded specimens generally presented with lower wear rates than the non- degraded samples. The wear rates of DLAZ and DAZ specimens at 2N and 4N were significantly less than those of the non-aged AZ and LAZ samples, as shown by Figure 4.23.

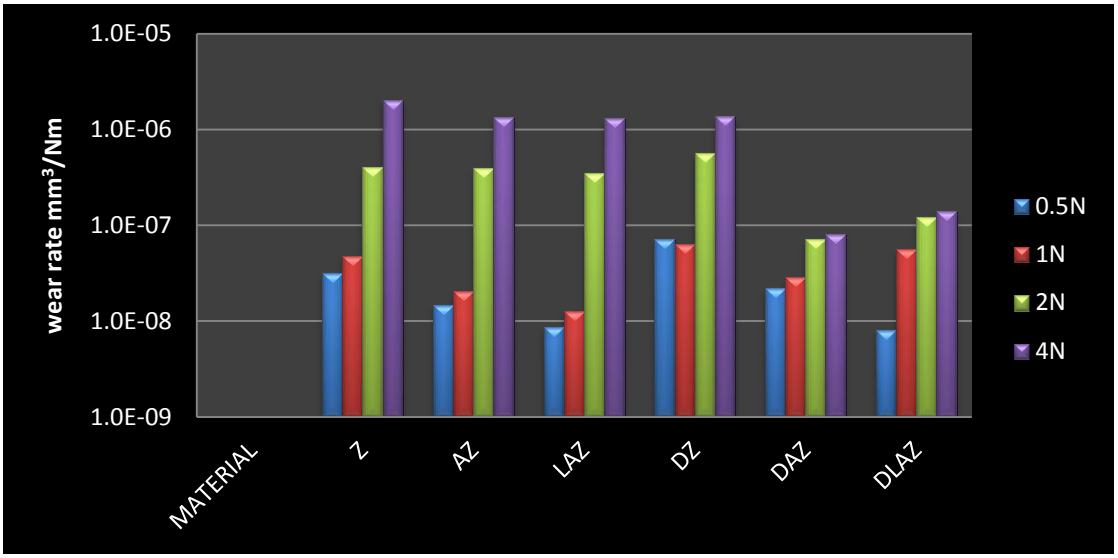

Fig 4.23: Specific wear rates for the reciprocating wear tests of all the material against high purity alumina ball lubricated with ultra-pure water, showing a comparison of the effect of load.

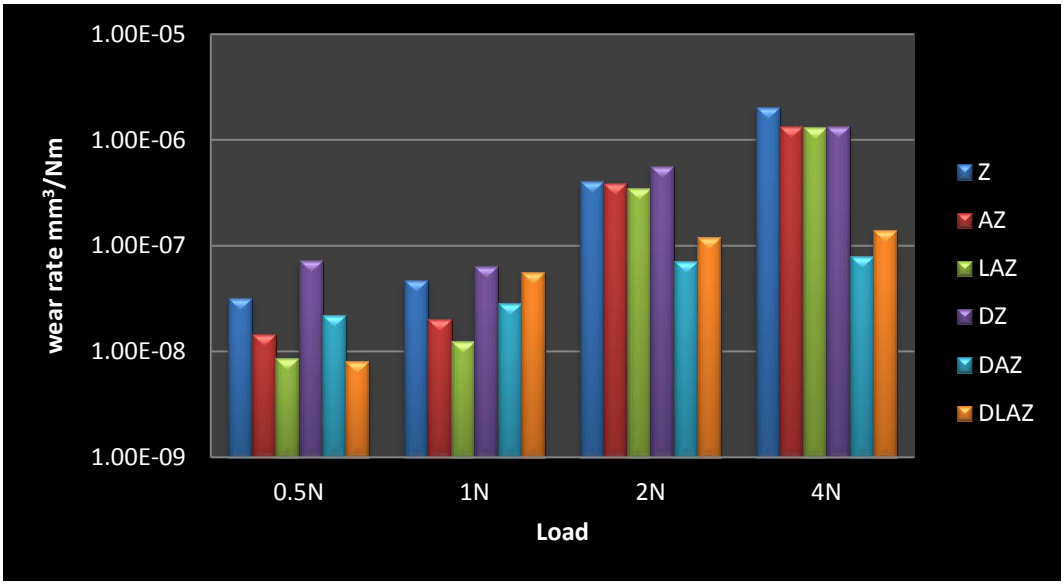

Fig 4.24: Specific wear rates for the reciprocating wear tests of all the material against high purity alumina ball lubricated with ultra-pure water. (Materials comparison).

4.5.2. Worn Surface Characterisation

4.5.2.1. VSI Imaging

Optical 3D (VSI) imaging of zirconia samples shows the surface evolution during sliding wear against alumina ball in water, Figures 4.25 to 4.34. Figure 4.25 and 4.26 demonstrate different wear zones. Z specimens worn at 1N and DZ specimens worn at 0.5N suffered

some localised severe wear damage even though other areas within the wear track surface were largely unaffected by wear. Wear debris accumulation to one side and at the head of the wear track showed more intensity in the DZ sample than in the Z one. The DZ samples worn in water under 0.5N, 1N and 2 N load, reveal that the wear track has a broader width and shallower depth with respect to the counterface geometry at higher applied loads (Figure 4.25, 4.27 and 4.28 respectively). In general at loads exceeding 1N the wear track in all specimens tended to be more obvious, Figure 4.27, 4.28, 4.30, 4.31 and 4.33. An abrupt increase in wear rate of the AZ specimen was observed for load 4N, Figure 4.31.

Figure 4.29 shows the worn surface of the AZ sample tested under 0.5N load. It exhibited parallel grooves along the sliding direction that appeared to be associated with third body abrasion.

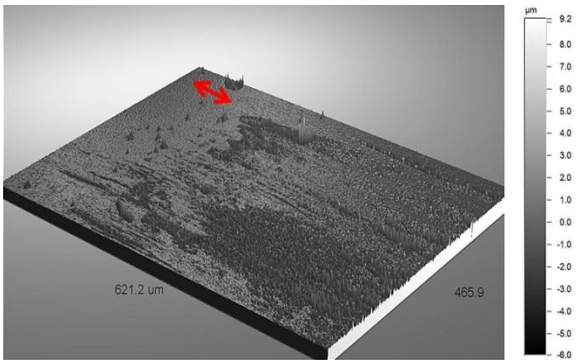

Fig 4.25: Z sample worn in water under 1N at 0.02 m/s

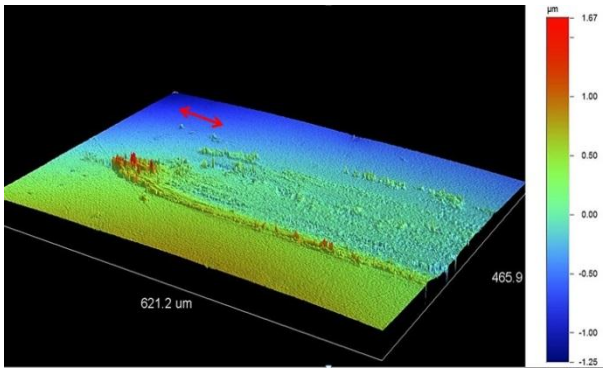

Fig 4.26: DZ sample worn in water under 0.5 N at 0.02 m/s

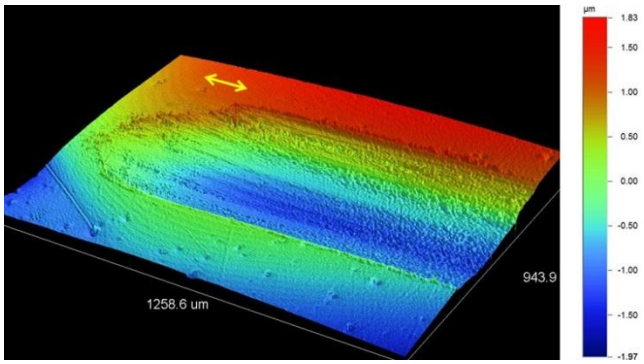

Fig 4.27: DZ sample worn water under 1N at 0.02 m/s

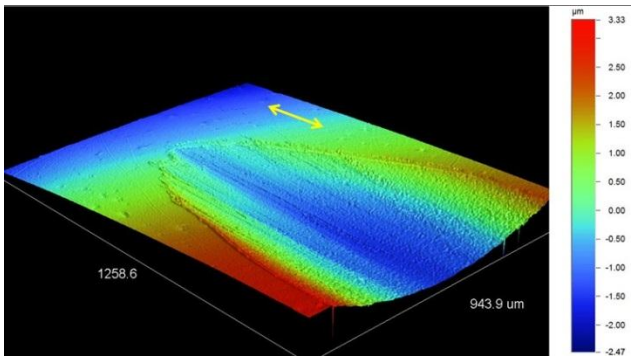

Fig 4.28: DZ sample worn in under water 2N at 0.02 m/s

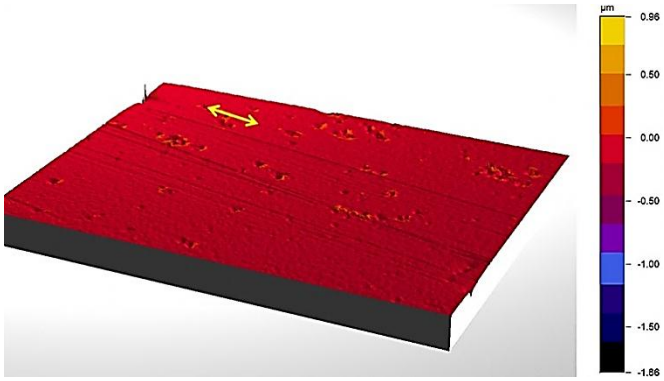

Fig 4.29: AZ sample worn in water under 0.5 N at 0.02 m/s

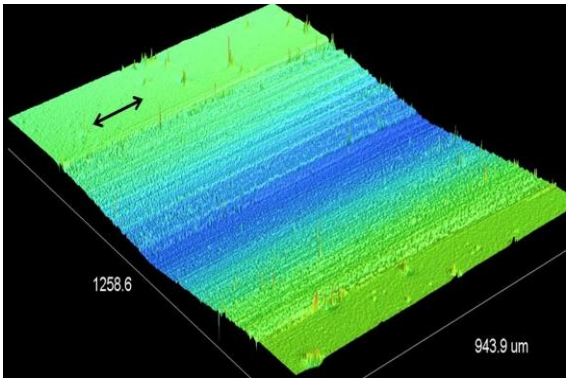

Fig 4.30: AZ sample worn under 2N in water at 0.02 m/s

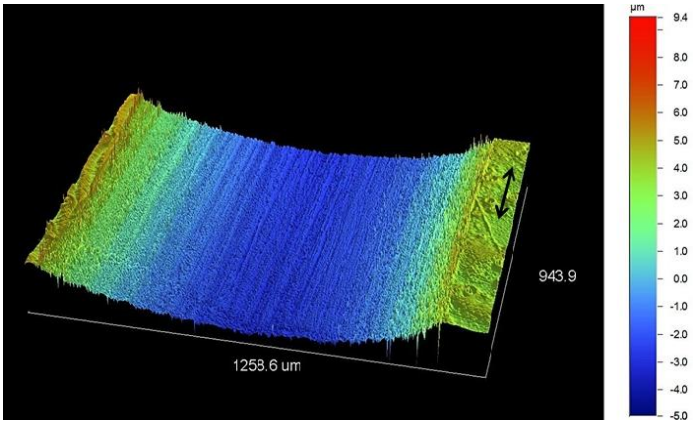

Fig 4.31: AZ sample worn under 4N in water at 0.02 m/s

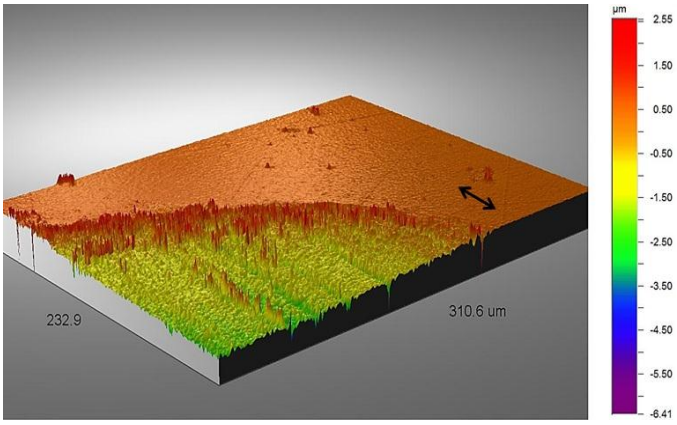

Fig 4.32: DAZ sample worn in water under 4N at 0.02 m/s

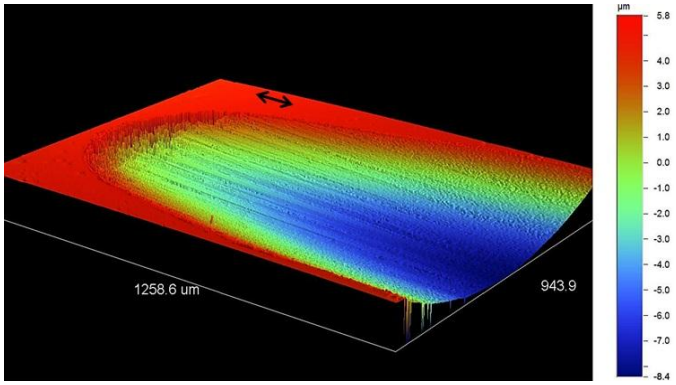

Fig 4.33: LAZ sample worn in water under 4N at 0.02 m/s

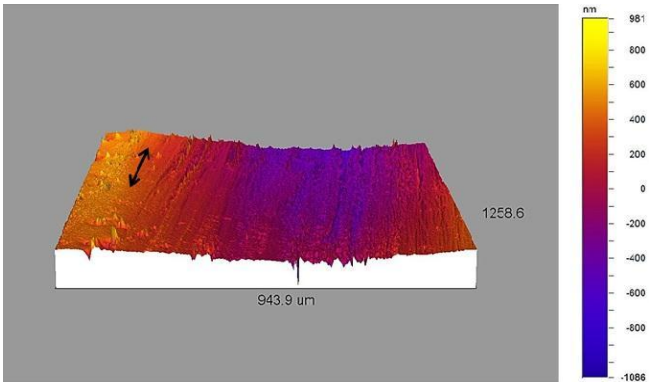

Fig 4.34: DLAZ sample worn under 4N in water at 0.02 m/s

Frequent grooves inside the wear scar in Figure 4.32 and 4.34 evidence the presence of embedded or loose third bodies with higher hardness than the zirconia surface. The wear rate of the DAZ specimen was higher than that of the DLAZ sample under the same load of 4N as shown by Figures 4.32 and 4.34.

4.5.2.2. SEM Imaging

Secondary electron scanning microscopy was used to characterise the worn surface damage including wear debris of a selection of worn surfaces. These surfaces exhibited both commonly observed features and extremes of behaviour. Surface changes as a function of load were consistent with that observed by optical microscopy. SEM imaging identified the existence of a surface tribolayer which covered almost the entire surface on all the water worn samples. Figure 4.35 shows the Z sample worn under 2N load. The surface layer in this image shows a more polished structure compared to that of the same sample worn under higher load (4N), Figure 4.36. The variable intensity of detached material in different locations of the surface in these two images is significant. Both images show embedded wear debris on the surface layer which is identifiable from the different contrasts in the surface layer. There is some loose wear debris over the surface which, depending on its hardness and size can produce further wear on the surface. In the Z specimen worn under 4N load (Figure 4.36) there appears to be an area of delamination in the surface layer (top left of the image) and also some surface ripples. The ripples are on two scales, one with a wavelength of around a micron (bottom right) and the other on a much finer scale.

Figure 4.37 is a low magnification SEM image in showing a general view of a wear scar (middle of the image). As already identified from the optical image, the wear debris accumulation is more pronounced in one side of the wear track (bottom of the image) and more material detachment is observable in the middle of the scar. The micro-ripples structure of DZ sample worn at 2N was captured in Figure 4.38, using high magnification of x20000. This wear morphology characteristic was found in most of the water worn zirconia surfaces.

Figure 4.39 shows the grain relief structure in AZ sample worn at 1N load. This structure is rarely observed in water worn zirconia surfaces. Interestingly, the AZ sample worn at the higher load of 2N, still show grain relief on the surface alongside another mechanism that occurred within the imaged area, Figure 4.40.

Figure 4.41a is a low magnification image of an AZ sample worn under 4N in water. In this image the edge of the wear track was smooth and it gets progressively rougher towards the scar centre. The higher magnification of Figure 4.41b indicates grain pull out, with the recess being filled by wear debris (exhibited as darker contrast in this image), leaving a relatively smooth surface overall. The grooved lines along the sliding direction which are often formed in sliding wear could be due to a foreign body between the two rubbing surfaces or could be due to an asperity on the counterface. The randomly oriented scratches were considered to be residual from surface preparation.

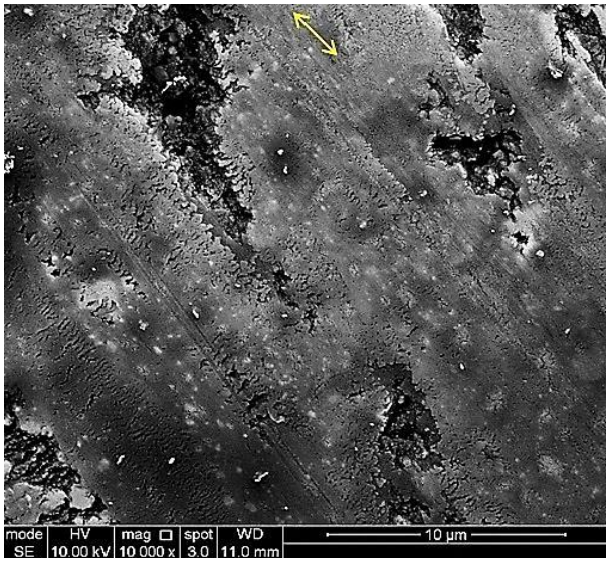

Fig 4.35: Z sample worn in water under 2N at 0.02 m/s

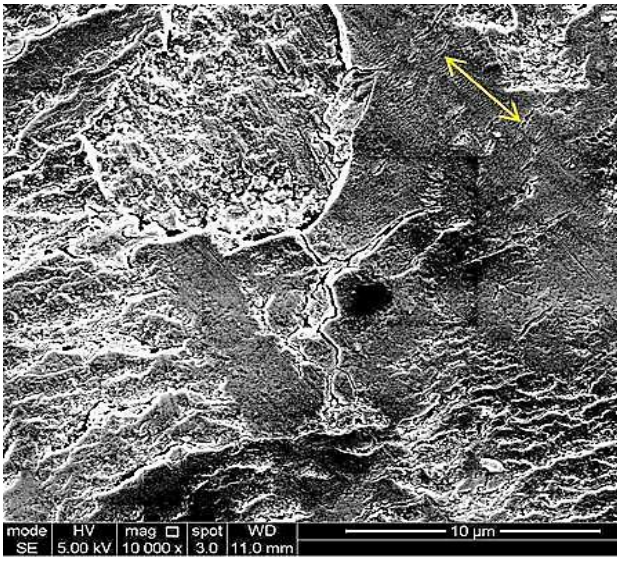

Fig 4.36: Z sample worn under 4N in water at 0.02 m/s

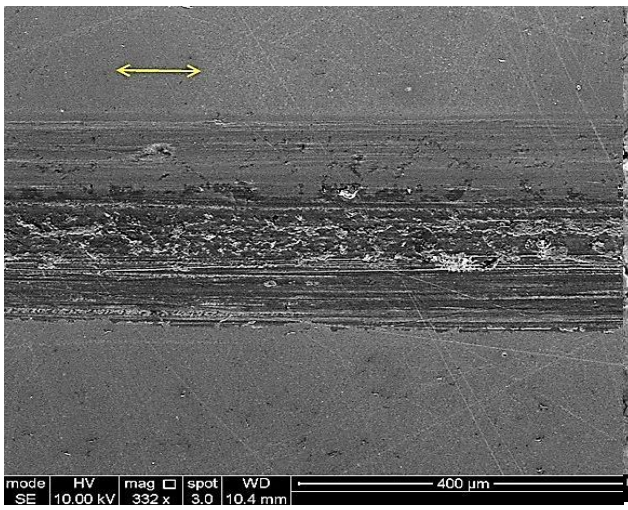

Fig 4.37: DZ sample worn in water under 0.5N at 0.02 m/s

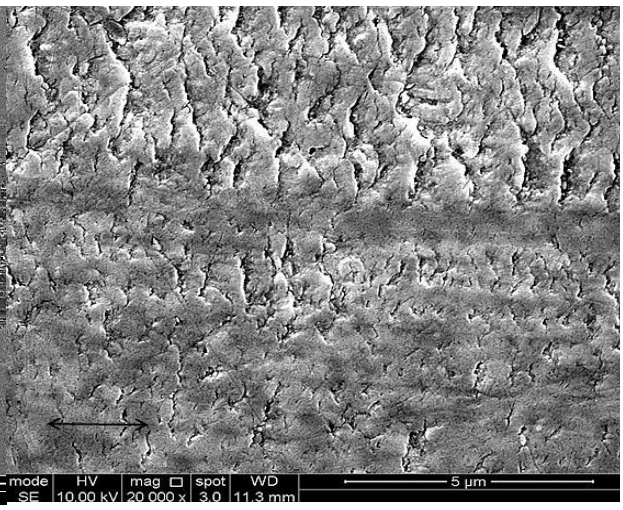

Fig 4.38: DZ sample worn in water under 2N at 0.02 m/s

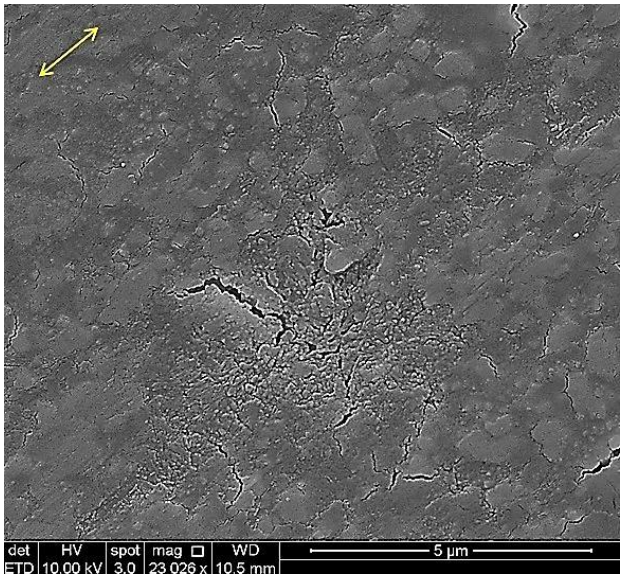

Fig 4.39: AZ sample worn in water under 1N at 0.02m/s

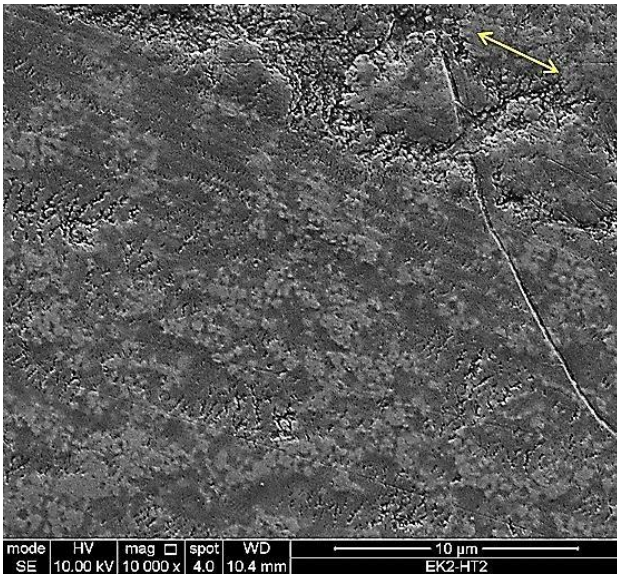

Fig 4.40: AZ sample worn in water under 2N at 0.02 m/s

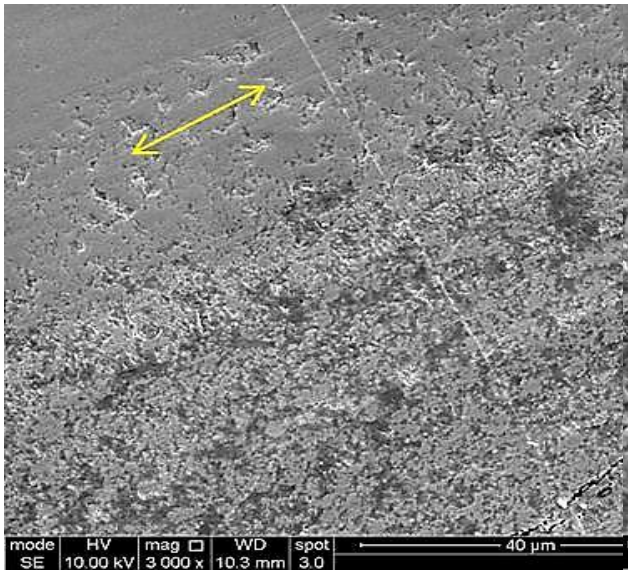

Fig 4.41a: AZ sample worn in water under 4N at 0.02 m/s

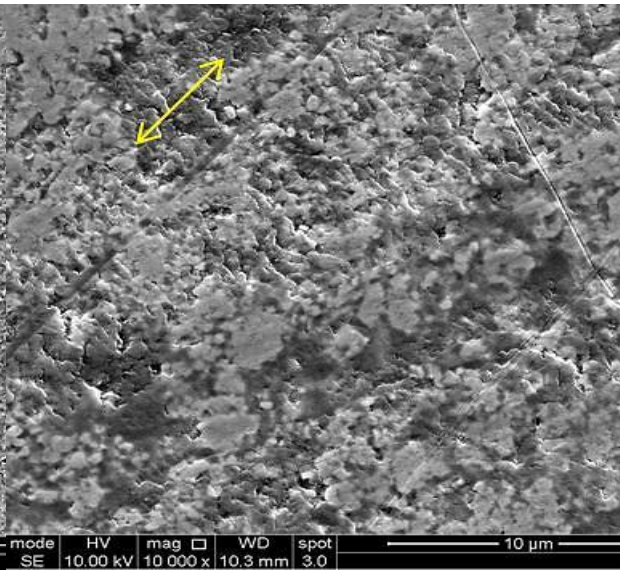

Fig 4.41b: AZ sample worn in water under 4N at 0.02 m/s

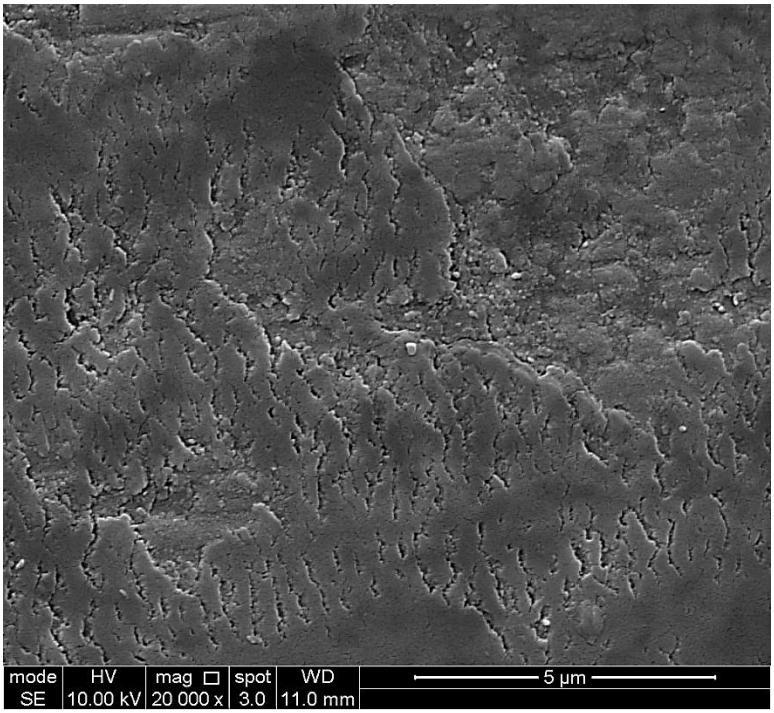

Fig 4.42: DLAZ sample worn under 1N load in water at 0.02 m/s

Figure 4.42 shows typical quasi-parallel cracks perpendicular to the sliding direction for the DLAZ specimen worn at 1N in water. This appearance is typical of stick slip behaviour, producing a surface layer that became wear debris when it detached (top right of image).

4.5.2.3. AFM Imaging

AFM imaging was employed to provide higher resolution information of the wear zone. Wear damage intensity is not uniform across the wear scar, but Figure 4.43 of Z sample under 1N load in water evidences surface modification during the wear process. The significant appearance of lubricant layer existence on top of the surface this layer considerably modified its surface. Figure 4.44 is a lateral force microscopy image of the specimen shown in Figure 4.43 evidencing grain boundary recesses which were not detected in normal contact mode AFM imaging. The amplitude image of this sample shows ripples of compacted layer on the worn region with 5µm wavelength, Figure 4.45.

Figure 4.46 shows an AFM image of the worn degraded DZ sample at 2N load. Two different wear mechanisms occurred in this image; the upper part of the image demonstrates slip - slide wear damage in zirconia. In this motion, attachment of some hard particles by frequent arrangements over zirconia surfaces was caused alumina ball's slip on the surface. In absence of such features the lower side of the image shows smoother wear morphology.

In Figure 4.47 the location of the grain boundaries can still be seen clearly in the AZ sample worn under 0.5N load. In the AFM images, the regions with brighter contrast correlate to features on the surface such as wear debris which stand proud of the surface. The AZ sample worn under 2N and 4N loads has approximately parallel grooves perpendicular to the sliding direction, Figure 4.48 and 4.49, which is consistent with SEM images of the same feature. These features appeared to be a result of fragmentation of a smeared surface layer.

Figure 4.50 shows an LAZ specimen worn under 1 N loads in water. A tribolayer covered a large portion of the surface. LAZ samples worn under 4N load shows slip-slide, grooving and grain pull out wear damage within the wear track, Figure 4.51 and the grain outline is still visible, Figure 4.52.

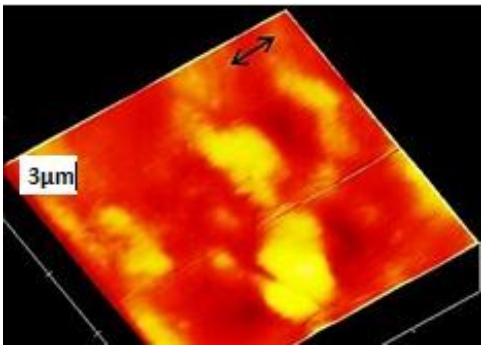

Fig 4.43: Z sample worn under 1N in water at 0.02m/s

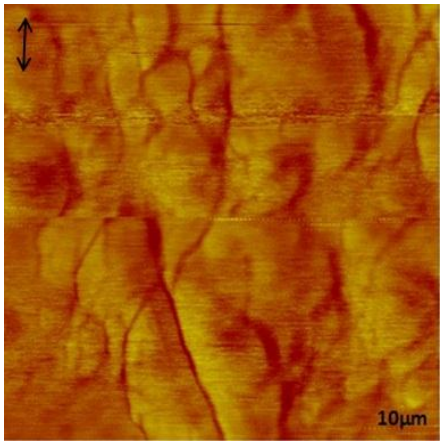

Fig 4.44: Lateral force microscopy of Z sample worn in water under 1N at 0.02 m/s

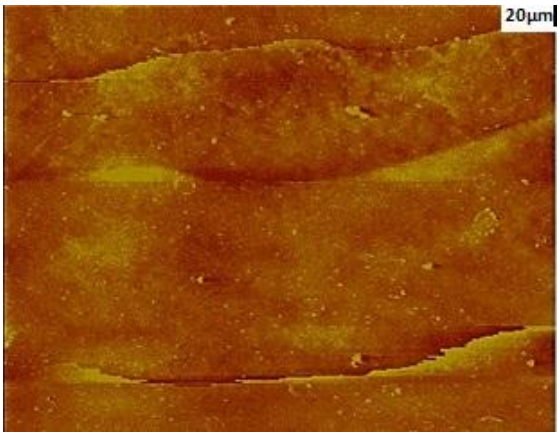

Fig 4.45: AFM amplitude image of Z sample worn under 1N in water at 0.02 m/s

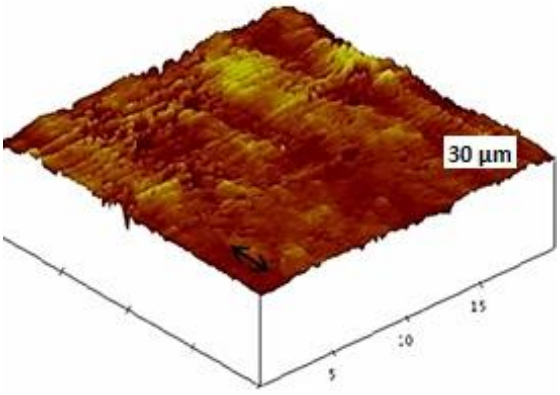

Fig 4.46: DZ sample worn under 2N in water at 0.02m/s

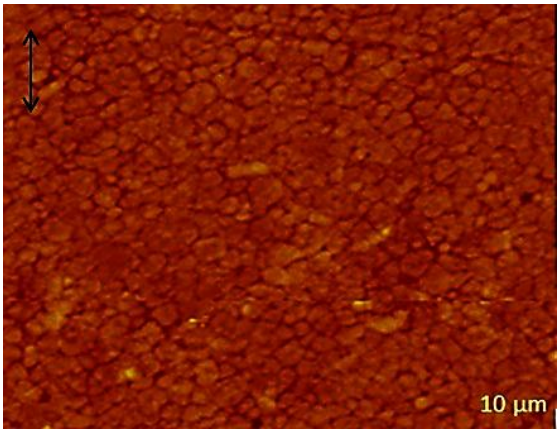

Fig 4.47: AFM image of the AZ sample worn under 0.5N load in water at 0.02 m/s

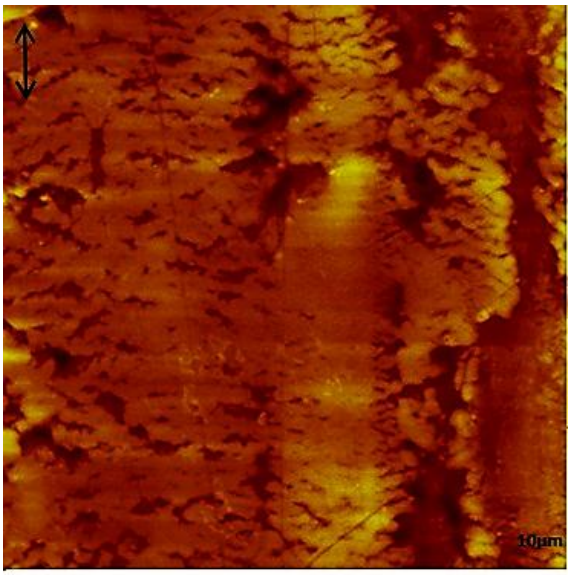

Fig 4.48: AZ sample worn under 2N load in water at 0.02 m/s

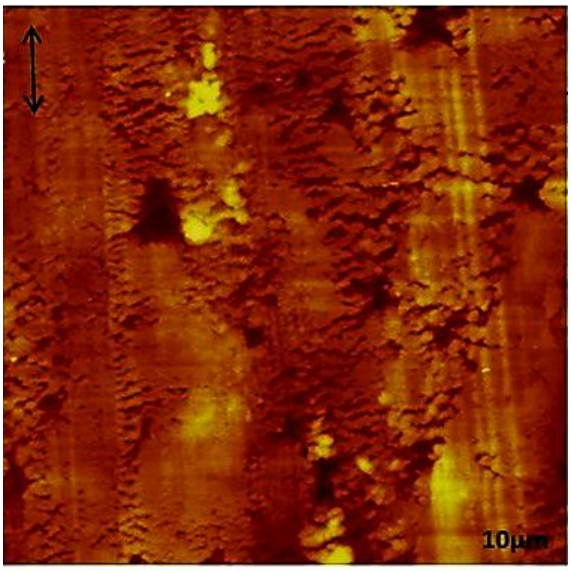

Fig 4.49: AZ sample worn under 4N load in water at 0.02 m/s

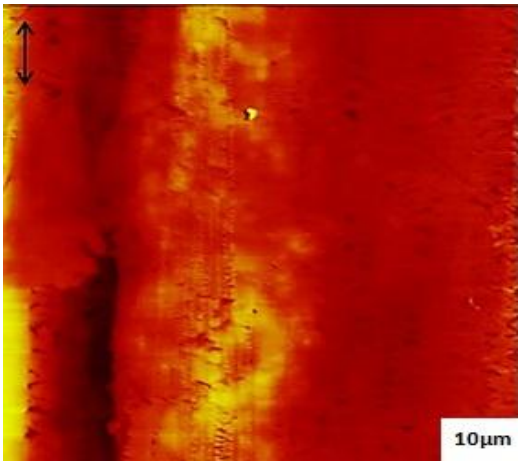

Fig 4.50: LAZ sample worn under 1N in water at 0.02 m/s

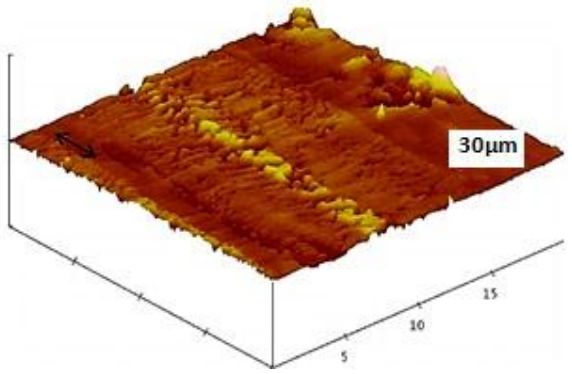

Fig 4.51: LAZ sample worn under 4N in water at 0.02m/s

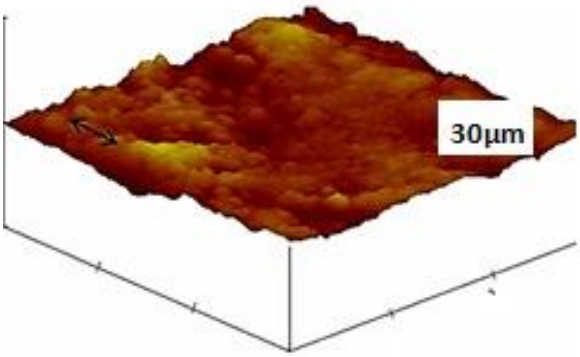

Fig 4.52: DLAZ sample worn under 2N load in water at 0.02 m/s

4.5.2.4. Subsurface Wear Damage Characterisation

A surface layer with around 50 nm thickness was generally found on the surface of the water worn specimens. A detailed sub-surface damage study was carried out using transmission electron microscope.

The labelled area in Figure 4.53 (top image), which is an SEM image of an AZ surface worn at 4N was selected for cross-sectional TEM sample. It was prepared using the focus ion beam (FIB) lift-out method. The corresponding TEM image, Figure 5.33 (bottom image) shows the carbon deposition layer which was mostly removed by damage of gallium ion beam during sample ion milling. A protective gold coating on top was present to label the original surface. A large region filled with lubricant can be seen in the corner of the TEM image. This could be due to the existence of subsurface pores which aid pull-out grains. Figure 4.54 shows major sub-surface cracking and also the tribolayer created over the very rough surface. Figure 4.55 evidences monoclinic twins the presence of which was also confirmed by diffraction pattern. These structures were formed due to either stress or tribochemical reaction of surface and environment (the circled regions).

Although Figure 4.56 indicates the existence of some nano particles within the tribolayer, only an amorphous structure could be detected from the diffraction pattern. The origin of the nano particles could be identified with high resolution TEM.

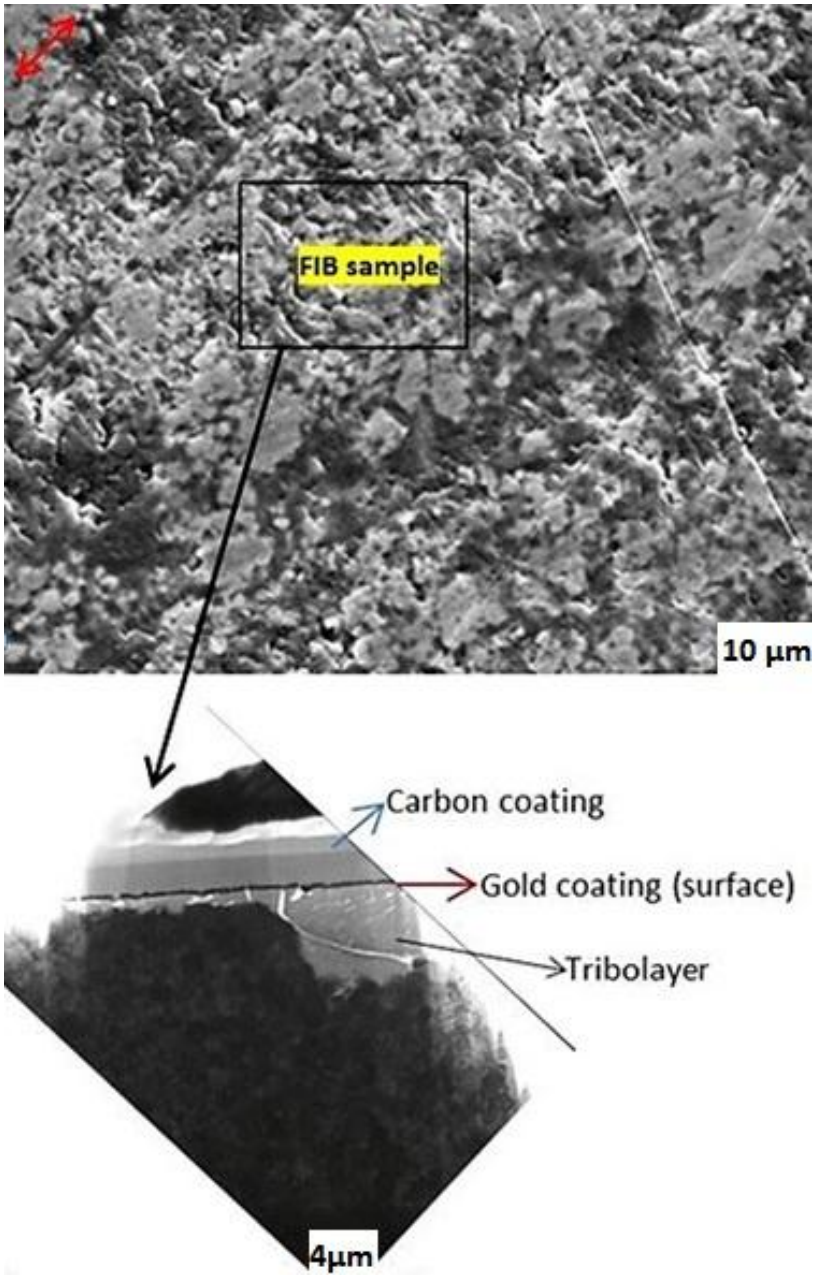

Fig 4.53: SEM image of typical damage pit on AZ worn surface under 4N load in water for 24 hours with reciprocating sliding speed 600 rpm with selected area for TEM imaging purpose by FIB lift out method.

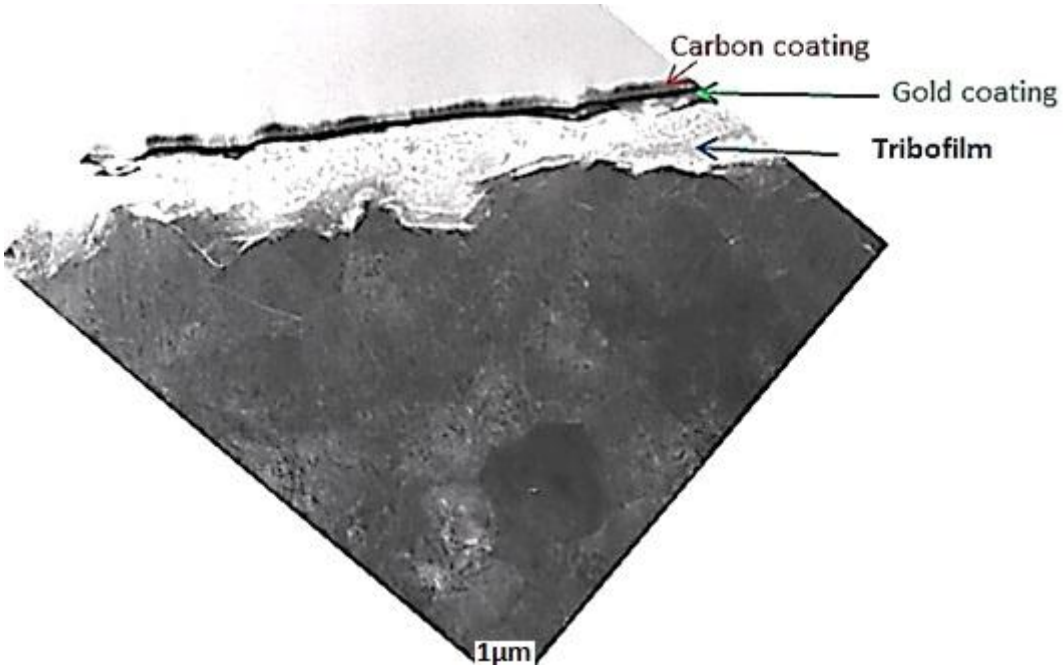

Fig 4.54: Tribolayer and microcracks underneath the surface.

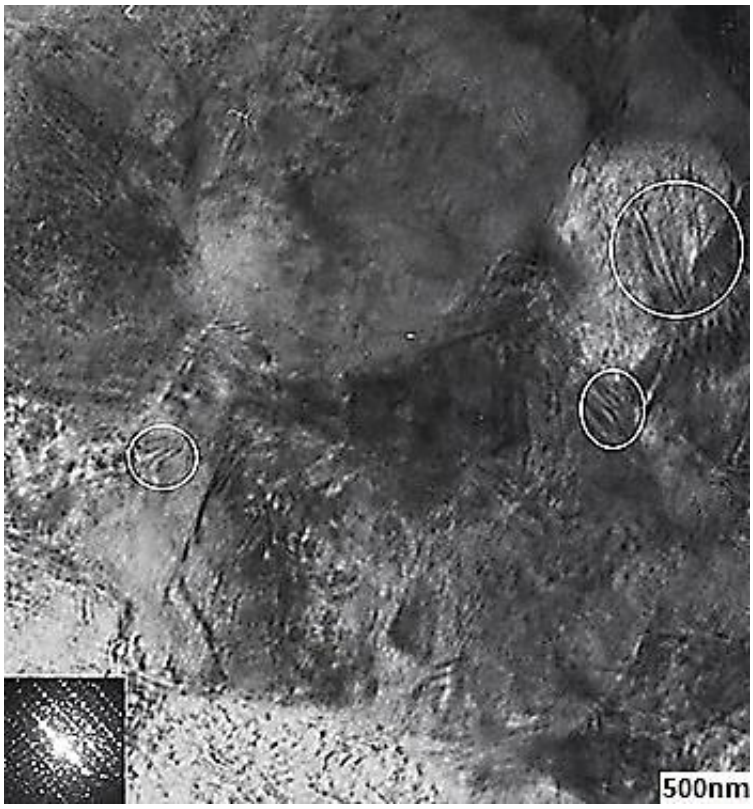

Fig 4.55: TEM image of damaged surface with monoclinic twins' formation.

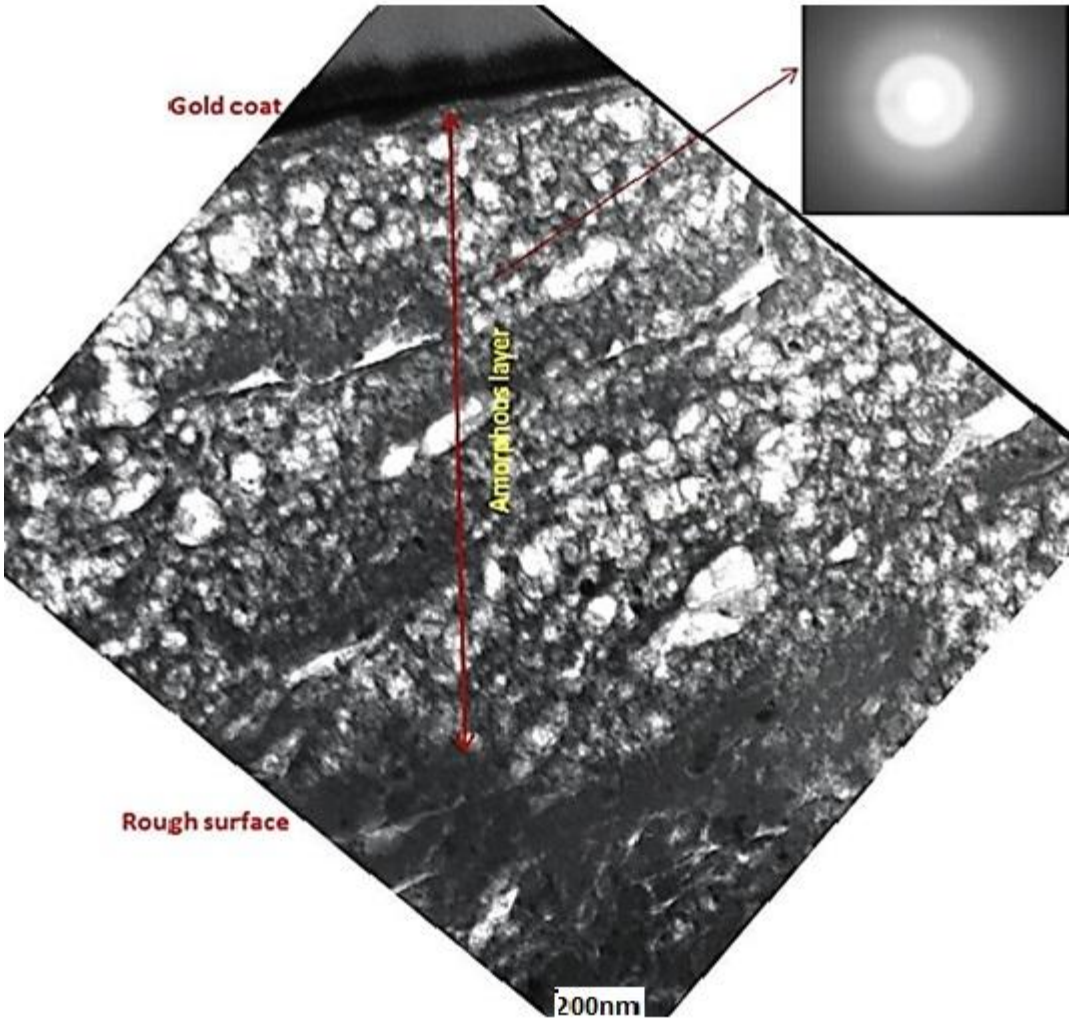

Fig 4.56: Tribolayer with nano particle floating on that.

4.6. %25 Bovine Serum Lubricated Condition

Lower wear rates would be expected when using %25 bovine serum lubricant rather than water. The sliding wear mechanism of zirconia surfaces against alumina ball was studied by applying loads ranging from 0.5N to 4N at 600rpm (0.02m/s) constant speed to simulate different wear zones i.e. the same testing regime as the water lubricated samples. A typical COF (coefficient of friction)-time graph for reciprocating sliding wear of the DLAZ (degraded LAZ) sample worn under 0.5 N load for 24h at 600rpm in bovine serum was plotted in Figure 4.57. Initial contact of the intact surfaces of alumina counter ball and zirconia disk caused

early COF fluctuation which then steadily increased from around 2 hours attaining a steady state value of about 0.014.

The lubricated regime was identified from the Stribeck curve constructed for six samples of Z, AZ, LAZ, DZ, DAZ and DLAZ, Figure 4.58. As with water lubrication then two main lubricated regime, mixed and full fluid were identifiable in most graphs, Table 4.3 COF value for zirconia surface in presence of bovine serum is very low being within the range at [0.003±0.002, 0.042±0.008].

As with the water lubricated tests, then surprisingly the DLAZ sample worn at 1N and 2 N load exhibited lower COF value than the non –aged specimen worn in the same condition.

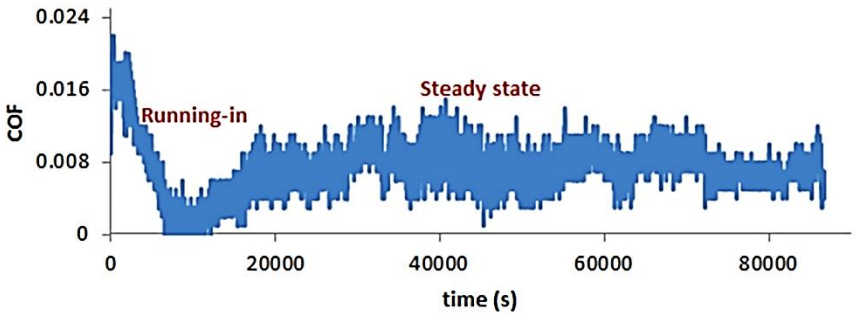

Fig 4.57: DLAZ sample worn under 0.5N load in bovine

Table 4.3: Minimum, maximum of COF with respect to the applied load and lubrication regime for Z, DZ, AZ, DAZ, LAZ and DLAZ specimens in bovine

Material	COF MIN	COF MAX	Lubricant regime
Z	0.001±0.002(1N)	0.011± 0.004 (4N)	Mix-Full-Mix
DZ	0.014±0.001(0.5N)	0.021±0.015(4N)	Mix
AZ	0.003±0.002(1N)	0.042±0.008(0.5N)	Full-mix
DAZ	0.002±0.002(2N)	0.025±0.001(0.5N)	Full -mix
LAZ	0.007±0.004(4N)	0.035±0.004(0.5N)	Full
DLAZ	0.004±0.003(4N)	0.035±0.004(0.5N)	Full

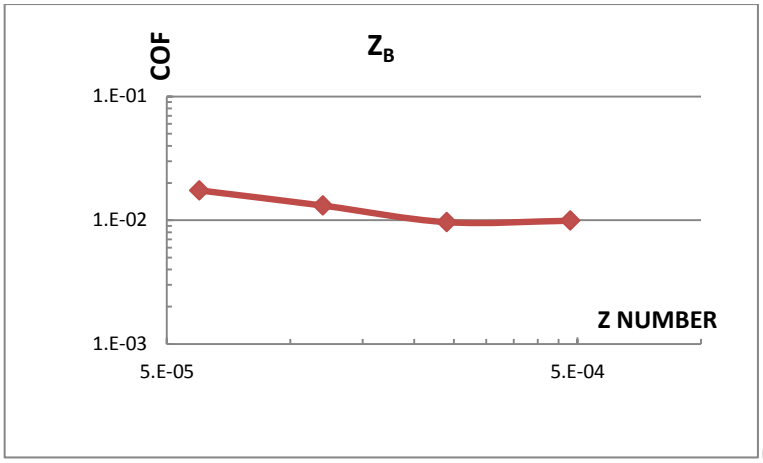
Z_B
COF
1.E-01
1.E-02
1.E-03
5.E-05
5.E-04
Z NUMBER

(a)

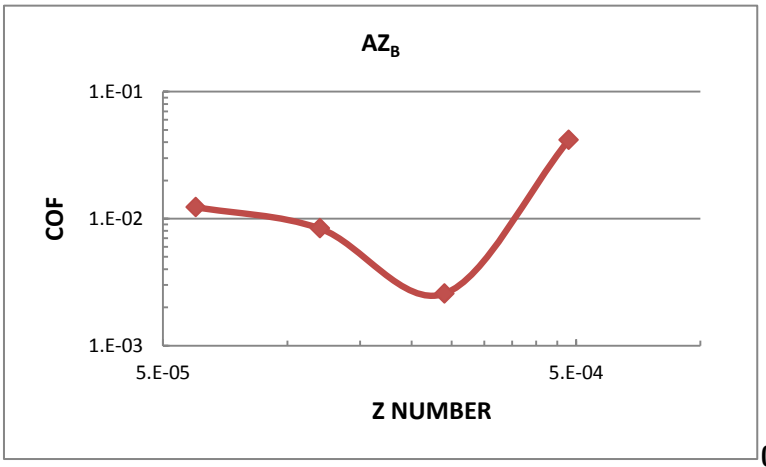
AZ_B
1.E-01
1.E-02
1.E-03
COF
5.E-05
5.E-04
Z NUMBER

(b)

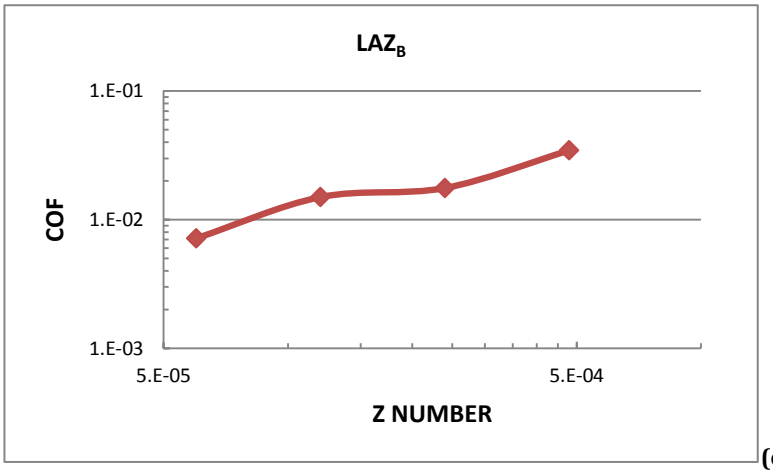
LAZ_B
1.E-01
1.E-02
1.E-03
COF
5.E-05
5.E-04
Z NUMBER

(c)

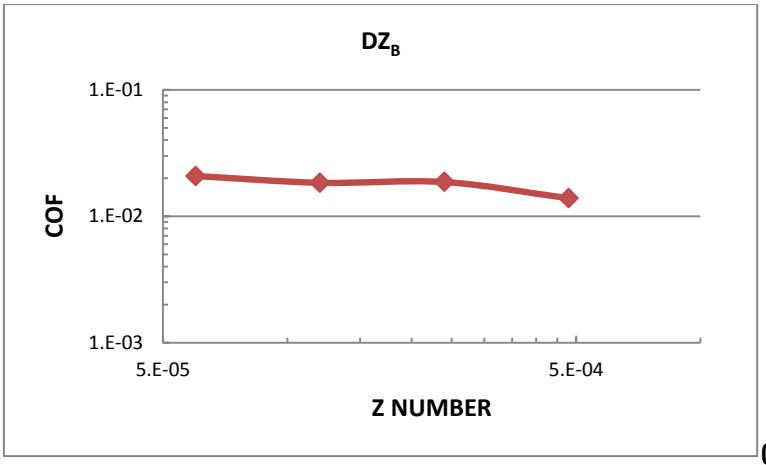

(d)

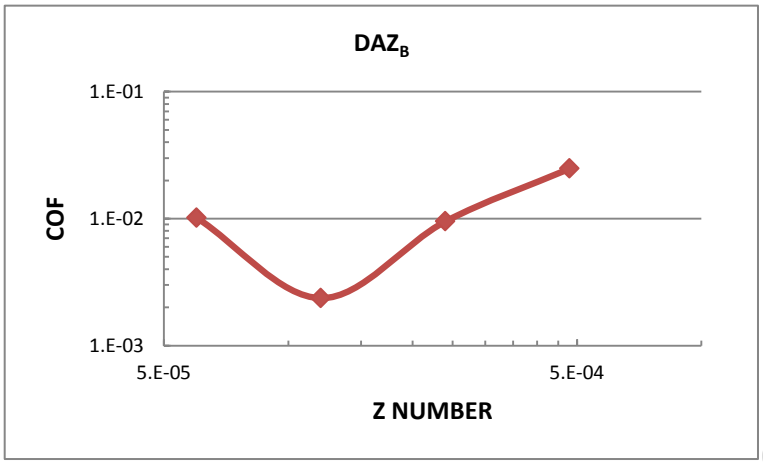

(e)

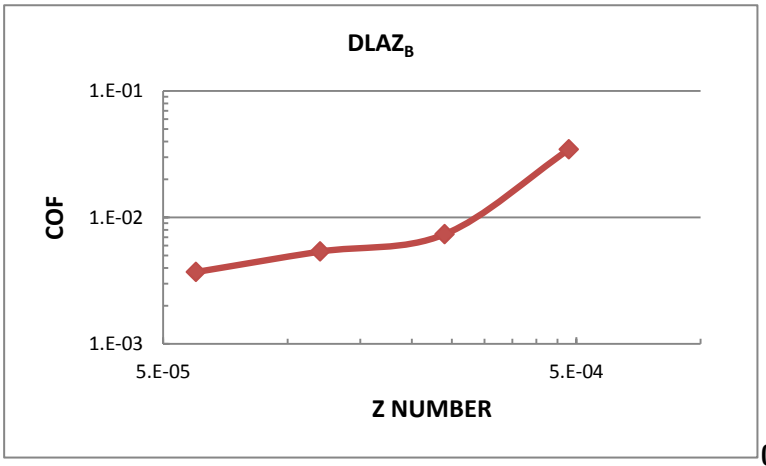

(f)

Fig 4.58: The Stribeck curve for (a) Z, (b) AZ, (c) LAZ, (d) DZ, (e) DAZ and (f) DLAZ samples *lubricated* with bovine serum(B) under 4, 2, 1 and 0.5N load . D represents degraded specimen.

Obtaining the lowest value of COF at 4N load for LAZ and DLAZ samples might be due to change of the lubricant viscosity. During the wear the mechanical stresses coupled with heat

generated in higher loads modifies the surface property in a way to improve the wear resistance significantly.

4.6.1. Wear Rate

Obtaining the lowest value of COF at 4N load for LAZ and DLAZ samples might be the result of changes to lubricant viscosity, but was difficult to explain. Figure 4.59 and 4.60 compare the wear rate in bovine serum of the 6 different materials over this load range. The highest wear rate recorded was 8.73 $x10^{-8}$ mm^3/Nm during the 4N load of the DZ specimen. The wear scar could usually be observed with the naked eye by comparing the contrast on the wear track to that of the original surface, but interestingly in the DLAZ sample worn at 0.5N no wear damage was detectable even by SEM microscopy.

All of the wear tests were conducted in the mild wear zone based on the specific wear rates measured. The DLAZ sample showed the best wear resistance and was situated entirely within the full fluid film lubricated regime.

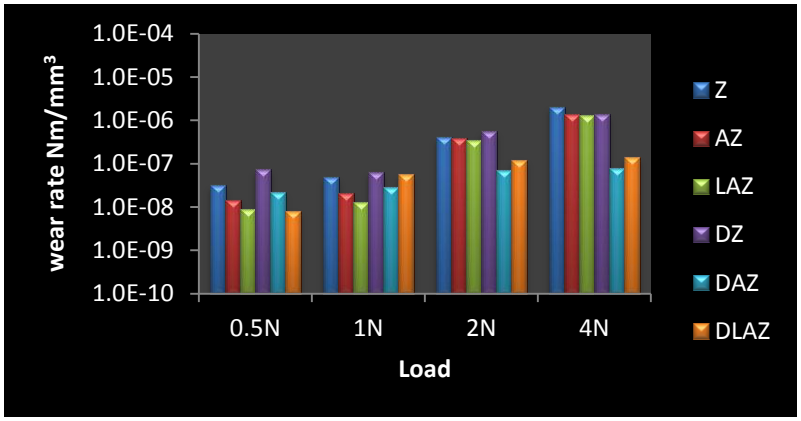

Fig 4.59: Specific wear rates for the reciprocating wear tests of all the material against high purity alumina ball lubricated with bovine serum showing the effect of test load.

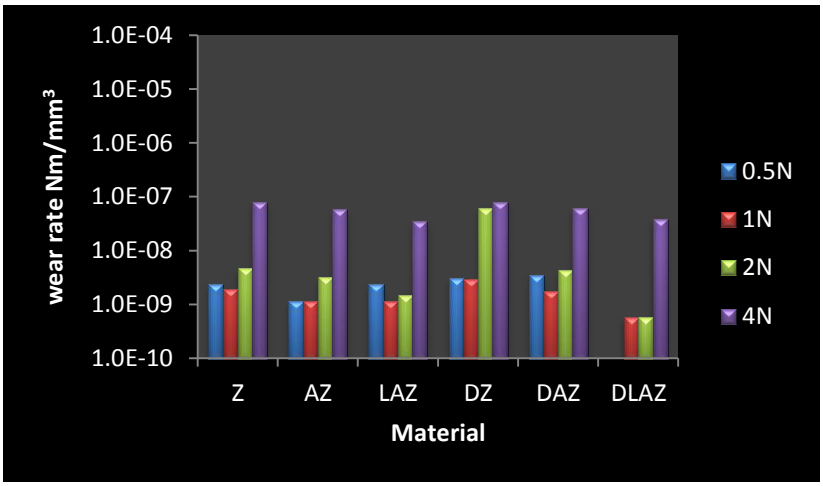

Fig 4.60: Specific wear rates for the reciprocating wear tests of all the material against high purity alumina ball lubricated with bovine serum, showing the effect of materials.

4.6.2. Worn Surface Characterisation

4.6.2.1. VSI Imaging

Surface evolution of Z, AZ and LAZ samples under bovine lubricated condition was imaged by 3D optical microscope (VSI), Figure 4.61 to 4.64. Figure 4.61 shows the worn surface of a Z sample tested under 0.5 N load. No wear debris accumulation was found on the surface indicating full fluid lubricated regime, but a deep groove parallel with sliding direction was found on the surface indicating the presence of an abrasive wear mechanism. The Z

specimen worn under 4N load, Figure 4.62, shows a rough surface towards the centre of the wear track and a few parallel grooves at the edge of the wear scar.

The LAZ sample worn at 4N load, Figure 4.63, shows two different wear regions. The left side image is of the head of the wear track and shows wear debris accumulation at one side of the wear track whilst the right side image is from middle of the scar where the wear damage is more inform. The levels of wear damage detected in the LAZ and DLAZ samples was very similar, Figures 4.63 and 4.64.

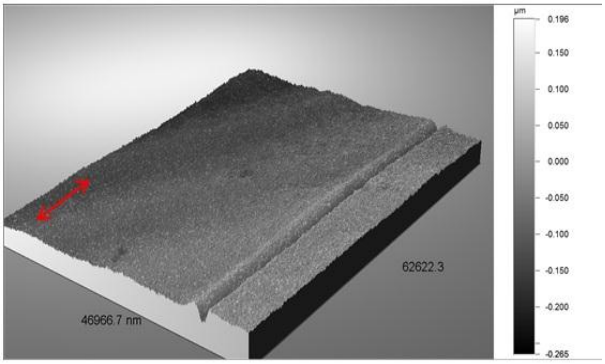

Fig 4.61: Z sample worn under 0.5 N in bovine.

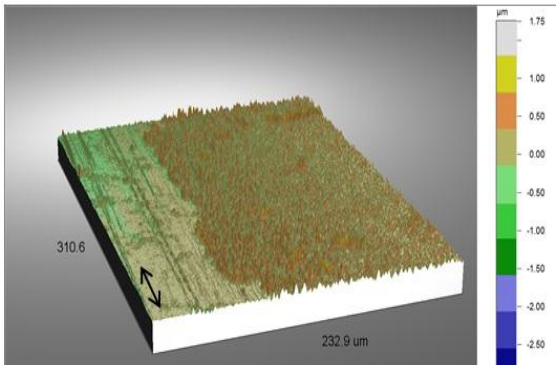

Fig 4.62: Z sample worn under 4N load in bovine.

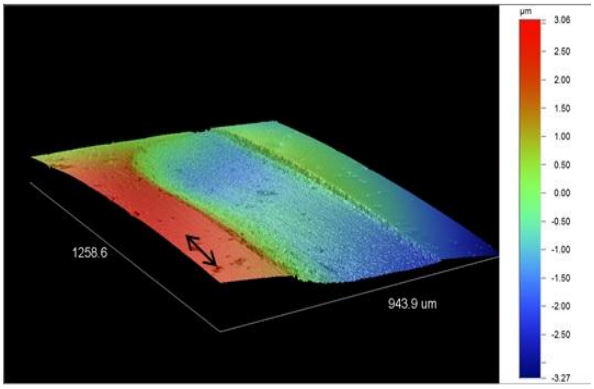

Fig 4.63: LAZ sample worn under 4N load in bovine.

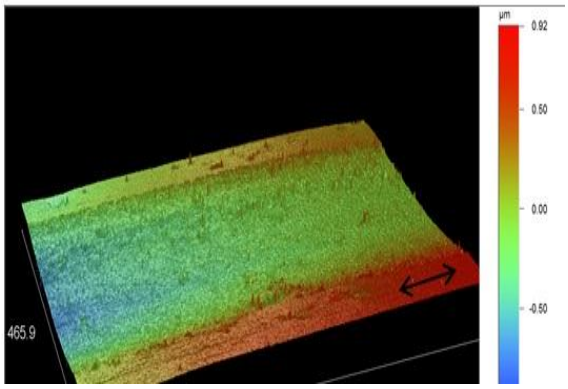

Fig 4.63: LAZ sample worn under 4N load in bovine.

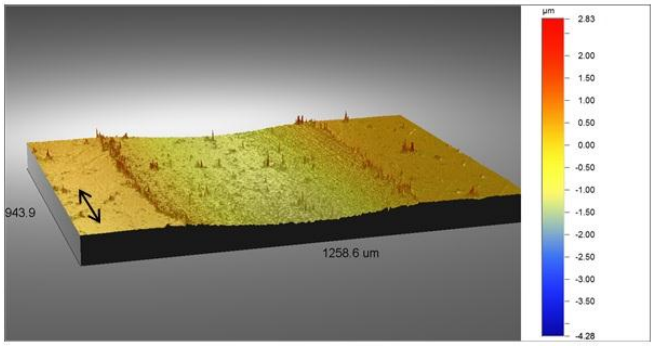

Fig 4.64: DLAZ sample worn under 4N load in bovine.

4.6.2.2 SEM Imaging

Figure 4.65 shows the surface layer of the AZ sample worn at 4N load. Surprisingly retention of the grain outline is clear within the image indicating that the original surface protected the surface layer. Comparison of Figure 4.66 with Figure 4.2c evidences modification of the

grain boundary outline in the LAZ sample which is a sign of tribochemical wear. The specific wear of this sample was extremely low and wear scar on the surface was difficult to detect even microscopically. The random scratch lines on the surface are residual from the sample preparation stage. The darker contrast in 4.66 and 4.68 images is a result of fixing carbon on the surface of the specimen by the action of the electron beam. Figure 4.67 of the LAZ sample worn at 1N load shows the intact grain outline but some surface wear particles were detectable which, dependent on their hardness and size could cause surface damage. Interestingly even under the highest applied load of 4N no sign of grain damage to the LAZ sample could be detected, Figure 4.68. The observable scratch lines were either residual from sample preparation or could have been caused by abrasive foreign body particles where the scratches were in line with the sliding direction.

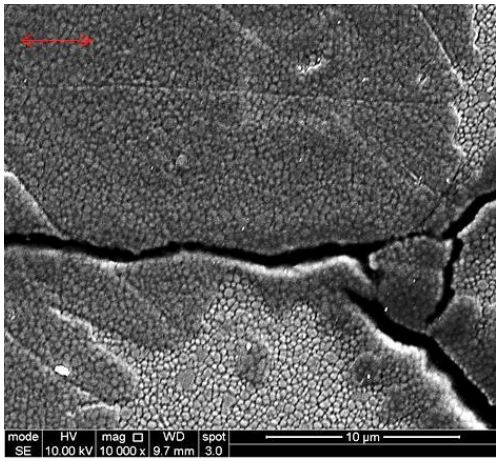

Fig 4.65: AZ sample worn in bovine under 4N load in for 24 hours at 0.02 m/s

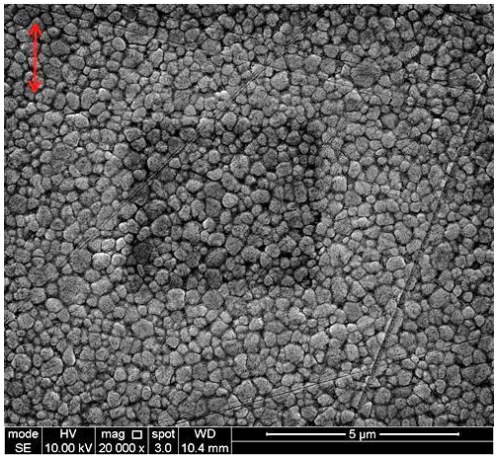

Fig 4.66: LAZ sample worn in bovine under 0.5 N load for 24 hours at 0.02 m/s

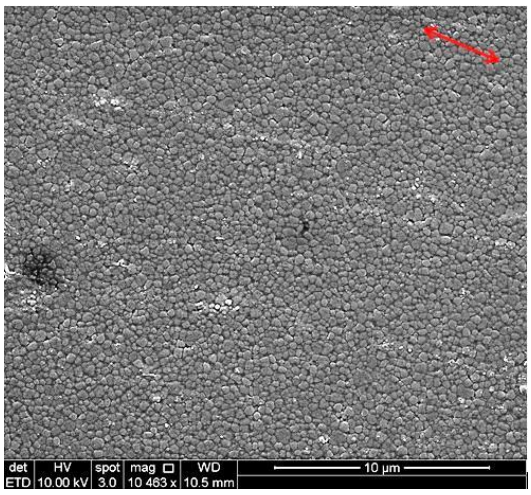

Fig 4.67: LAZ sample worn in bovine under 1N load for 24 hours at 0.02 m/s

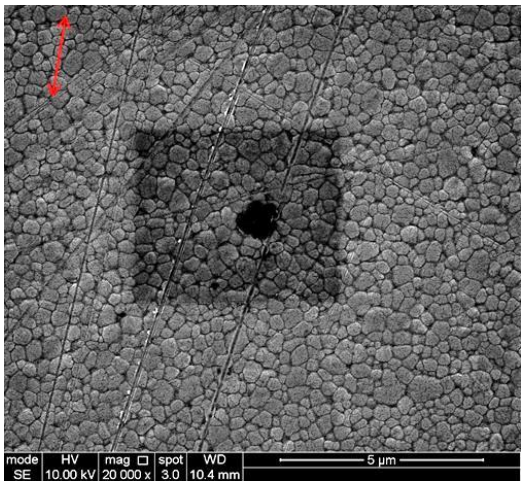

Fig 4.68: LAZ sample worn in bovine under 4N load for 24 hours at 0.02 m/s

4.6.2.3. AFM Imaging

The modified zirconia surface after wear in bovine serum was also investigated using AFM imaging. This indicated an irregular wear morphology and multiple wear mechanisms. The LAZ sample worn at 4N presents a totally polished surface but abrasive grooving along the sliding direction is visible, Figure 4.69(a). Localised grain relief is evident within the wear scar, Figure 4.69 (b). Interestingly the grain relief region was not detected in normal contact

mode imaging of AFM but only when using lateral force mode. The stable crystal orientation of some grains was attributed to the high fracture toughness of LAZ sample. AFM section analysis of the abrasive groove depth profile indicates that the abrasive particles participate in further wear damage, Figure 4.70 (bottom image).

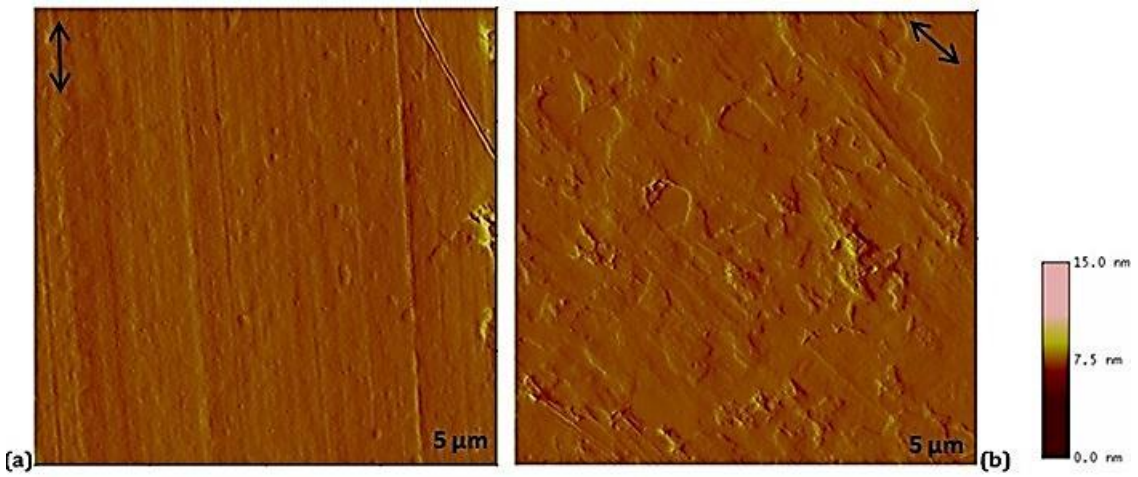

Fig 4.69: Lateral force microscopy image of LAZ sample worn under 4N load in bovine serum for 24 h. The polished area (a) belongs to worn surface adjust to fractured area (b) grain relief traces are clear.

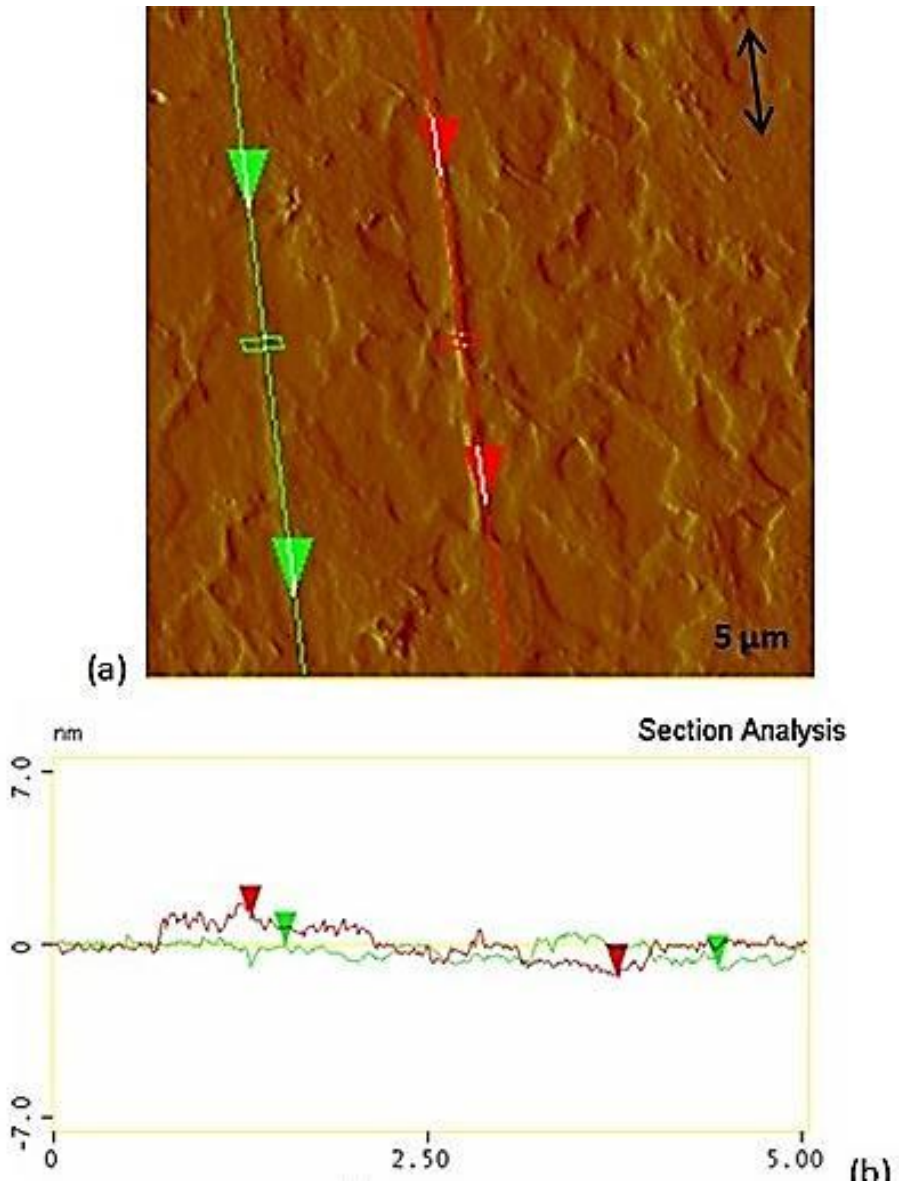

Fig 4.70: AFM 2D height image of grooves in DAZ sample worn inside bovine under 4N load (a) with corresponding section analysis of grooves depth.

4.6.2.4. Subsurface Wear Damage Characterisation

Determining actual wear damage of zirconia surface against alumina ball required analysis of sub-surface images. An AZ sample worn under 4N load in bovine serum for 24h at speed 0.02 m/s was investigated using TEM. Focus ion beam microscopy technique was applied to prepare the transparent sample if mechanical grinding was not a practical method for thinning TEM samples of the worn region. The boxed area of the SEM image in Figure

4.71(top image) was selected for cross-sectional TEM sample by FIB lift-out method. A gold coating layer protected the surface from further damage due to the gallium ion beam damage where it helped to label the actual surface. The TEM cross-section, Figure 4.71(bottom image) shows extensive subsurface microcracking and grain pull out. The diffraction pattern taken from an area beneath the tribolayer presents a monoclinic structure. Figure 4.72 (top image) shows the presence of a thick tribolayer on top of the original surface. The very rough structure of the original wear surface is clear from this image. The sub-surface microcracking (bottom image) extended to grains a considerable depth beneath the surface. In this image the subsurface porosity can be observed which makes this region vulnerable to grain pull, which then causes further damage.

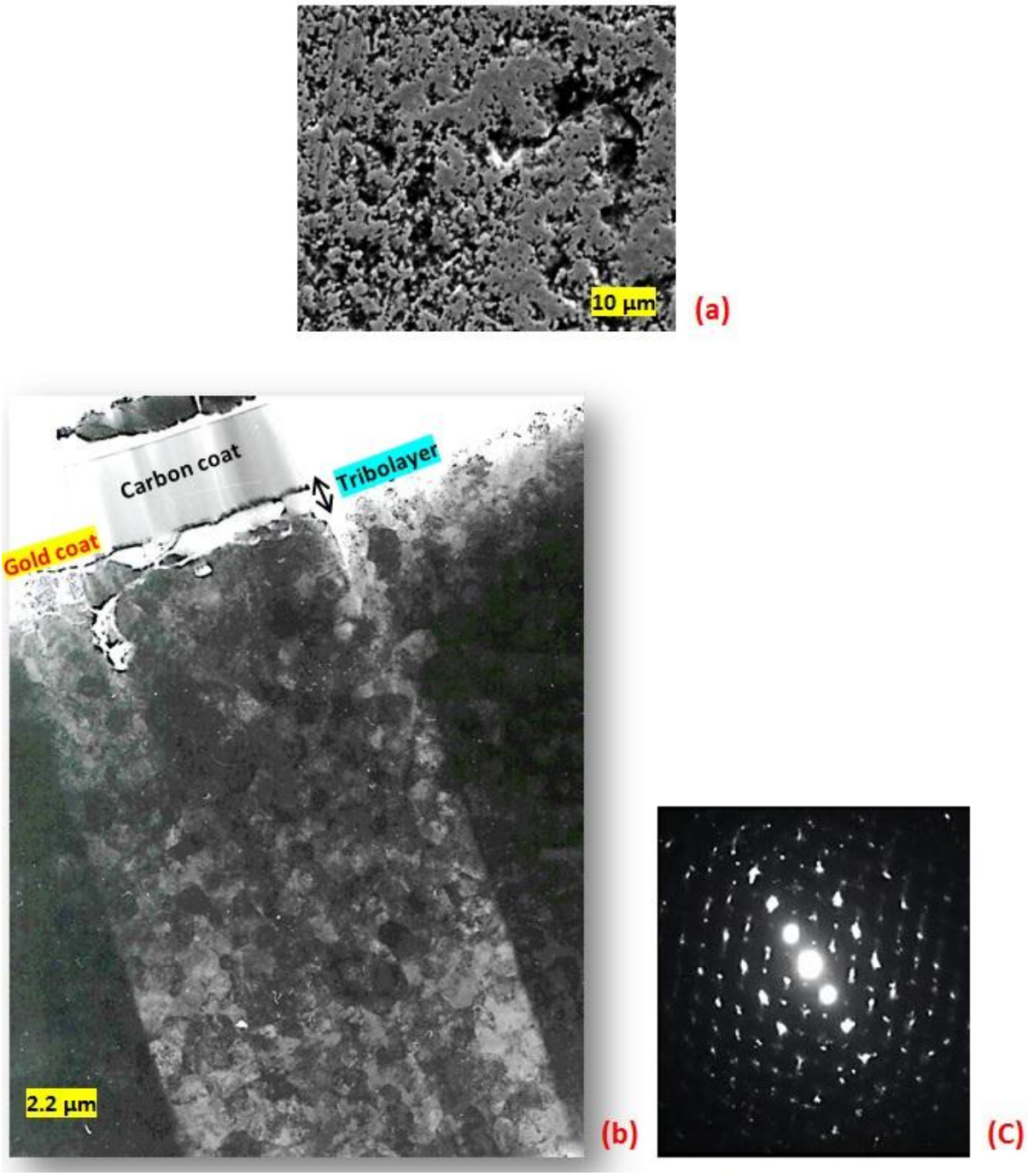

Fig 4.71: (a) A SEM image of worn AZ sample under 4N load in bovine shows a typical pit damage on which the location of cross-section TEM sample prepared by FIB lift-out method . (b) The plan view of the corresponding TEM cross-section sample and diffraction pattern(c).

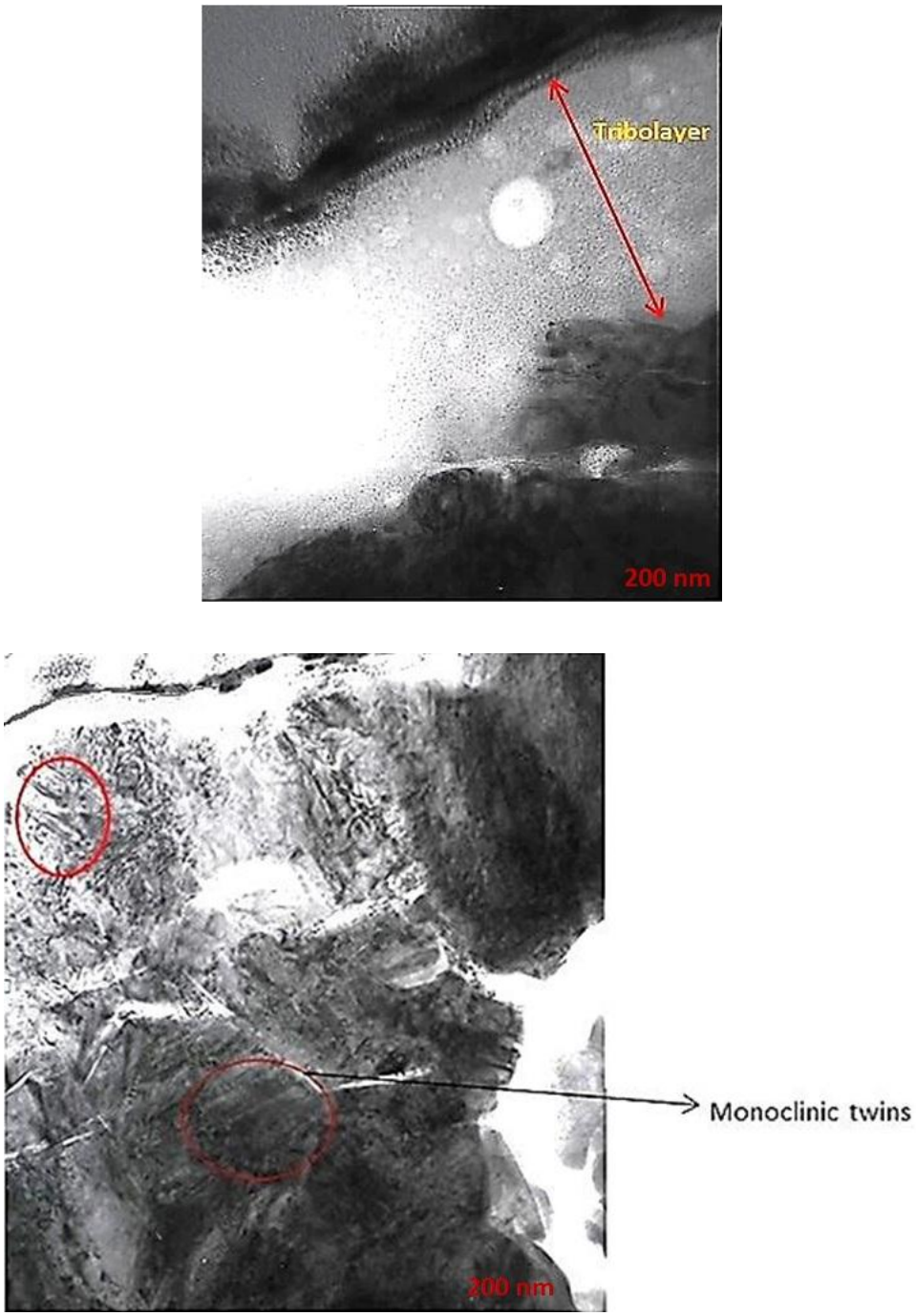

Fig 4.72: (Top image) shows floating wear particles inside surface layer. Bottom image shows the detail of wear damage followed by micro- cracking and monoclinic Twining.

5. Discussion

In this chapter the results of the degradation and wear tests are analysed. The benefit of dopant additions (Al_2O_3 and La_2O_3) in reducing the kinetics of the tetragonal to monoclinic phase transformation, on the zirconia's wear behaviour and interlinking mechanisms between degradation and wear are discussed.

5.1. Material Processing

High purity 3Y-TZP, B-grade Tosoh powder was used in this test due to it producing a sintered microstructure of faceted grain boundaries with no glassy phase at the grain boundaries or triple points. This is important as the glassy phase is known to effect the degradation kinetics and also could preferentially dissolve the dopant additions, thereby negating their beneficial effect [7]. Zirconia balls were used as milling media to eliminate any possible impurities introduce during milling process. Nogiwa [60] in her TEM study of the same composites used in the present work discovered some voids within the doped material's structure and attributed them to the removal of the amorphous phase in the triple point due to ion milling of TEM sample preparation process. However, these were few and far between and high resolution TEM analysis demonstrated that the grain boundaries were free from glassy phase.

The schedule of the sintering process was that developed by Burke [70] to achieve optimum grain size and fracture toughness. In particular, this sintering schedule allowed materials with different additions to be developed with the same grain size and fracture toughness, thereby allowing the role of the dopant additions to be determined without the complication of these variables. Grain size has a critical effect on the mechanical properties

of zirconia and its role in the tetragonal to monoclinic phase transformation has been discussed extensively in the literature. For zirconia in biomedical applications, the British standard requirement is of a grain size is less than 400 nm. This is a reduction in grain size compared to that stated previously of 600nm, followed by catastrophic failure of the Prozyr zirconia hip joint implants manufactured in 2001. The grain size produced in the current work is in agreement of the British standard requirement although all three compositions showed some degree of ageing regardless of grain size. The range of the measured grain size was 260-310 nm (Table 4.1) where AZ had the closest value to the undoped Z material, while the LAZ grain size was 20 nm smaller, but this value is within experimental error. Similarly, the fracture toughness measured for all materials was the same, within experimental error.

The grain size observed in the current work does not fit in the suggested ranking for dopants additions suggested by Huan and Chen [19]. The sintering schedule used provided essentially the same grain size and fracture toughness for all materials. This is in contrast to Huan and Chen who suggested that the grain sizes should be a function of the characteristics of the ternary dopant, in particular the ionic size and valence. Moreover, there are several reports in the literature that the alumina addition should act as a sintering aid [7]. The difference between the current research and the literature is because relatively small additions were made in the current work, and a relatively low sintering temperature was also used.

Lepisto and Mantyla [71] in their research pointed to the creation of the oxygen vacancies as a result of the alumina addition, which aids the ageing resistance. The number of oxygen vacancies is the key factor in tetragonal phase stabilization. Ross and Rodrigues Pulido also

discuss about the effect of the alumina and lanthena additions on oxygen ion vacancy accumulations at the grain boundaries, which is a major contributor in the stabilization of the tetragonal phase [72].

It is important to note that the fracture toughness of a zirconia ceramic depends strongly on the test method used to measure the fracture toughness. In the current work, indentation was used, because this was regarded as most relevant to the wear process, which is a surface specific phenomenon. One of the disadvantages of this technique is that there can be further crack propagation from the indent some time after the test. Moreover, locating the crack tip can be difficult, particularly by optical microscopy. In the current work, crack measurements were made in the SEM straight after indentation to minimise any time dependent crack propagation. The more accurate measurement of total crack length by SEM is likely to have produced a lower value of the fracture toughness than observed by Burke and Rodrigues Pulido for essentially the same material, as they used optical microscopy to measure crack length [72][73].

5.2. Topography of the Degraded Materials

Since the tetragonal to monoclinic phase transformation results in an increase in the lattice volume and thereby grain upheaval on a surface, AFM with its high vertical resolution was used to image the changes in grains height after aging. A significant height difference was observed between transformed and non-transformed regions, e.g. Fig. 4.16. Monoclinic twinning was not observed in any of the monoclinic grains, consistent with the work of Nogiwa [78], believed to be because of the small grain size. Twins in the monoclinic phase have been observed, but for significantly larger grain size materials. XRD of the degraded samples aged less than 24h did not detect any monoclinic phase but AFM imaging revealed

some transformed grains, indicating that AFM was more sensitive to detecting transformation than XRD. AFM imaging of the sample degraded for 24 hours showed circular monoclinic “spots” forming on the surface, Fig. 4.13. These “spots” are regions where transformation occurs in a small number grains and this triggers transformation in the adjacent grains such that the transformation front grows away from the original grains with an approximately circular appearance when viewed at the surface. The structure of these spots was revealed by Nogiwa and Rainforth [23].

The AZ material exhibited similar behaviour to the Z material, Fig. 4.12 and 4.13. However, AFM imaging of the LAZ specimen showed a different behaviour of monoclinic nucleation and growth compared to the other compositions. In the LAZ specimen, monoclinic spots were not observed; rather transformation appeared to occur in individual or small clusters of grains, as can be seen in the light contrast area in 24h, Figure 4.14. This behaviour has not been seen before, and is different to that observed by Nogiwa and Rainforth for material with similar composition. However, the current work was undertaken with a degradation temperature of 134^{o}C, whereas Nogiwa and Rainforth used 180^{o}C. This suggests that the co-addition of La^{3+} and Al^{3+} interferes with the autocatalytic nature of the transformation more at the lower temperature than the higher temperature. Nevertheless, Nogiwa and Rainforth observed a fundamental difference in transformation behaviour between the Z and LAZ materials, with the latter exhibiting far slower transformation kinetics.

Phase transformation in zirconia is triggered by an applied stress. As it is shown in Figure 4.6 defects such as scratches on the surface appeared to be preferential regions for nucleation

of the monoclinic phase. This is consistent with the work by Nogiwa for samples aged at 180 °C.

5.3. Propagation of the Transformation

Degradation of zirconia starts from the surface and propagates inside the bulk. SEM imaging of surface cross-sections of the aged specimens revealed the transformation front as a result of grain pull-out and intergranular fracture which occurred during metallographic preparation, a consequence of the low mechanical strength and microcracking of the monoclinic phase, Fig. 4.19. This showed the dramatic difference in the degradation rate between the different materials. The small addition of alumina approximately halved the depth of transformation. The addition of alumina and lanthana reduced the depth of transformation by a factor of around 4. This is in-line with the observations of Nogiwa and Rainforth [43], although the effect of a combined alumina and lanthena addition was much more pronounced at 134^{o}C degradation temperature used in the current work compared to the 180^{o}C used by Nogiwa and Rainforth.

5.4. Sliding Wear Mechanisms

5.4.1. Friction and Lubrication Behaviour

Lubricated reciprocating wear tests were carried out at four different loads in water and 25 vol% new-born calf serum. Generally the average COF for all the materials was very low. The COF value was in range of 0.010-0.070 for water and 0.002-0.041 for bovine serum. Ma undertook tests of a commercial zirconia toughened alumina (ZTA) using the same test conditions as those in the present work and observed higher friction for tests using water as a lubricant compared to the bovine serum. However, as such low values of the friction coefficient, the accuracy of the test method has to be called into question. Nevertheless, it is interesting that the values observed in the current work for zirconia were similar to those that Ma observed for ZTA [30]. The higher COF value for the tests in water compared to bovine serum could indicate zirconia's inherent sensitivity to water. Rainforth in his research showed that water was not a suitable lubricant for zirconia during the wear simulated wear tests, with similar wear behaviour observed in wet and dry tests [53]. This suggests that the surface of zirconia is hydrophilic.

In ceramic on ceramic in-vitro wear tests, the wear rate and COF in bovine serum depends on the viscosity of the serum. For example 100% bovine serum exhibited a higher coefficient of friction than that of 25% bovine serum [75]. This could be related to the absorption of the protein layer on the ceramic surface which creates an organic surface layer which is believed by some to act as a solid lubricant.

To identify the lubrication regime during the wear tests, the Stribeck curve construction for all the materials in both lubricants was constructed. Figure 5.1 shows a comparison of all the data. Some curves followed a classic shape for a Stribeck curve (as shown in Fig. 2.1), while

some do not. One problem is that the range of test conditions used was not sufficient to fully establish a Stribeck curve, with a range of sliding speeds also required to provide a comprehensive plot. In addition, it was difficult to measure friction accurately given the low friction coefficient values observed and therefore any noise in the system would dominate the measured value.

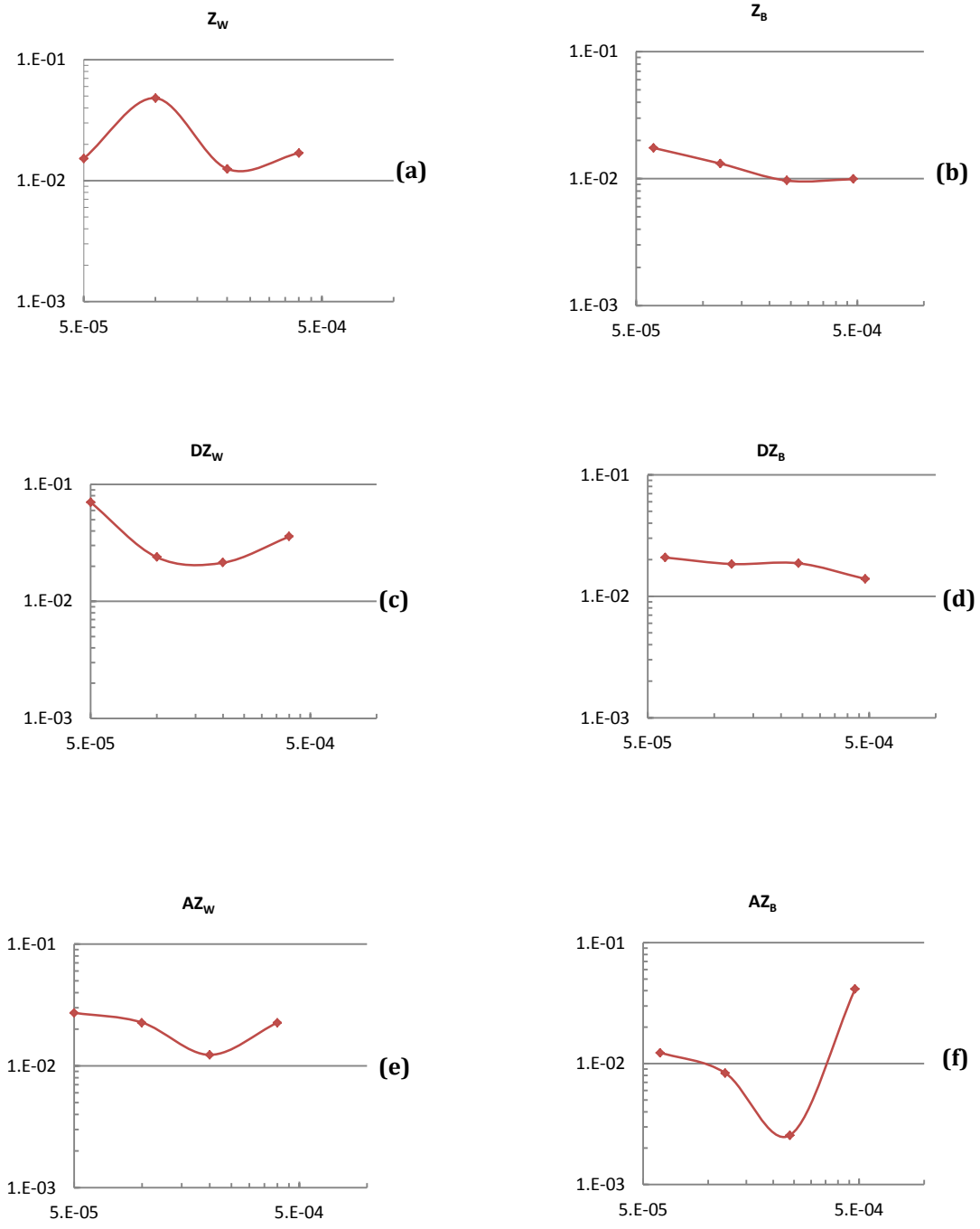

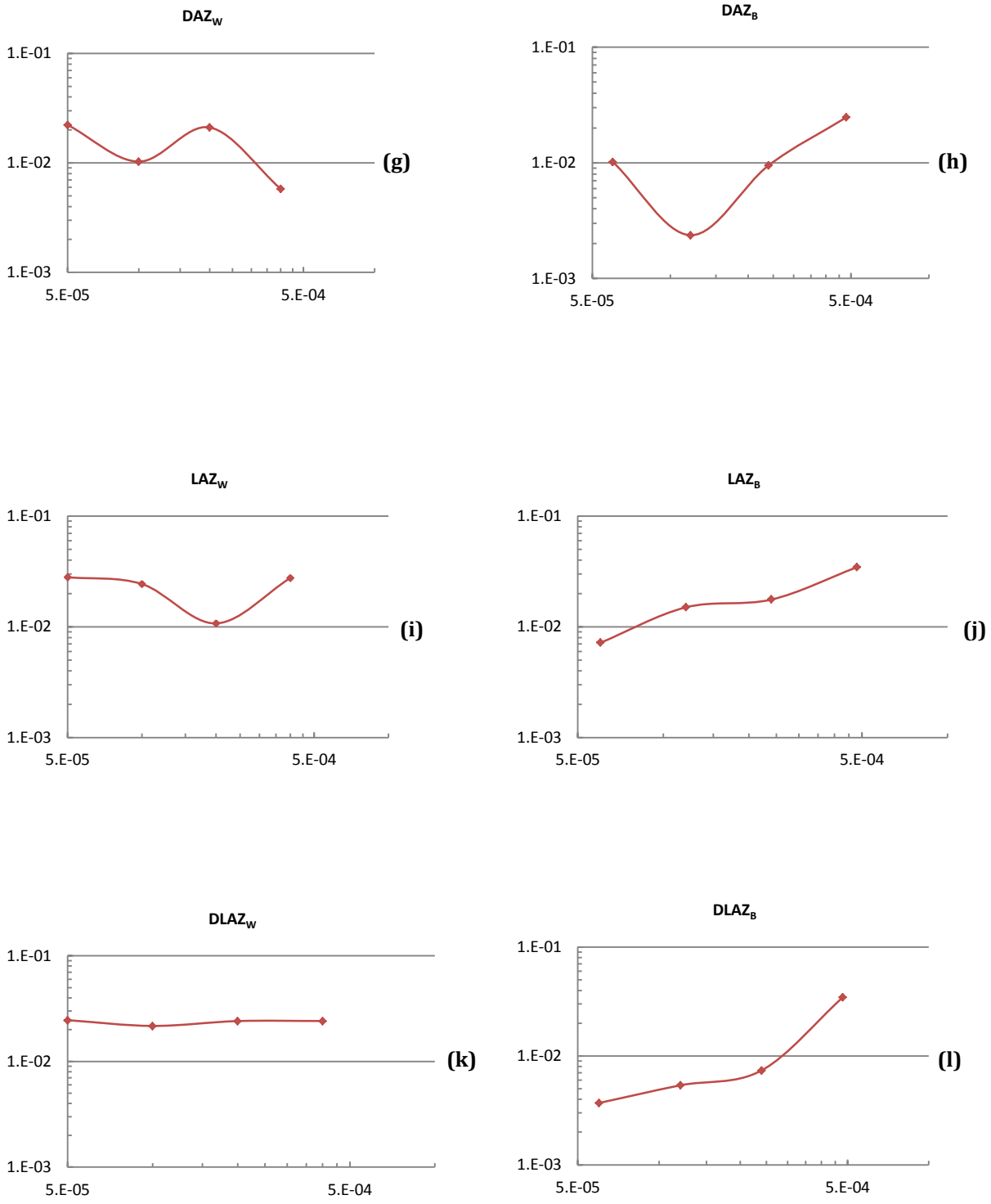

Fig 5.1: Partial Stribeck curves for : a) Z sample worn in water, b) Z sample worn in bovine, c) Degraded Z sample worn in water , d) AZ sample worn in Water ,e) AZ sample worn in water ,f) AZ sample worn in Bovine , g) Degraded AZ sample worn in water , h) Degraded AZ sample worn in Bovine , i) LAZ sample worn in water , J)LAZ sample worn in Bovine , K) Degraded LAZ sample worn in water, L) Degraded LAZ sample worn in Bovine .

Ma in her Stribeck curve construction for ZTA material found a specific trend to suggest a mixed and hydrodynamic lubricated regime. The Stribeck curves she observed for three

lubricants were much more consistent with the classic behaviour shown in Fig. 2.10, so that she was able to determine the lubrication regime operating for each test condition. The available evidence from studying the worn surfaces was that the zirconia in the current tests was operating predominantly in the boundary-lubricated regime.

5.4.2. Specific Wear Rates

The highest specific wear rates for all materials tested in water were $2.03x10^{-6}$ mm^3/Nm for water and $8x10^{-8}$ mm^3/Nm for bovine serum. These values are in the mild wear regime, as defined by Rainforth [52] who suggested a specific wear rate below 10^{-6} mm^3/Nm or less can be defined as the mild wear regime for ceramics. Le tested a commercial ZTA material using the same test conditions and obtained specific wear rates of 9.75×10^{-10}-1.33×10^{-8} mm^3/Nm in serum solution, which are smaller than the specific wear rates for the materials tested here. Jin [37] in his screening test suggested wear rates range of 10^{-8} mm^3/Nm for ceramic-on-ceramic hip joint combinations. So based on these findings bovine serum lubricated specimens with a lower wear rate than water are in the accepted range of mild wear. The specific wear rate here in this test is agreement with Rainforth's plot of specific wear rate against sliding speed for all the data available in the literature at that time [52], Figure 5.2.

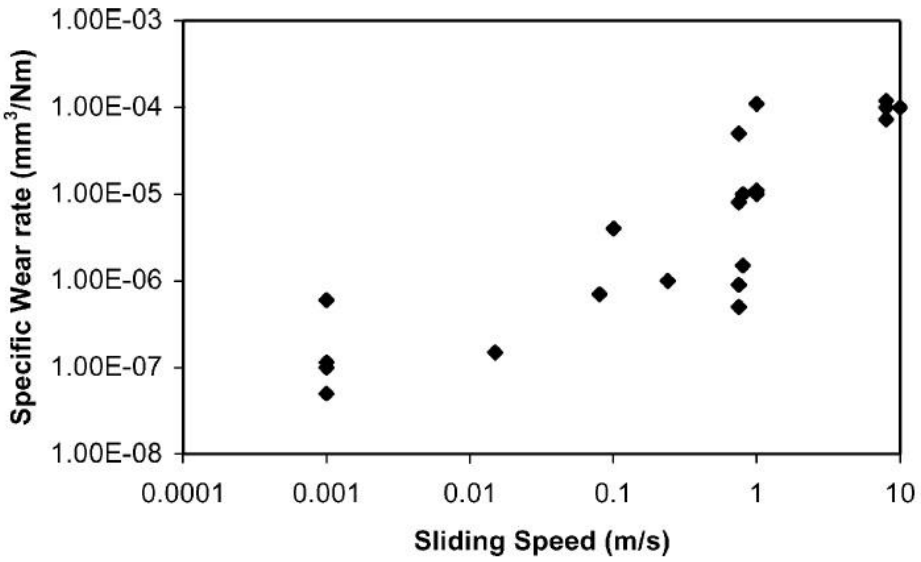

Fig 5.2: Specific wear rate as a function of sliding speed [52]

Rainforth and Stevens [50] reported similar specific wear rates for non-lubricated and water lubricated sliding for zirconia against alumina. Detailed microstructural observation of the worn surface revealed surprising high strain deformation at the surface that could only be explained by high flash temperatures during sliding. The surface structure was similar for water lubricated and dry sliding, again strongly suggesting that water does not act as a lubricant, rather that zirconia is hydrophilic.

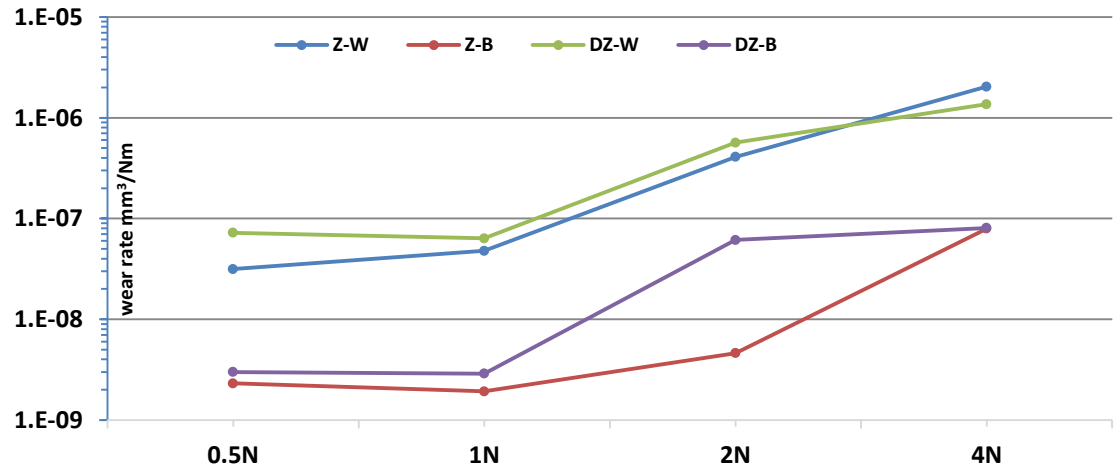
1.E-05
1.E-06
1.E-07
1.E-08
1.E-09
wear rate mm³/Nm
Z-W
Z-B
DZ-W
DZ-B
0.5N
1N
2N
4N

(a)

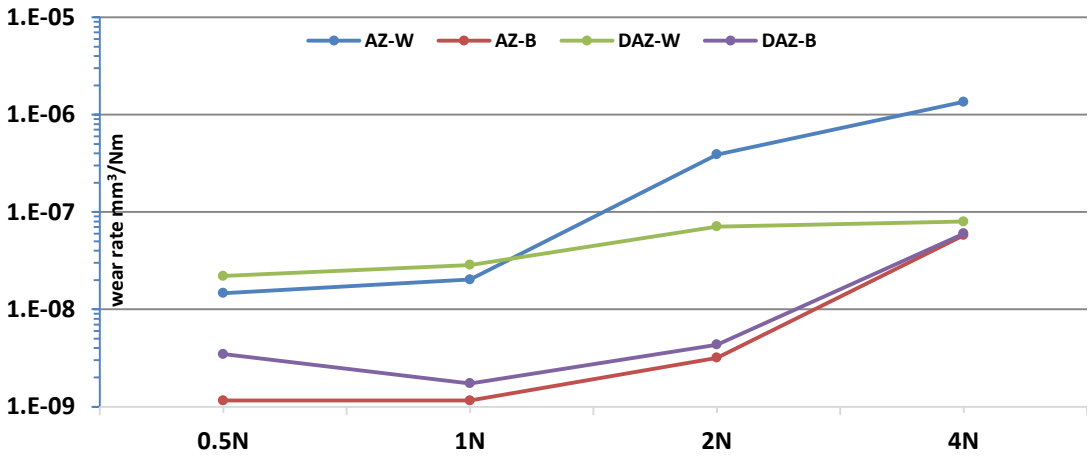
1.E-05
1.E-06
1.E-07
1.E-08
1.E-09
wear rate mm³/Nm
AZ-W
AZ-B
DAZ-W
DAZ-B
0.5N
1N
2N
4N

(b)

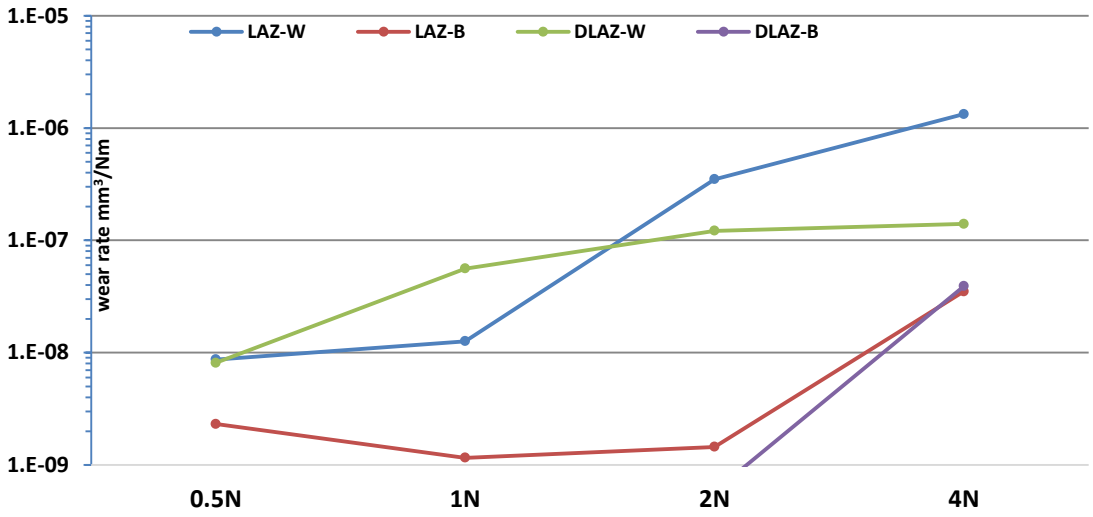

(c)

Figure 5.3: Specific wear rate as a function of load for a) Z, b) AZ and c) LAZ materials respectively. "D" represents degraded specimens. "W" and "B" are water and bovine lubricants.

5.4.3. Worn Surface Morphology

The worn surfaces of the materials tested in water differed from those tested in bovine serum. Generally, the surfaces worn in water were generally rougher and contained a more distinct tribolayer. Also, the surfaces worn in water tended to show characteristics of stick-slip (e.g. Figs. 4.38, 4.42, 4.46), while this characteristic was not evident on the surfaces worn in bovine serum. There was some evidence of grain pull-out, but this was more pronounced on the water surface and was generally obscured by the tribolayer.

TEM cross-sections of the worn surface showed that the surface regions were dominated by monoclinic zirconia for both the water lubricated and bovine serum lubricated surfaces, Fig. 4.56,4.71 and 4.72. The monoclinic grains were heavily microcracked in both cases, and evidence of grain pull-out was found for both lubricants. Such grain pull-out would be easy since the monoclinic phase was full of microcracks and has little mechanical strength, Fig. 4.72. Thus, the evidence was that the wear process was dominated by the transformation

from tetragonal to monoclinic zirconia at the surface, followed by detachment of the monoclinic grains as wear debris.

Detached wear debris would be re-deposited on the worn surface through attrition of the wear debris between the sliding surfaces. During this attrition process, there was clearly a reaction between the zirconia wear debris and the lubricant, ultimately leading to the formation of an amorphous tribolayer, with fine nanocrystals within the layer, Figs. 4.56, 4.72. SEM showed that this tribolayer covered much of the surface, e.g. Fig. 4.41, 4.53. The tribolayer becomes thicker at higher loads. The layer appeared to fill in recesses on the surface and form much of the contacting surface. Detachment of this layer occurred, giving the appearance of delamination wear, e.g. Fig. 4.36.

One surprising observation on the worn surface was the absence of monoclinic zirconia when using Raman spectroscopy to search for it. However, the laser wavelength penetration limit is less than the tribofilm thickness on the surface. Given the clear evidence in the TEM of a thick layer of monoclinic zirconia at the surface, it is concluded that the failure to observe it by Raman spectroscopy must have been because of the tribofilm prevented a signal escaping from the monoclinic layer.

One particular difference between the water and bovine serum lubricated surfaces was that grain relief was observed for the bovine serum lubricated conditions, e.g. Fig. 4.69, but was rarely seen in the water lubricated case. Grain relief morphology is usually linked to tribochemical mechanism, and has mostly been observed for the wear of alumina. This and the significant other differences in surface morphology indicate the significant differences in wear behaviour with water compared to bovine serum lubrication.

For both water lubricated tests and bovine serum tests for the non-degraded surfaces, the wear resistance of the alumina (AZ) containing material was better than the base 3Y-TZP, while the alumina-lanthana containing (LAZ) material offered the best wear resistance of all materials. Broadly speaking, the wear resistance scaled with the resistance to hydrothermal degradation. This, therefore, gives direct evidence that reducing the extent of transformation from tetragonal to monoclinic zirconia improves the wear resistance. It is also consistent with the TEM observations that wear occurred predominantly by removal of monoclinic grains from a heavily microcracked surface. The same observation of LAZ being better than AZ being better than Z is broadly speaking true for the wear tests on prior degraded surfaces, although the difference was more pronounced at low load. This again, suggests that the smaller the transformed layer the lower the wear rate.

One question that has been very difficult to answer has been why the surfaces degraded prior to wear testing tended to offer similar or better wear resistance to those that had not. Given that the degradation results in extensive microcracking in the monoclinic layer, it would be expected that such a surface would wear at a greater rate, but this was not observed. One possible reason could be that the surface transformation induced by the degradation results in surface compressive stresses that reduce wear rate. Such a hypothesis would be difficult to verify. However, it is difficult to envisage any other reason why a degraded surface could offer superior wear resistance in both water and bovine serum lubricated conditions.

6. Conclusions

6.1. Degradation in Zirconia

The effect of Al_2O_3 and La_2O_3 oxide additions on the ageing behaviour of a 3Y-TZP zirconia ceramic was studied. Powder processing and sintering schedule resulted to achieve a fully dense 3Y-TZP ceramics with homogeneous microstructures of faceted equiaxed grains. The structure was 100% tetragonal confirmed by XRD. These dopants additions did not significantly effect on the grain size of the base material (Z) material. The mean linear intercept measured grain size ranged between 260-300 nm with average grain size 286nm. This grain size is in agreement of the British Standards for Y-TZP surgical implants [11]. In addition, no statistically significant difference in fracture toughness or hardness was observed between doped and undoped materials. As shown in previous work by Nogiwa, dopants addition by segregation to the grain boundary create oxygen ion vacancies which make the tetragonal phase of zirconia more stable.

To simulate the degradation for zirconia in hydrothermal condition, all three samples were place in a degradation vessel for 6, 12 and 24 hours at 134 °C. The tetragonal to monoclinic phase transformation initiated at the free surface, usually from an isolated grain. Transformation then grew in an autocatalytic manner from the original transformation site forming monoclinic “spots”. Due to the volume expansion of the monoclinic grains the area of transformed grains starts to form conical structure, standing proud of the surface. Atomic force microscope with high vertical resolution was able to detect the monoclinic spots earlier than XRD. AFM is more sensitive to height differences on the surface. At the same time as forming these protuberances, the transformation of tetragonal zirconia propagated

into the bulk. Surface defects such as scratches were preferential regions for monoclinic nucleation.

Dopant additions reduced the rate of monoclinic phase transformation. The added dopants segregate to the grain boundary and by increasing the local stabilising effect from higher dopant concentration inhibit the transformation. It has been shown that the t→m transformation kinetics follows a sigmoidal behaviour typical of the nucleation and growth mechanisms described by the Mehl-Avrami-Johnson laws [84].

SEM cross-section imaging of the aged structure easily revealed the penetration depth as a result of intergranular microcracking and grain pull out which occurred during polishing the cross-sections. This revealed major differences in depth is minimum in LAZ sample and maximum in undoped Z sample.

In conclusion, alumina and lanthana-alumina additions to 3Y-TZP resulted in a significant improvement in ageing resistance in this material by creating oxygen ion vacancies at the grain boundaries to retain the tetragonal phase.

6.2. Sliding Wear Mechanisms in Zirconia

Based on the findings from reciprocation wear tests on sintered zirconia disks using water and bovine lubricants at 0.5, 1, 2 and 4 N loads at a constant speed of 0.02 m/s , the following conclusions were drawn:

Results from reciprocating sliding wear tests in water and bovine lubrications were used to understand the lubricant regime during zirconia performance against alumina ceramic. To determine this purpose the Stribeck curve was constructed with friction coefficients and Sommerfeld number. Mixed and full fluid films lubrication regimes were detected for zirconia performance during wear. Degradation and low thermal conductivity in zirconia made the wear behaviour of zirconia very complicated and quiet unexpected.

In general worn surfaces for materials worn in water showed higher wear rate than those worn in bovine serum. At 4N load however, the wear rate was few orders of magnitude higher than the other loads. The wear zone in fact changed from mild to severe by moving towards higher loads.

Surface pitting and intergranular fracture were the dominant wear morphology was seen for the surfaces. Differential wear between individual grains was detected in bovine serum worn specimens. Third body abrasive grooving was observed in many loads and also in both lubricants. Liberated grains from pits contribute in the abrasive wear mechanism.

An amorphous tribolayer was formed on top of the fractured surface imaged by FIB microscopy. The nature of the tribofilm and how it formed does need to be investigated

7. Future Work

Alumina and lathena additions in small amount made a positive contribution in mechanical property improvement in zirconia to aid the ageing and wear resistance. It is important to further investigate what exactly the role of the dopant additions is.

A systematic study of FIB samples is suggested to study the distribution of tetragonal and monoclinic grains across a region exposed to hydrothermal conditions.

For the further study of reciprocating sliding wear behaviour of zirconia tests that were carried out in these different conditions an investigation of longer and shorter wear durations are suggested. A wear map construction in different lubricants might assist to study the wear mechanisms in zirconia ceramics.

A further investigation on tribolayer required to investigate which in the origin of the layer.

While protein reaction on implant surface has critical importance to investigate, so XPS could be applied to study this reaction on the surface. Tribolayer on serum lubricated worn surface is strongly affected by protein precipitation.

Viscosity of the lubricant need to be study in more details. More controllable environment such as temperature, shear rate, speed, could be add to the wearing system to compare the viscosity effect to the wear.

8. References

1. McKee GK, Watson-Farrar J. Replacement of arthritic hips by the McKee-Farrar prosthesis. Bone and Joint Surgery (Br) journal, 1966; 48-B (2):245-259.
2. Gomez PF, Morcuende JA. Early attempts at hip arthroplasty-1700s to 1950s. The Lowa Orthopaedic Journal 2005; 25:25-29.
3. Dowson D. New joints for the millennium: wear control in total replacement hip joints. Proceedings of the Institution of Mechanical Engineers, Part H: Journal of Engineering in Medicine 2001; 215(4):335-358.
4. Semlitsch M, Willert HG. Clinical wear behaviour of ultra-high molecular weight polyethylene cups paired with metal and ceramic ball heads in comparison to metal-on-metal pairings of hip joint replacements. Proceedings of the Institution of Mechanical Engineers, Part H: Journal of Engineering in Medicine 1997; 211(1):73-88.
5. Joshi RP, Eftekhar NS, McMahon DJ, Nercessian OA. Osteolysis after Charnley primary low-friction arthroplasty: a comparison of two matched paired groups. Journal of Bone and Joint Surgery (Br) 1998; 80-B (4):585-590.
6. Chevalier J. What future for zirconia as a biomaterial? Biomaterials. 2006; 27,535-543.
7. Lee WE, Rainforth WM. Ceramic microstructures property control by processing, London: Chapman and Hall, 1994, 359-360.
8. Cited; available from http://www.anatomie-physiologie.de/ana_site/anato064.html.
9. Jenabzadeh AR, Pearce SJ, Walter WL. Total Hip Replacement: Ceramic-on-Ceramic Seminars in Arthroplasty. 2012, 23:4, 232–240.

10. Rainforth WM, Zeng P, Ma L, Valdez AZ, Stewart T. Dynamic surface microstructural changes during tribological contact that determine the wear behaviour of hip prostheses: metals and ceramics. The royal society of chemistry. 2012; 156: 41-57.

11. Barnes CL, DeBoer D, Corpe RS, Nambu S, Carroll M, Timmerman I. Wear performance of large-diameter differential-hardness hip bearings. J Arthroplasty. 2008; 23:56-60.

12. Clarke IC, Green D, Williams P, Pezzotti G, Donaldson T. Wear performance of 36mm Biolox® forte/delta hip combinations compared in simulated 'severe' micro-separation test mode. 12th Biolox® Symposium, Seoul. 2007; 33-44.

13. Rahaman MN, Yao A, Bal BS, Garino JP, Ries MD. Ceramics for prosthetic hip and knee joint replacement. Journal of the American Ceramic Society 2007; 90(7):1965-1988.

14. Tetsuya Y, Masanobu S, Masaru U, Takehito H, Yusuke T, Kazuo Y. Wear analysis of retrieved ceramic-on-ceramic articulations in total hip arthroplasty: Femoral head makes contact with the rim of the socket outside of the bearing surface. Journal of Biomedical Materials Research. Part B: Applied Biomaterials 2005; 73B (2):301-307.

15. Taylor S, Manley MT, Sutton K. The role of stripe wear in causing acoustic emissions from alumina ceramic-on-ceramic bearings. The Journal of Arthroplasty 2007; 22(7 Supplement 1):47-51.

16. Stewart TD, Williams S, Tipper JL, Ingham E, M.H. S, Fisher J. Advances in simulator testing of orthopaedic joint prostheses. 29th Leeds-Lyon Symposium on Tribology, Leeds: Elsevier, 2002. p. 291-296.

17. Christel P, Meunier A, Dorlot JM, Crolet JM, Witvoet J, Sedel L, Boutin P. Biomechanical compatibility and design of ceramic implants for orthopaedic surgery, Annuals of the New York Academy of Sciences, 1988, 523, 234-256.

18. Green DJ, Hannink RHJ, Swain MV. Transformation Toughening of Ceramics. CRC Press, 1989, 138-139.

19. Hwang SL, Chen IW. Grain size control of tetragonal zirconia polycrystals using the space charge concept. American Ceramic Society, 1990. 73[11], pp. 3269-3277.

20. Masaki T. Mechanical properties of Y2O3 stabilized tetragonal ZrO2 polycrystals after ageing at high temperature. Journal of the American Ceramic Society.1986, 69,7. 519-522, 1986.

21. Lange FF. Transformation toughening, Journal of Materials Science. 1982, 12, 225-234.

22. Schubert H, Frey F. Stability of Y-TZP during hydrothermal treatment: neutron Experiments and stability considerations. Journal of the European Ceramic Society, 2005, 25, 1597-1602.

23. Nogiwa-Valdez AA, Rainforth WM, Zeng P, Ross IM. Deceleration of hydrothermal degradation of 3Y-TZP by alumina and lanthana co-doping. Acta Biomaterialia. 2013, 9, 4, 6226–6235.

24. Sato T, Shimada M. Control of the tetragonal-to-monoclinic phase transformation of yttria partially stabilized zirconia in hot water. Journal of Materials Science. 1985, 20, 3988-3992.

25. Yoshimura M, Noma T, Kawabata K, Somiya C. Role of H_2O on the degradation process of Y-TZP. Journal of Materials Science Letters.1987, 465-467.

26. Guo X. Hydrothermal degradation mechanism of tetragonal zirconia. Journal of Materials Science. 2001, 26, 3737-3744.

27. Ross IM, Rainforth W.M, McComb DW, Scott AJ, Brydson R. The role of trace additions of alumina to yttria-tetragonal zirconia polycrystals (Y-TZP) Scripta Materialia. 2001, 45, 653-660, 2001.

28. Lawson S. Environmental degradation of zirconia ceramics. Journal of the European Ceramic Society, 1995, 15485-50.

29. Ma L. Wear Behaviour of Biolox® delta ceramic Composite for Joint Replacements. PhD Thesis. Sheffield: University of Sheffield; 2010.

30. Kato K, Adachi K. Wear of advanced ceramics. Wear, 2002, 253, 1097-1104.

31. Chen M, Kato K, Adachi K. The Comparisons of Sliding Speed and Normal Load Effect on Friction Coefficients of Self-mated Si3N4 and SiC Under Water Lubrication, Tribology International, 2002, 35, 129–135.

32. Hutchings IM. Tribology: friction and wear of engineering materials. London: Edward Arnold, 1992.

33. Williams JA. Engineering tribology. Oxford: Oxford University Press, 1994.

34. Archard JF. Contact and rubbing of flat surfaces. Journal of applied physics 24, 1953, 981-988.

35. Hatton A, Ingham E, Matthews JB, Fisher J. Cytokine release by human peripheral blood macrophages after stimulation with alumina ceramic particles in vitro. 6th World Congress of Biomaterials, Hawaii, 2000, 1186.

36. Jin ZM, Stone M, Ingham E, Fisher J. Biotribology. Current Orthopaedics 2006; 20(1):32-40.

37. Jacobson A. Biotribology: the tribology of living tissues. Tribology and Lubrication Technology 2003; 59(12):32-38.

38. http://www.substech.com/dokuwiki/doku.php?id=lubrication_regimes. Accessed on September 2014.

39. Rainforth WM. The wear behaviour of oxide ceramics-A Review. Journal of materials science, 2004, 39, 6705 – 6721.

40. Stewart TD, Tipper JL, Insley G. Severe wear and fracture of zirconia heads against alumina inserts in hip simulator studies with microseparation.

41. Fukui K, Kaneuji A, Sugimori T, Ichiseki T, Matsumoto T. Wear comparison between conventional and highly cross-linked polyethylene against a zirconia head: a concise follow-up, at an average 10 years, of a previous report. J Arthroplasty. 2013 Oct; 28(9):1654-8.

42. Valefi M, Rooij M, Schipper DJ, Winnibst L. Effect of temperature on friction and wear behaviour of CuO-zirconia composites. European ceramic society journal, 32, 2012, 2235, 2242.

43. Nogiwa-Valdez AA, Rainforth WM, Stewart DT. Wear and degradation on retrieved zirconia femoral heads .2012

44. Fischer TE, Anderson PM, Jahanmir S. Influence of Fracture Toughness on the Wear Resistance of Yttria-Doped Zirconium Oxide , American Ceramic Society journal.1989,72, I2, 252–257.

45. Birkby, Harrison P, Stevens R. The effect of surface transformation on the wear behaviour of zirconia TZP ceramics J. Eur. Ceram. Soc., 5 (1989), 37–46.

46. Lee SW, Hsu SM, Shen MC, American society journal, 1993. 76[8], 1937-47.

47. Mahdiar Valefi, Wear and friction of self-lubricating CUO-TZP composites, 1980. Iran.

48. Barceinas-Sanches JDO, Rainforth WM. 1998, Acta matter.56, 18, 6475-6483.

49. Rainforth WM, Stevens R. A transmission electron microscopy study of wear of magnesia partially stabilised zirconia, 1993, 162–164, Part A, 322–33.

50. Khanna R, Basu B. Sliding Wear Properties of Self-Mated Yttria-Stabilized Tetragonal Zirconia Ceramics in Cryogenic Environment, 2007, Journal of the American Ceramic Society 90, 8, 2525–2534.

51. Rainforth WM, The sliding wear of ceramics. Ceramics International 1996; 22:365-372.

52. Stachowiak GW, Stachowiak GB. Environmental effects on wear and friction of toughened zirconia ceramics .Wear journal.1993.160.153-162.

53. Rainforth WM, Zeng P, Ma L, Valdez AZ, Stewart T. Dynamic surface microstructural changes during tribological contact that determine the wear behaviour of hip prostheses: metals and ceramics. The royal society of chemistry 2012; 156:41-57.

54. Fischer TE, Zhu Z, Kim H, Shin D.S, Genesis and role of wear debris in sliding wear of ceramics , Wear , 2000, 245:1–2.53–60.

55. Kalin M, Novak S, Vizintin J. Wear and friction behaviour of alumina ceramics in aqueous solutions with different pH. Wear 2003; 254(11):1141-1146.

56. Novak S, Kalin M, Kosmac T. Chemical aspects of wear of alumina ceramics. Wear, 2001; 250(1-12):318-321.

57. Min-Soo S, Bup-Min K, Seock-Sam K. Friction and wear behavior of structural ceramics sliding against zirconia. Int. J. Mod. Phy, 2006, B 20, 4407.

58. http://www.gordonengland.co.uk/wear.htm. Accessed on September 2014.

59. Nogiwa A. Effect of ternary oxide additions on the hydrothermal degradation resistance of 3Y-TZP. PhD Thesis. Sheffield: University of Sheffield; 2009.

60. Higginson RL, Sellars C. Worked examples in quantitative metallography, London: Maney Publishing, 2003, 31.

61. Shetty DK, Wright IG, Mincer PN, Clauer AH. Indentation fracture of WC Cocermets, Journal of Materials Science, 1985, 20.1873-1882.

62. Garvie RC, Nicholson PS. Phase analysis in zirconia systems. Journal of the American Ceramic Society, 1972, 55, 303-305.

63. Toraya H, Yoshimura M, Somiya S. Calibration curve for quantitative analysis of the monoclinic-tetragonal ZrO2 systems by XRD. Journal of the American Ceramic Society, 1984, 67[6], C-119-C-121.

64. Clarke DR, Adar F. Measurement of the crystallographically transformed zone produced by fracture in ceramics containing tetragonal zirconia. Journal of the American Ceramic Society.1982, 65[6], 284-288.

65. http://www.inspectionengineering.com/Bruker_Tribology.htm.Accessed on September 2014

66. ISO 6474. Implants for surgery-ceramic materials based on high purity alumina. International Standard, 1994.

67. Stachowiak GW. Engineering Tribology, 2005. Engineering Tribology. Elsevier Butterworth-Heinemann, Oxford, UK.

68. Burke D. Low temperature degradation of yttria stabilised tetragonal zirconia polycrystals (TZP's). Ph.D. Thesis, Department of Engineering Materials, University of Sheffield, Sheffield, 1998.

69. Lepistö TT, Mäntylä TA. A model for structural degradation of Y-TZP ceramics in humid atmosphere. Ceramic Engineering and Science Proceedings.1989, 10[7-8], 658-667.

70. Rodriguez-Pulido A, Ross IR, Rainforth WM. Processing and structural characterisation of 3Y-TZP ceramics resistant to hydrothermal ageing, Key Engineering Materials,2002, 206-213, 1053-1056.

71. Rodriguez-Pulido A. Degradation Mechanism of Y-TZP, Ph.D. Thesis, Department of Engineering Materials, University of Sheffield, Sheffield, 2006.

72. Ma L, Rainforth WM. The effect of lubrication on the friction and wear of Biolox_delta. 2012, Acta Biomaterialia, 8, 2348–2359.

73. Scholes S, Unsworth A, Goldsmith A. A frictional study of total hip joint replacements. Physics in Medicine and Biology 2000; 45:3721-3735.